Université catholique de Louvain

Louvain Drug Research Institute

Biomedical Magnetic Resonance Unit

MULTI-MODALITY IMAGING

TO ASSESS METABOLIC SHIFT IN TUMORS

Marie-Aline NEVEU

2016

Thesis presented in fulfillment of the requirements for the degree of

'Docteur en Sciences Biomédicales et Pharmaceutiques'

Supervisor : Bernard GALLEZ

Co-supervisor : Olivier FERON

« C'est dans l'effort que l'on trouve la satisfaction et non dans la réussite.

Un plein effort est une pleine victoire. »

Gandhi

A l'issue de la rédaction de ce manuscrit, je suis convaincue que la thèse repose sur un effort collectif et l'entraide. Je tiens donc à remercier les personnes qui, par leur soutien ou leur aide précieuse, m'ont permis de progresser et finaliser ce projet.

Je tiens tout d'abord à remercier mon promoteur, le Professeur Bernard Gallez. Merci de m'avoir ouvert les portes du labo il y a déjà 6 ans. Merci de m'avoir accordé votre confiance pour ce projet et pour votre grande disponibilité pour l'encadrement de la thèse, même lorsque j'étais à l'autre bout du globe.

Je remercie aussi mon co-promoteur, le Professeur Olivier Feron, pour sa disponibilité à chaque fois que j'ai sollicité son aide, ainsi que pour ces nombreuses encouragements lors de nos différentes entrevues.

Je remercie également le Docteur Bénédicte Jordan pour avoir suivi de près mon projet. Ses conseils et nos différents échanges ont amené à une réflexion plus raffinée et m'ont toujours permis d'aller de l'avant.

I wish to express my gratitude to the Professor Murali Krishna for giving me the opportunity to spend 6 months at the National Institute of Health. Thank you for your interest in my project, your time and your kindness. I sincerely thank the lab members, especially Ketha, Shun, Jeffery, Mouli and Anastasia, for the time they spent with me during my stay.

I extend my sincere thanks to all the members of my jury for their involvement during the committee meetings. Thank you to Professor Nathalie Delzenne and Professor Vincent Grégoire for their valuable suggestions and the constructive discussions. Thank you also to Professor Laure Bindels for accepting to be part of the jury. I am deeply grateful to Professor Tom Scheenen and Professor Jan Henrik Ardenkjær-Larsen for agreeing to read the manuscript and to participate in the defense of this thesis.

Je remercie tous les membres du team REMA pour leur soutien logistique et moral ainsi que pour la très bonne ambiance ! Merci à Anne-Catherine, qui a été la première à m'initier à la recherche durant mon Master et qui m'a consacré beaucoup de son temps. Un tout grand merci à Florence pour avoir pris le temps au début de ma thèse de me former. Merci pour tout ! Merci à mes collègues de bureau, Géraldine et Céline pour leur bonne humeur et les bons moments passés aux congrès, lors des manips ou durant une pause. Merci à Nicolas pour ton aide précieuse pour les manips Oxygène-

17 et pour toutes ces discussions qui ont animé le labo. Merci à Lionel pour tout ce temps et les discussions lors de nos différents co-voiturages. Merci à Pierre pour avoir toujours eu un sujet de conversation ainsi que pour tes conseils US. Merci à Philippe pour le partage de tes connaissances. Merci à Stefania pour ton dynamisme et ta bonne humeur. Merci à An, Trang, Linda, Valérie, Julie et Samantha pour les bons moments passés avec vous. Je souhaite également bonne chance aux nouvelles recrues. Bonne route à tous !

J'exprime ma gratitude à toutes les personnes des équipes FATH, MIRO et ANIM avec lesquelles j'ai interagi, et plus particulièrement merci à Pierre Sonveaux, Paolo Porporato, Cyril Corbet, Caroline Bouzin, Laurenne Petit, Anne Bol, et Jean-Paul Dehoux. Merci pour votre accueil ainsi que pour vos conseils logistiques et scientifiques.

Special thanks to the BMIC members. It was a pleasure to prepare exciting events with you!

J'aimerais également remercier le FNRS ainsi que l'UCL pour avoir financé ce projet.

Je terminerai par remercier ma famille et plus particulièrement mes parents. Merci pour votre soutien, votre patience à toute épreuve et votre aide lors des moments de panique à toute heure du jour et de la nuit. Merci de m'avoir toujours poussé dans mes retranchements, de m'avoir aidé à voir et donner le meilleur de moi-même. Merci à mon frère pour les paniques voitures du dimanche matin et son soutien. Merci à Marie-Christine et Paul pour avoir toujours montré de l'intérêt pour mon épanouissement, qu'il soit personnel ou professionnel. Merci à Jimmy pour sa présence, ses encouragements et pour avoir toujours trouvé le moyen de me faire rire même dans les moments critiques…

FOREWORD

Enhanced glycolysis has been recognized as a common metabolic feature of cancer. However, new evidence of oxidative activities in tumor cells has challenged this paradigm. Indeed, some tumor cells majorly rely on oxidative phosphorylation for energy production and besides the glycolytic and oxidative phenotypes, some cancers exhibit hybrid phenotypes with an amazed metabolic flexibility. All these adaptive behaviors represent major challenges for therapies. A better understanding of the process associated with the characterization of metabolic patterns for each tumor patient would lead to the development of more efficient anticancer strategies.

Therefore, this thesis work aims at exploring the value of different non-invasive imaging modalities to assess tumor metabolic profiles and their pharmacological modulations. Advanced imaging techniques including ^{18}F-FDG PET, EPR oximetry, ^{13}C-hyperpolarized MRI and ^{17}O MRS were used to characterize glucose uptake, oxygenation, pyruvate transformation and oxygen consumption in well-established tumor models in vivo.

In the introduction, the patterns that govern glucose metabolism in tumors are described and anticancer strategies derived from these patterns are presented. We will consider how and why cancer cells exhibit a high rate of glycolysis. But even if the glycolytic phenotype has for long been considered as a hallmark of cancer, cancer cells can also adopt other metabolic profiles. Some tumor cells can rely on glucose oxidation for energy production or can also exhibit a metabolic flexibility. Current strategies that target glucose

metabolism are presented, focusing on glycolysis inhibition, glycolysis reversion with a particular focus on dichloroacetate agent and mitochondrial inhibition. Finally, available imaging technologies for tumor phenotyping, especially to appraise glucose metabolism, are described.

In the second part, specific aims of the thesis work are described.

The third part of this manuscript will present the four articles written during the thesis work. The first article presents the feasibility of ^{17}O MRS to assess oxygen metabolism in tumors. The second article aims at following the metabolic changes induced by the administration of dichloroacetate in glycolytic and oxidative tumor models, using different imaging modalities. The third article presents the preliminary results obtained with ^{18}F-FDG PET to assess the impact of oxygenation on tumor metabolism. And finally, the fourth article describes the metabolic behavior of glycolytic and oxidative tumors in vitro and in vivo during a reoxygenation challenge.

The fourth and last part of the manuscript will discuss the results obtained and the remaining challenges in the field but will also suggest possible future directions.

TABLE OF CONTENT

LIST OF ABBREVIATIONS

ADP	adenosine diphosphate
AIF	arterial input function
AMP	adenosine monophosphate
ATP	adenosine triphosphate
AUC	area under the curve
B_0	external magnetic field
3-BP	3-bromopyruvate
^{13}C	carbon 13
CHC	α-cyano-4-hydroxycinnamate
$CMRO_2$	cerebral metabolic rate of oxygen
CoA	coenzyme A
CSC	cancer stem cells
CT	computed tomography
2-DG	2-deoxyglucose
DCA	dichloroacetate
DNA	deoxyribonucleic acid
DNP	dynamic nuclear polarization
EPR	electron paramagnetic resonance
ETC	electron transfer chain
^{18}F	fluorine 18
^{18}F-FDG	18-fluorodeoxyglucose
F1,6-BP	fructose-1,6-bisphosphate
F2,6-BP	fructose-2,6-bisphosphate
FADH2	flavin adenine dinucleotide
G6P	glucose-6-phosphate

GEM	genetically engineered mouse
GLUT	glucose transporter
^{1}H or H^{+}	proton
$H_2{}^{17}O$	^{17}O-labeled water
HIF	hypoxia inducible factor
HK	hexokinase
IDH	isocitrate dehydrogenase
IGFR	insulin-like growth factor receptor
LDH	lactate deshydrogenase
MCT	monocarboxylate transporter
MIBG	metaiodobenzylguanidine
MRI	magnetic resonance imaging
MRS	magnetic resonance spectroscopy
mtDNA	mitochondrial deoxyribonucleic acid
NADH	nicotinamide adenine dinucleotide
NADPH	nicotinamide dinucleotide phosphate
NMR	nuclear magnetic resonance
^{17}O	oxygen 17
$^{17}O_2$	^{17}O-enriched gas
OXPHOS	oxidative phosphorylation
^{31}P	phosphorus 31
3PO	3-(3-pyridinyl)-1-(4-pyridinyl)-2-propen-1-one
PDC	pyruvate dehydrogenase complex
PDH	pyruvate dehydrogenase
PDK	pyruvate dehydrogenase kinase
PDP	pyruvate dehydrogenase phosphatase
PET	positron emission tomography
PFK	phosphofructokinase
PFKFB	phosphofructo-2-kinase/fructose-2,6-bisphosphatase

pHe	extracellulat pH
pHi	intracellular pH
Pi	inorganic phosphate
PK	pyruvate kinase
PPP	pentose phosphate pathway
ROI	region of interest
ROS	reactive oxygen species
SNR	signal-to-noise ratio
SPECT	single photon emission computed tomography
SUV	standardized uptake value
TCA	tricarboxylic acid
β^+	positron
w_0	precession frequency or Larmor frequency

INTRODUCTION

1. Altered metabolism in cancer, the case of glucose

Glucose plays a key role in cellular metabolism. Like amino acids, lipids or other nutrients, glucose is a major fuel to produce energy, mostly in the form of adenosine triphosphate (ATP), in most mammalian cells and its metabolism is highly regulated to ensure normal tissue function (**Figure 1**). Glucose is taken up by the cells via specific transporters (GLUT) and is transformed into pyruvate via the enzymatic cascade of glycolysis. During this process, 2 molecules of ATP are generated. Under appropriate oxygen concentration, glycolysis is coupled with the oxidative phosphorylation (OXPHOS) to produce the majority of energy needed. The pyruvate is transferred to the mitochondria and oxidized to acetyl-CoA and CO_2 by the pyruvate dehydrogenase (PDH). Then, acetyl-CoA enters the Krebs cycle (also known as citric acid cycle or tricarboxylic acid (TCA) cycle) and is oxidized to generate NADH and FADH2, that will in turn account for the production of a large amount of ATP. The complete oxidation of one glucose molecule generates 36 molecules of ATP. In the absence of oxygen, OXPHOS is inhibited and the anaerobic glycolysis occurs. Pyruvate produced during the glycolysis is transformed into lactate by the lactate deshydrogenases (LDH). Lactate molecules are finally exported from the cells by the monocarboxylate transporters (MCT). The metabolism of glucose to lactate generates only 2 molecules of ATP per molecule of glucose. The phenomenon of redirection of the metabolism depending on the oxygen content is known as the Pasteur Effect. This reversible process regulates glucose metabolism through an allosteric regulation exerted by metabolites on key enzymes of the glycolytic pathway. Hexokinase (HK) is inhibited by glucose-6-phosphate (G6P). High levels of ATP inhibit

phosphofructokinase (PFK) and pyruvate kinase (PK). PFK is also regulated by citrate and PK by alanine and acetylCoA. Other metabolites can also be involved like inorganic phosphate (Pi), adenosine monophosphate (AMP), adenosine diphosphate (ADP) and fructose-1,6-bisphosphate (F1,6-BP) (Porporato, 2011). The Pasteur Effect is essential to maintain appropriate energy production in proportion to the oxygen level.

Enhanced glycolysis has been recognized as a common metabolic feature of cancer. Otto Warburg identified in the 20's the presence of a faster glycolytic flux in tumor cells, characterized by a high glucose uptake and an increased lactate production even in the presence of oxygen (Warburg, 1925). During decades, the loss of coupling between glycolysis and OXPHOS in tumor cells has been assigned to major mitochondrial dysfunctions. However, new evidence of oxidative activities in tumor cells has challenged this paradigm. Indeed, some tumor cells mainly rely on OXPHOS for energy production and besides the Warburg and oxidative phenotypes whereas, for many tumors, hybrid phenotypes with a large metabolic flexibility is the rule.

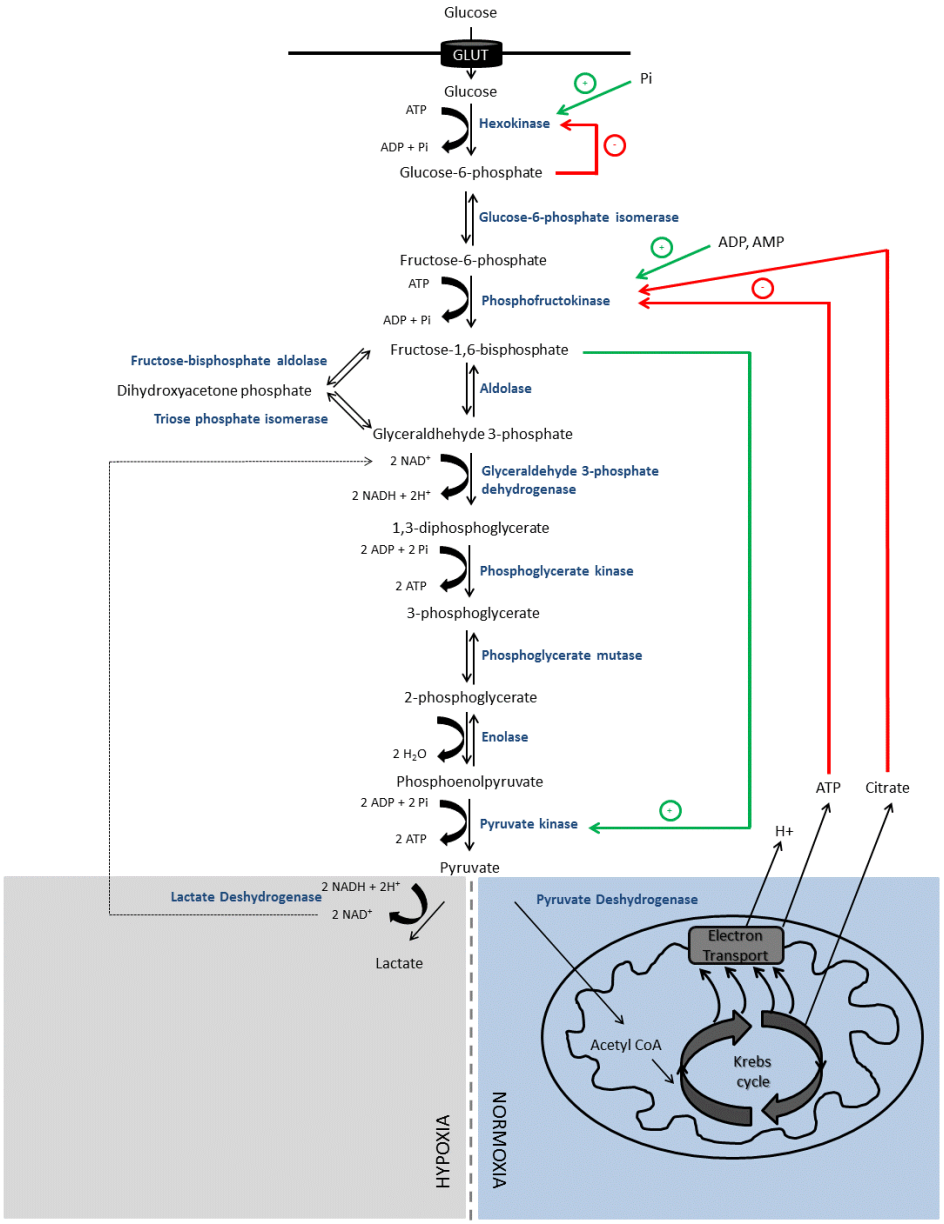

Figure 1: Glucose metabolism in mammalian cells. Adapted from (Porporato, 2011) (Payen, 2014) (Ngo, 2015)

1.1. Glycolytic metabolism and Warburg phenotype

The most common metabolic phenotype of cancer is known as the Warburg effect. The observations of Otto Warburg highlighted that cancer cells exhibit high rates of glucose consumption and lactate production under normoxic conditions, phenomenon called aerobic glycolysis (Warburg, 1925). Despite a limited capacity of ATP production, many cancer cells reprogram the glucose metabolism to produce ATP via the glycolytic process and avoid glucose oxidation through mitochondrial pathways and OXPHOS. Even if the functions and the benefits of the Warburg effect remains controversial, clues emerged to explain this metabolic strategy. Cancer cells seem to maintain a high glycolytic flux in order to support cell growth and proliferation (Lunt, 2011). Controlled by intrinsic genetic mutations and external responses to the tumor microenvironment, a metabolic shift to glycolysis occurs in tumor cells to support 1) a rapid ATP generation to maintain energy status; 2) an increased biosynthesis of macromolecules; and 3) a tightened maintenance of appropriate cellular redox status (**Figure 2**) (Cairns, 2011). Aerobic glycolysis is also associated with aggressiveness and invasiveness.

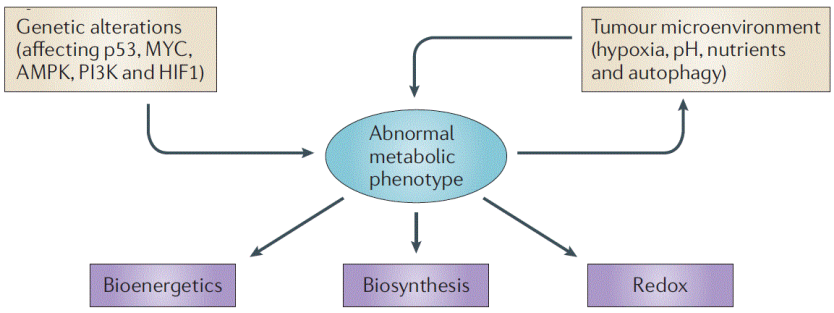

Figure 2: Determinants of the tumor metabolic phenotype (Cairns, 2011)

The Warburg phenotype can also be observed in non-transformed cells (López-Lázaro, 2008). We can cite several normal tissues like the retina, the kidney, the medulla, the cartilage, the bone marrow, the skin, the intestinal mucosa, the placenta but also the fibroblasts and some proliferating thymocytes (Hockenbery, 2013). Nevertheless, normal cells shift their metabolism back to OXPHOS when they return to a resting state, while cancer cells keep this advantage.

1.1.1. Metabolic reprogramming to support proliferation

Cells generally regulate their biochemical pathways in order to support energy needs and fuel the anabolic process to grow and produce new cells. Phenotype adaptations are thus required during the early stages of the carcinogenesis to support rapid cell division and the expansion of the tumor mass. Glycolysis has been selected by the majority of invasive cancer cells as the preferred pathway to generate biomass as well as to produce ATP and to maintain redox balance for the support of uncontrolled cell division.

Glycolysis only provides 2 molecules of ATP per glucose and represents an inefficient way for ATP synthesis compared to a complete glucose oxidation that can provide up to 36 molecules of ATP. However, as long as glucose is available, glycolysis represents a faster pathway for ATP production (Pfeiffer, 2001): lactate production from glucose is 10-100 faster than complete glucose oxidation (Liberti, 2016). This process seems to fulfill the cancer cell needs in ATP, which is mainly required for biosynthetic precursors and macromolecular synthesis. For example, nucleotide and lipid biosynthesis rely on unfavorable biosynthetic reactions that consume significant amounts of ATP. Also, ATP is necessary to maintain

homeostasis and ensure cell survival, as ATP depletion is leading to cell death. Nevertheless, ATP/AMP ratio needs be tightly regulated to keep a high glycolytic rate. As previously mentioned, the activities of PFK and PK, two key enzymes of the glycolysis, are sensitive to ATP levels. By selecting a weak ATP synthetic pathway (López-Lázaro, 2008) and by increasing the ATP consumption (Fang, 2010), cancer cells can escape a slow-down of the glucose metabolism generally induced by high ATP levels. Therefore, cancer cells select glycolysis, a pathway capable of a quick adjustment for ATP production.

Beyond a rapid way to generate ATP, glycolysis represents an advantageous tool for biomass synthesis. Glucose is an abundant source of carbon. To support proliferation, glucose is deviated from carbon catabolism (for ATP production) and redirected for anabolic reactions. Glycolysis can generate numerous building blocks and intermediates involved in nucleotide, lipid synthesis or amino acid and can provide crucial cofactors for macromolecular biosynthesis (**Figure 3**). The synthesis of nucleotides for nucleic acids formation is essential for cell replication. G6P, the product of the glycolytic enzyme hexokinase, can be redirected through the pentose phosphate pathway (PPP) to generate ribose-5-phosphate, the starting point for the purine and pyrimidine nucleotide synthesis (Dang, 2012) (López-Lázaro, 2008). Glycolysis is also a source of carbon for lipid precursors, lipids representing an important component of cell membranes. The glycolytic intermediate dihydroxyacetone phosphate is the precursor to glycerol-3-phosphate, which is crucial for the biosynthesis of the phospholipids and triacylglycerols that serve as major structural lipids in cell membranes (Lunt, 2011). As proteins represent a high proportion of cell

mass, an efficient production of amino acids is required during proliferation. G6P, through the PPP, can generate histidine. 3-phosphoglycerate provides the carbons for cysteine, glycine and serine, and pyruvate provides the carbons for alanine, valine and leucine. Together, 3-phosphoglycerate and phosphoenolepyruvate can generate tryptophan, phenylalanine and tyrosine (Lunt, 2011) (López-Lázaro, 2008). Nevertheless, the generation of cofactors is required to drive anabolic biochemical reactions. Nicotinamide adenine dinucleotide (NADH), flavin adenine dinucleotide (FADH2), nicotinamide dinucleotide phosphate (NADPH), and coenzyme A (CoA) are necessary as reducing agents for nucleotide, amino acid and lipid biosynthesis. NAD+, generated during the pyruvate to lactate conversion, is also required to maintain a high glycolytic flux ensuring the conversion of glyceraldehyde-3-phosphate to 3-phoshopglycerate (Feron, 2009). FADH2, NADH, NADPH and CoA are generated via the purines pathway, itself derived from glycolysis. (Lunt, 2011) NADPH can also derive from the PPP.

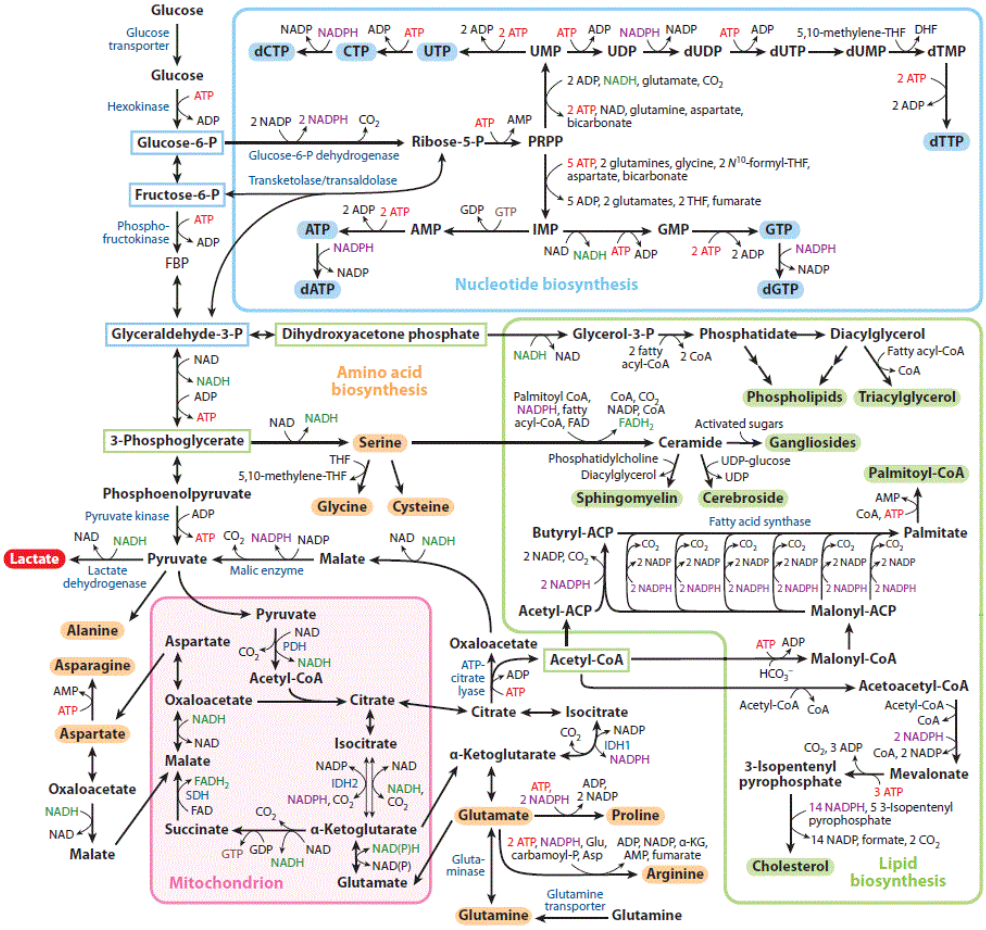

Figure 3: Glucose fueled anabolic pathways (Lunt, 2011)

Proper cell functions and cell survival also rely on the balance between generation and elimination of reactive oxygen species (ROS). In cancer cells, ROS are required to promote carcinogenesis but a ROS excess will conduct to tumor suppression (Gupta, 2012). The high proliferative rate of glycolytic cells contributes to the oxidative stress by different ways. By avoiding glycose oxidation in favor to glycolysis, the electron transport is impaired leading to ROS generation and the production of numerous Krebs

cycle intermediates with antioxidant properties is reduced (Costa, 2014) (El Sayed, 2013). To generate antioxidant systems like the glutathione and the thioredoxin systems, the production of reductive equivalents like NADPH is essential. Fueled by the G6P, the oxidative reactions of the PPP generate this key molecule providing the reducing power required in tumor cells. Also the regeneration of NAD^+ during lactate production, controlled by the LDH, represents an alternative way to maintain a favorable NAD^+/NADH redox balance (Lunt, 2011). Thus, cancer cells rely on glycolysis to counteract the deleterious effects of ROS by producing high levels of antioxidants (Cairns, 2011).

1.1.2. Metabolic reprogramming to promote invasion

Glycolysis turning at full speed in highly proliferating cancer cells, waste products are profusely generated and need to be evacuated from the cells. Beside lactate, protons (H^+) are another end product of the glycolysis, generated during the hydrolysis of ATP mediated by HK and PFK. Given the toxicity of intracellular acidification, tumor cells increase their H^+ export leading to the acidification of their microenvironment. Non-invasive measurements have shown that extracellular pH (pHe) ranges from 6.5 to 6.9, values which are typically not observed in normal tissue, while intracellular pH (pHi) remains neutral to alkaline (Wojtkowiak, 2011). Lactate production and extracellular acidosis favor uncontrolled proliferation such as evasion of the immune system and induction of angiogenesis and metastasis (Warmoes, 2014). Although the molecular mechanisms are poorly understood, exogenous lactate can increase tumor cell motility. Moreover, exogenous lactate can enter endothelial cells through MCT1 (Vegran, 2011) to initiate pro-angiogenic pathways and can

also play an immunosuppressive role (Icard, 2012). Extracellular acidosis can induce death of normal cells, improve tumor cell migration by promoting the degradation of the extracellular matrix, can inhibit immune response and induce resistance to treatment (Fais, 2014). Glycolytic phenotype creates optimal microenvironmental conditions to promote tumor progression that correlates with poorer clinical outcomes (Gatenby, 2004).

1.1.3. Regulations and molecular adaptations

Decades of research has fostered the debate around the driving forces of glycolytic phenotype. Warburg observed high rates of lactate generation in cancer cells under normoxic condition. While the Pasteur effect should cause the inhibition of glycolytic process under well oxygenated conditions and thus reduce lactate production, Warburg's observation led him to the conclusion of a mitochondrial impairment, making glycolysis the only way for cancer cells to produce ATP (Warburg, 1956). For a long time, mitochondrial impairment was presented as the driver of Warburg phenotype. It is only recently that researchers were able to identify that mitochondrial defects are occasional in cancer cells and that most of the cancer cells keep their oxidation capacities, even if a diminished oxidative metabolism is observed. More interestingly, some cancers seem to rely exclusively on OXPHOS to support the carcinogenesis (this phenomenon will be presented in Introduction section 1.2.). Another hypothesis has emerged presenting glycolysis as a phenotypic adaptation to hypoxia during the early stages of carcinogenesis that allows ATP production in absence of oxygen (Vaupel, 2012) (Gatenby, 2004). Beside the interaction of cancer cells with their environment, multitude of genetic changes occurring during

the carcinogenesis can lead to the selection of a particular phenotype in cancer (Jose, 2011).

Multiple cellular pathways support the glycolytic phenotype in cancer cells (Gillies, 2008). Indeed, major adaptations are required to accelerate the glycolytic flux, maintain a high glycolytic rate, support an increase in glucose uptake, lactate export, glycolytic enzyme activity and a decrease in pyruvate use by the mitochondria. The implication of key proto-oncogenes and tumor suppressors such as HIF-1, MYC, PI3K, AMPK, RAS and p53 has been reported in the literature (**Figure 4**) (Cairns, 2011) (Dang, 2012) (Lunt, 2011). Hypoxia inducible factor 1 (HIF-1) is the major force driving the upregulation of glycolysis that activates the transcription and translation of glycolytic genes in tumor cells. GLUT1 and GLUT3, numerous glycolytic enzymes like HK1 and HK2, PFK2, PK2, LDHs (Porporato, 2011) and the mitochondrial activity (Pyruvate dehydrogenase kinase 1 (PDK1) and the electron transport complex) were reported as regulated by HIF-1. The oncogene c-MYC activates glycolytic genes, such as those for GLUT1, glucose-6-phosphate isomerase, PFK1, and LDH. Another major regulator of glucose metabolism is the PI3K/Akt signaling pathway. This pathway stimulates glycolysis by impacting HK and PFK2 enzymes but also activates mTOR that in turn alters metabolism in various ways and enhances HIF-1 activity (Dang, 2012) (Cairns, 2011). AMPK stimulates energy production in proliferating cells and inhibits mTOR. Mutated RAS also enhances glycolysis, partly through increasing the activity of MYC and HIF-1 and by enhancing glucose uptake. Finally, glycolysis can be promoted by the loss of p53 function in cancer (Lunt, 2011). All those pathways act as a coordinated system to regulate tumor metabolism and

favor the expression of specific isoforms of metabolic enzymes (Ward, 2012) (Yeung, 2008). Epigenetic modifications represent another mechanism involved in the deregulation of enzymatic activities during glycolysis (Ward, 2012). Epigenetic regulations are reported for GLUT, HK, PK and Fructose-1,6-bis phosphatase (Upadhyay, 2013). Alternative splicing, increased copy number of genes in cancer cells, gene regulation by microRNAs and post-translational modifications of proteins are other mechanisms involved in metabolic reprogramming and enhanced glycolysis in cancer cells (Ward, 2012) (Upadhyay, 2013).

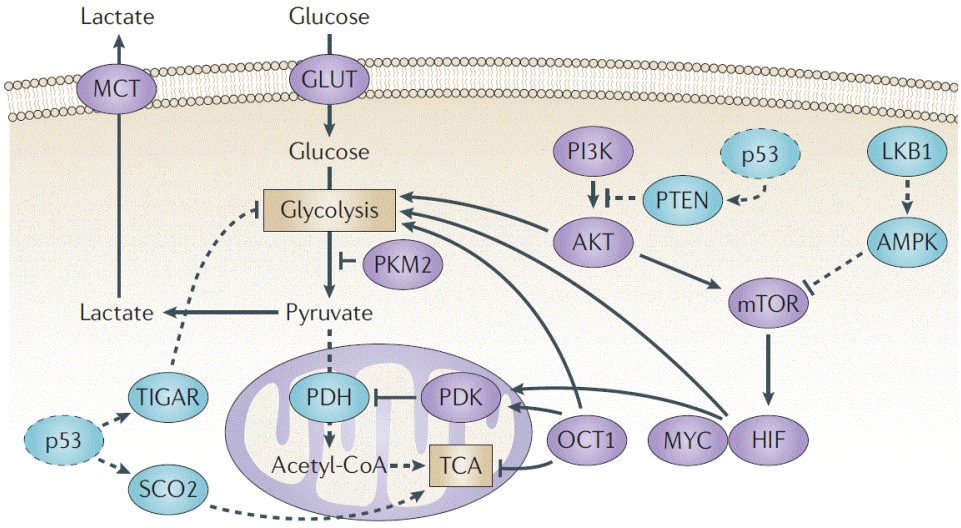

Figure 4: Molecular mechanisms driving the Warburg effect (Cairns, 2011)

1.2. True evidence of oxidation activities in cancer

In 1956, Otto Warburg proposed that enhanced glycolysis in cancer cells was driven by irreversible mitochondrial damages (Warburg, 1956). Indeed, glycolysis must be enhanced to maintain ATP level constant if OXPHOS function is weakened. Since then, the Warburg effect reinforced by this hypothesis represents a universal dogma in oncology barely contested during decades. While numerous studies emerged to support Warburg's hypothesis, only a few studies on cancer mitochondrial metabolism appeared to discredit this categorical view. Various mechanisms were reported in favor of the mitochondrial disorder hypothesis such as: an altered mitochondrial function, mutations in mitochondrial DNA (mtDNA), a lower mitochondrial content, the Crabtree effect (inhibition of OXPHOS by glycolysis), a truncated Krebs cycle and an altered ATP synthase (reviewed by Moreno Sanchez, 2007). These data also presented glycolysis as a universal mechanism to produce energy in cancer cells. Even if studies highlighted mitochondrial dysfunctions in a few cell lines, these explanations were unfortunately assumed to be applicable to all tumor cell types. During decades, an increased gene transcription or protein content of glycolytic enzymes or transporters has generally been over-interpreted. Indeed, a diminution/alteration of one enzyme or transporter does not automatically lead to a diminution in the pathway flux or metabolite concentration. Also, the quantitative contribution of each pathway to ATP supply has rarely been determined. Further, the assessment of protein activity associated with pathway flux studies were generally missing. Recently, the mitochondrial function in tumor cells has become a hot research topic. By exposing human cancer cells to low concentrations of

ethidium bromide to deplete mitochondrial deoxyribonucleic acid (DNA) and consequently reduce OXPHOS activity, a state known as ρ0 (rho-0), researchers found that cancer cells showed an impaired ability to grow and became sensitive to cytotoxic drugs, highlighting the crutial role of OXPHOS in some cancer cells (as reviewed by Viale, 2015). While OXPHOS activity is generally not suppressed in cancer cells, the OXPHOS function is even higher in some cases than in normal cells (Zheng, 2012). Oxidative phenotype was found in lymphomas, melanomas, glioblastomas, breast cancer, pancreatic cancer and leukemia (Obre, 2015) (Moreno Sanchez, 2007) (Moreno Sanchez, 2014). OXPHOS is also present in circulating tumor cells and promotes metastasis (LeBleu, 2014). Quiescent cells seem also to rely on OXPHOS (Viale, 2014) (Lagadinou, 2013).

A considerable amount of cancers use OXPHOS or a mixture of glycolysis and OXPHOS for ATP production (Moreno Sanchez, 2007) (Moreno Sanchez, 2014). But beyond the ATP production, proliferating cells desperately rely on strong pathways able to generate macromolecules and many TCA cycle intermediate can support macromolecule biosynthesis and thus tumor expansion. Also, other nutrients like amino acids, fatty acids, glutamine and lactate are consumed by cancer cells which require an efficient oxidative function. While hypoxia remains the major factor affecting OXPHOS activity, the activation of MYC oncogene also supports mitochondrial gene expression, mitochondrial biogenesis and promotes glutamine utilization by increasing the expression of glutaminase (Ward, 2012).

1.3. Metabolic heterogeneity in cancer

The cancer cells population in a tumor mass represents a heterogeneous group expressing distinct metabolic patterns. Cancer stem cells (CSC) represent one of the key driver of the metabolic heterogeneity in cancer. Beside their self-renewal capacity, CSC exhibit metabolic flexibility. In response to the microenvironment and (epi)-genetic modulations, cancer stem-like cells can differentiate in non-stem cancer cell with different metabolic profiles contributing to a heterogeneous cellular society (Yoshida, 2015) (Peiris-Pages, 2016). While each individual cell within the tumor mass can express a distinct metabolic profile, a metabolic dialogue can also emerge between different types of cancer cells but also with cells composing the stroma.

Nutrients have to diffuse from the blood vessels through different layers of cells in order to reach the center of the tumor mass. As cancer cells located near the blood vessels intensively extract nutrients to support their proliferation, a gradient of nutrient deprivation is created at increasing distances from the nourishing vessel. While some cancer cells die from this deprivation, other cells struggle to survive and tend to adapt. In 2008 (Sonveaux, 2008), a lactate shuttle was discovered between oxygenated (close to the nourishing vessels) and poorly oxygenated or hypoxic cancer cells (distant from nourishing vessels), mediated by MCT expression heterogeneity. Hypoxic cells, relying only on glucose and glycolysis, produce and export lactate that is taken up by oxygenated cells, which in turn use it as their principal substrate to support OXPHOS. Hypoxic cells providing an alternate nutrient source for oxygenated cells, glucose pool is preserved and can diffuse to feed hypoxic cells. MCT and LDH, under the

control of HIF-1, play an essential role in lactate exchanges between hypoxic and oxygenated cells. While glycolytic cells rely on LDH5 to convert pyruvate into lactate and on MCT4 (low-affinity lactate transporter) to export lactate, oxygenated cells express MCT1 (high-affinity lactate transporter) to take up extracellular lactate and LDH1 to convert lactate into pyruvate. This cell to cell lactate shuttle, that occurs as a physiological process in muscle cells during exercise and also in the brain between astrocytes and neurons (Draoui, 2011), is usurped by cancer cells.

Besides a metabolic symbiosis observed between cancer cells, they also metabolically interact with cells composing the stroma. A new concept of metabolic interplay between cancer associated fibroblast and epithelial cancer cells was introduced in 2009 and called the reverse Warburg effect (Pavlides, 2009). In this concept, cancer associated fibroblasts exhibit the Warburg effect and epithelial cancer cells express an oxidative profile. An oxidative stress induced by cancer cells, in association with loss of Caveolin-1, mitophagy, mitochondrial dysfunction and increased production of NO, forces cancer-associated fibroblasts to shift their metabolism: they become glycolytic and secrete lactate and pyruvate. Epithelial cancer cells can in turn take up these energy-rich metabolites and use them in the mitochondrial TCA cycle (Gonzalez, 2014) (Yoshida, 2015).

While glucose metabolism represents the major pathways studied, cancer cells also exhibit metabolic reprogramming such as increased de novo lipid synthesis, increased citrate oxidation and glutaminolysis where metabolic interplay can also exist. All these adaptative behaviors represent major challenges for therapies. A better understanding of the process associated

with the characterization of metabolic patterns for each tumor patients would lead to the development of more efficient anticancer strategies.

2. Targeting glucose metabolism for cancer therapy

Given the numerous metabolic alterations identified in tumors during the last decades, tumor metabolism has become a new privileged target for the development of anticancer treatment. Tumor metabolism had already been favorably exploited in the past. Indeed, methotrexate therapy is the first successful antimetabolite therapy to treat cancer and is still used in the clinic. Targeting dihydrofolate reductase and thymidylate synthase, metothrexate disrupt nucleotide synthesis. Together with nucleoside analogues, such as 5-fluorouracile and gemcitabine, antimetabolite drugs demonstrate effective antineoplastic activity by targeting specific enzymes involved in nucleotide synthesis.

Treatments targeting glucose metabolism should impact specific metabolic adaptations that support malignant phenotypes (Vander Heiden, 2011) and could present a unique strategy to selectively attack tumor cells. Altered expression of metabolic enzymes or changes in metabolic pathway regulation identified in cancer already permitted to develop promising compounds (**Figure 5**). While some of them presented major side effects and toxicity, others are about to be translated to the clinic or are currently tested in various cancer types. Also antiglycolytic agents have demonstrated promising results in combination with conventional chemotherapy by overcoming drug resistance (Butler, 2013) (Ganapathy-Kanniappan, 2013). In this chapter, direct strategies, targeting specific metabolic enzymes and transporters, and indirect strategies, targeting signaling pathways, will be presented. While glycolysis remains the main target, oxidation and mitochondrial metabolism also represent a major potential strategy that will be discussed.

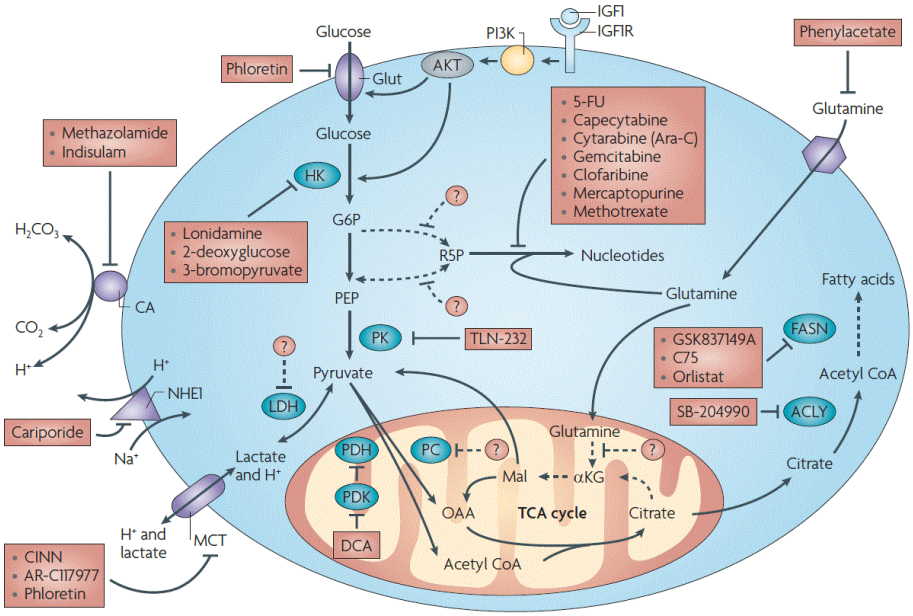

Figure 5: Targeting tumor metabolism (Tennant, 2010)

2.1. Inhibition of glycolysis

Upregulated glycolysis being presented as a hallmark in various cancers, disrupting tumor glycolysis was an evident anticancer strategy. Several molecules deregulating metabolic enzymes and pathways were studied to impact tumor growth by inducing energy depletion and a resensitization to chemotherapy (Ganapathy –Kanniappan, 2013).

2.1.1. Glucose uptake and glycolytic enzymes

Enhanced glycolysis is supported by the enhancement of different transporters and enzymes involved the glycolytic process.

The overexpression of GLUTs, transporters that facilitate glucose uptake in cells, has been found to be associated with tumor progression (Szablewski, 2013). High affinity glucose transporters GLUT1 and GLUT3 are frequently upregulated in cancers but the overexpression of GLUT2, GLUT4 and GLUT5 were also observed in gastric, breast, colon, liver, melanoma and pancreatic tumors. Also the expression of different isoforms can coexist within tumors. Natural and synthetic small organic molecules showing GLUT-inhibitory properties have been discovered (Granchi, 2012). Some molecules presented successful results in vivo and showed potential of GLUT-targeting, leading them to clinical trials, as presented in **Figure 6**. While most of the studies have been completed, 2 flavonoïd compounds are still under investigation in clinical trials. Quercetin, firstly presented as an effective non-competitive GLUT2 inhibitor, is presently tested in clinical Phase I for prostate cancers (NCT01912820). Silibinin (or silybin), presenting inhibitory effects on cancer growth in preclinical models, has been tested in clinical Phase I and Phase II trials (NCT00487721) for prostate cancer and presented a good safety profile. Despite relatively weak GLUT4 inhibitory activity, silibinin's anticancer effects are likely to be elicited from multiple mechanisms (Qian, 2014). This promising molecule will be tested in combination with erlotinib (a tyrosine kinase inhibitor) in lung adenocarcinoma patients (NCT02146118). Although glucose uptake inhibition represents an attractive way to impact cancer cells, lack of specificity has actually limited the potential of this strategy. GLUTs being

ubiquitously expressing in all mammalian cells, the therapeutic window is limited.

Inhibitor	Target GLUT	Status	Ref.
WZB117	GLUT1	Animal study	Liu *et al*[238], 2012
STF-31	GLUT1	Animal study	Chan *et al*[240], 2011
Fasentin	GLUT1	*In vitro*	Wood *et al*[242], 2008
Apigenin	GLUT1	Phase Ⅱ	NCT00609310
Genistein	GLUT1	Phase Ⅱ / Ⅲ	NCT00118040; NCT00584532
Oxime-based GLUT1 inhibitors	GLUT1	Animal study	Tuccinardi *et al*[255], 2013
Pyrrolidinone derived GLUT1 inhibitors	GLUT1	*In vitro*	Ulanovskaya *et al*[257], 2011
Phloretin	GLUT2	Animal study	Wu *et al*[258], 2009
Quercetin	GLUT2	Phase Ⅰ	NCT01912820
DNA-damaging anticancer agents	GLUT3	*In vitro*	Watanabe *et al*[269], 2010
GSK-3 inhibitors	GLUT3	*In vitro*	Watanabe *et al*[270], 2012
Ritonavir	GLUT4	Phase Ⅰ / Ⅱ	NCT01009437; NCT01095094
Silibinin	GLUT4	Phase Ⅰ / Ⅱ	Flaig *et al*[260], 2007; NCT00487721

Figure 6: Glucose transporter inhibitors (Qian, 2014)

Hexokinase, phosphofructokinase and pyruvate kinase are irreversible and rate limiting steps of the glycolysic process, making them also attractive targets to disrupt tumor glycolysis.

Hexokinase, the first enzyme in the glycolytic cascade, presents an increased activity in tumor, HK2 (and to a lesser extend HK1) being preferentially expressed. 2-deoxyglucose (2-DG), lonidamine and 3-bromopyruvate (3-BP) are currently known to target HK2. 2-DG, a glucose analogue, competes with glucose for uptake and is phosphorylated by HK2. In its phosphorylated form, 2-DG cannot be further metabolized (due to a lack of the hydroxyl group in position 2) and is metabolically trapped in cells. 2-DG accumulation leads to growth arrest and cell death. Efficient but toxic in patients as a monotherapy (due to high concentrations required), 2-DG seems efficient at lower doses in combination with doxorubicine, paclitaxel, trastuzumab and Bcl-2 antagonists (Butler, 2013). Lonidamine specifically inhibits mitochondria-bound HK2. Bound enzyme is less

sensitive to feedback inhibition and presents an increased affinity for ATP (Pauwels, 2000) and this form is mainly expressed in cancer cells, not in normal cells (Qian, 2014). Efficient in preclinic, lonidamine went to Phase II clinical trials for glioblastoma patients, where it failed to show therapeutic benefit (Porporato, 2011). Other clinical trials Phase II/III for the treatment of prostate cancer were suspended due to severe pancreatic and hepatic toxicities (Ganapathy-Kanniappan, 2013). 3-BP, an alkylating agent, exhibits significant anticancer effects by inhibiting HK2 mitochondrial bounding but present a lack of specificity and strong alkylation potential (Dang, 2011). The development of more specific inhibitors of HK2 is required to assess the potential of HK as a relevant target.

PFK is allosterically regulated by ATP but also by fructose-2,6-bisphosphate levels (F2,6-BP). F2,6-BP levels are affected by enzymes of the phosphofructo-2-kinase/fructose-2,6-bisphosphatases (PFKFB), bifunctional enzymes that catalyze either the ATP-dependent phosphorylation of fructose-6-phosphate to fructose-2,6-bisphosphate or the dephosphorylation of fructose-2,6-bisphosphate to fructose-6-phosphate (Porporato, 2011) (Ros, 2013). 3-(3-pyridinyl)-1-(4-pyridinyl)-2-propen-1-one (3PO) is the only specific inhibitor of PFKBP3 (an enzyme isoform that exerts an important contribution to the glycolytic switch) and is reported to inhibit in vitro and xenograft tumor growth in vivo (Dang, 2011).

PKM2 is the preferred isoenzyme in tumor cells. Controlling the conversion of phosphoenolpyruvate to pyruvate, the inhibition of PKM2 should limit the generation of ATP in cancer cells. The TLN-232 inhibitor exhibited high selectivity even at low doses for cancer cells in vitro and in animal models and is well tolerated even at high doses (Butler, 2013). A phase II clinical trial to assess the efficacy and safety of TLN-232 in patients with renal

carcinoma has been successfully completed (NCT00422786) but another phase II clinical trial in patients with metastatic melanoma (NCT00735332) has been terminated for legal reasons.

Various small molecules that are inhibitors of the other steps of the glycolytic pathway (glucose-6-phosphate isomerase, aldolase, glyceraldehyde-3-phosphate dehydrogenase, enolase, phosphoglycerate mutase and phoshoglycerate kinase) have been identified (Granchi, 2012-2014) but further characterization is required to define the efficacy and to identify possible toxicity.

Targeting tumor glycolysis has emerged as a logical strategy. Numerous compounds have been tested with mixed success, but some drugs are currently tested in clinical trials. Beyond deregulating cancer cell metabolism, antiglycolytic agents can also overcome drug resistance in cancer. Glycolysis provides high ATP and NADH levels that can overcome oxidative stress induced by chemotherapies and can also support common mechanisms of drug resistance like enhanced DNA repair, misregulation of growth factor signaling, increased drug efflux, higher expression of antiapoptotic genes, or survival signaling pathways (Butler, 2013). Glycolytic inhibitors have already demonstrated promising results in combination with conventional chemotherapeutic drugs. Thus antiglycolytic agents may provide additional gain when used in combination therapy for treating resistant tumors (Ganapathy-Kanniappan, 2013).

2.1.2. Lactate production and transport

Pyruvate reduction into lactate, mediated by LDH, is essential in cancer cells to restore NAD+ pool and to regulate biomass production but also confer invasive advantage to tumor cells. LDH5 isoform, that preferentially catalyzes the reduction of pyruvate into lactate (Porporato, 2011), is mainly expressed in tumor cells. Oxamate, a structural analogue of pyruvate, presented an efficient antiglycolytic activity by competing with pyruvate for enzyme binding. Unfortunately, this small molecule was found to be non selective to LDH5, also inhibiting aspartate aminotransferase (a mitochondrial enzyme). Furthermore, due to poor cell penetration, high drug concentrations required to reach enough efficacy stopped further investigation with this drug (Granchi, 2012). The natural compound gossypol, or AT-101, firstly developed as an antimalaric agent showed a non selective inhibitory effect on LDH by blocking NADH binding leading this compound to Phase I and Phase II clinical trials (Doherty, 2013). AT-101 is currently tested as a monotherapy in non small cell lung cancer (Phase III, NCT01977209), in association with lenolidomide in chronic lymphocytic leukemia (Phase I/II, NCT01003769) and in association with docetaxel, cisplatin and carboplatin in laryngeal cancer (Phase II, NCT01633541). However, this compound showed also an inhibitory effect on glyceraldehyde-3-phosphate dehydrogenase. Derived from this compound, FX11 was reported to exert an efficient and selective inhibition of LDH5 (Granchi, 2012). Galloflavin and N-hydroxyindole–based compounds were also developed to inhibit LDH5 (Doherty, 2013). Even if these agents represent promising anticancer drugs, the development of more selective and potent compounds is needed.

Another strategy to tackle tumor cells is to block lactate transport, mediated by MCTs. While MCT4 inhibition still lacks characterization, MCT-1 inhibition is an intense field of research. The lactate shuttle between oxygenated/oxidative cancer cells and hypoxic/glycolytic cancer cells is targeted. The strategy is to force oxidative cell to rely on glucose instead of lactate, leading to glucose starvation in glycolytic cells. During decades, the only major MCT inhibitor described was α-cyano-4-hydroxycinnamate (CHC) but suffered from a lack of selectivity (Granchi, 2012). AR-C155858 and AZD3965 are more recent examples of drugs that interfere with lactate transport through blockade of MCT1 (van der Mijn, 2016). AZD3965 is currently in Phase I clinical trial for advanced solid tumors, such as prostate cancer, gastric cancer and lymphoma (NCT01791595). However, those molecules cannot block lactate influx mediated by MCT4. Novel strategies have been presented recently to block both MCT1 and MCT4 lactate mediated influx in some cancer cells (Draoui, 2014). The identification of potent and selective MCT4 inhibitors should also lead to interesting anticancer treatment, by targeting mainly lactate efflux in glycolytic cells.

2.1.3. Signaling pathways involved in glycolysis

Beside direct targeting of metabolic enzymes, indirect targeting represents another strategy explored to disrupt glycolysis. Signaling pathways involved in glycolytic process, like HIF-1, PI3K, AKT, mTOR, AMPK, MYC and insulin-like growth factor receptor (IGFR), have been explored as potent therapeutic targets (as reviewed in **Table 1**). Even though these molecules are mainly in clinical trials, it is important to mention that the inhibition of signaling cascades can also contribute to tumor regression in a metabolism-

independent manner as these pathways are tumorigenic in several different ways, contributing to cell proliferation and survival (Tennant, 2010).

Compounds	Target	Effect	Development stage
Torin1 and PP242	mTORC1 mTORC2	Inhibition	Preclinical
AZD8055, OSI-027, INK128, GSK795	mTORC1	Inhibition	Phase I
Ridaforolimus and other rapalogues	mTORC1	Inhibition	Phase I/II
Temsirolimus and everolimus	mTORC1	Inhibition	US FDA approved
Acriflavine	HIF-1α	HIF signalling inhibition	Preclinical
PX-478	HIF-1α	HIF signalling inhibition	Phase I
MK-0646, BIIB022, AVE1642 and others	IGF1R	Blocks IGF signalling	Phase I/II
BEZ235, XL765, SF1126, BGT226, NVP-BEZ235, GDC-0980, PF-04691502, GSK2126458, XL765	PI3K and mTOR	PI3K and mTORC1-mTORC2 signalling inhibition	Phase I/II
LY294002, Wortmannin	PI3K	PI3K signalling inhibition	Preclinical
GDC-0941, PX866, GSK-2636771, XL147, NVP-BYL719	PI3K	PI3K signalling inhibition	Phase I/II
NVP-BKM120, GDC-0032, CAL-101	PI3K	PI3K signalling inhibition	Phase III
Perifosine and GSK690693	AKT	Inhibition	Phase I/II
A-769662	AMPK	Activation	Preclinical
Metformin	AMPK	Activation	Phase I/II

Table 1: Compounds targeting signaling pathways involved in tumor metabolism. Adapted from (Tennant, 2010) (Hardie, 2013) (Guimarães, 2015)

2.2. Reversion of the Warburg effect using Dichloroacetate

Dichloroacetate (DCA) is a small molecule (150 Da) that is able to restore mitochondrial function in cancer cells. As some cancer cells are highly glycolytic and bypass the mitochondria to produce energy, reverting glycolytic metabolism is an attractive strategy for cancer therapy.

2.2.1. Mechanisms of action

DCA is a structural analogue of pyruvate (**Figure 7**). Firstly discovered as an antidiabetic and lipid-lowering drug, DCA has been universally exploited to lower lactate levels in acquired or congenital forms of lactic acidosis (malaria, sepsis, congestive heart failure, burns, cirrhosis, liver transplantation and congenital mitochondrial diseases) (Stacpoole, 2003). Administrated orally as a sodium salt, DCA is rapidly absorbed, presents a bioavailability of 100% and crosses plasma and mitochondrial membranes through monocarboxylate and pyruvate transporters respectively (Stacpoole, 1989). DCA also presents a good tolerability and safety even in young children (Michelakis, 2008). Its principal pharmacological target is the mitochondrial pyruvate dehydrogenase complex (PDC).

Pyruvate ***Dichloroacetate***

Figure 7: Structures of Pyruvate and Dichloroacetate

PDC is located in the mitochondrial matrix and catalyses the oxidative decarboxylation of pyruvate to AcetylCoA, NADH and CO_2. This complex plays a crucial role in metabolism by linking glycolysis, occurring in the cytoplasm, to the TCA cycle and to OXPHOS in the mitochondria and is thus highly regulated. The pyruvate dehydrogenase kinase (PDK) phosphorylates and inactivates the complex while pyruvate dehydrogenase phosphatase (PDP) phosphorylates and restores the catalytic activity of the complex. PDK and PDP are also highly regulated proteins (**Figure 8**) (Kankotia, 2014).

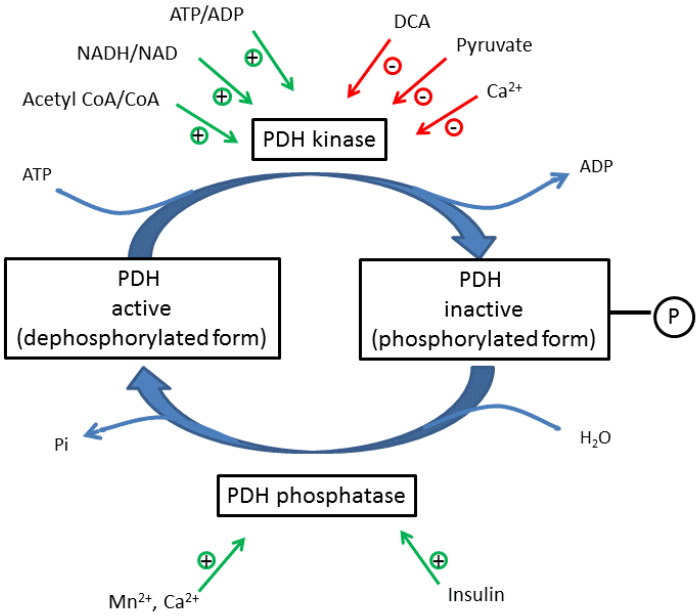

Figure 8: Pyruvate dehydrogenase complex. Adapted from (Kankotia, 2014)

DCA enhances PDC activity by inhibiting PDK that leads to a stabilization of PDC in its unphosphorylated (active) form. DCA occupies the pyruvate-blinding site of PDK. More specifically, DCA binds to the hydrophobic pocket in the N-terminal domain of PDK. DCA is a non selective inhibitor and targets the four PDK isoforms that present different sensitivity to DCA inhibition. PDK2 is the most sensitive, PDK3 the most resistant, while PDK1 and PDK4 are relatively sensitive (Papandreou, 2011). DCA also stimulates PDC activation by inhibiting the complex turnover and increases enzyme stability through unknown mechanisms (Kankotia, 2014).

2.2.2. Dichloroacetate in cancer

In cancer, PDK is generally upregulated to support high rate glycolysis. Favoring the production of building blocks to support proliferation and the production of lactate that promotes invasiveness, suppressed mitochondrial function also promotes mitochondrial hyperpolarization and suppresses apoptosis (Sutendra, 2013). PDK1 and PDK3 represent the 2 isoforms mainly upregulated in cancer, mediated by HIF-1α.

In 2007, Bonnet and colleagues investigated the effects of DCA in cancer and discovered that DCA was promoting apotosis in vitro and decreasing tumor growth in vivo (Bonnet, 2007). Since then, this orally available and cheap molecule, presented as a promising selective anticancer agent, has been further investigated in vitro, in vivo and successfully reached clinical trials (**Table 2**).

Trial status	Cancer Type	Treatment type	References
Phase I Completed (NCT00566410)	Metastatic solid tumors	Monotherapy	Chu, 2015
Phase I Completed (NCT01111097)	Brain tumors	Monotherapy	Dunbar, 2014
Phase I Completed (NCT01163487)	Head and neck cancer	Monotherapy	/
Phase II Completed (NCT00540176)	Gliomas and glioblastomas	Monotherapy	/
Phase II Terminated (NCT01029925)	Metastatic breast cancer and lung cancer	Monotherapy	Garon, 2014
Phase II Active (NCT01386632)	Head and neck cancer	Combination with cisplatin and radiotherapy	/

Table 2: Update of clinical trials involving dichloroacetate in cancer therapy

There are 2 fundamental changes in tumor metabolism elicited by DCA that antagonize tumor growth, metastasis and survival.

① Redirection of glucose metabolism from glycolysis to oxidation leading to inhibition of proliferation and induction of caspase-mediated apoptosis.

DCA reactivates the mitochondrial function, decreases the flux through the pentose phosphate pathway and decreases lactate production. DCA also decreases mitochondrial membrane potential, stimulates the mitochondrial

production of Krebs cycles intermediates (especially α-ketoglutarate), NADH and ROS that activates plasma membrane Kv channels (K+ channels), induces a stabilization of HIF-1 and a reactivation of p53. This mitochondrial remodeling results in a decreased cellular proliferation, cell cycle arrest and increased apoptosis. These effects were not found in non-cancer cells exposed to DCA (Bhat, 2015) (Sutendra, 2013) (Michelakis, 2008) (Kankotia, 2014).

② Oxidative removal of lactate and buffering effect.

Since lactate production is reduced by DCA and consequently lactate/H+ export, remaining lactate in the microenvironment will feed oxidative cancer cells, inducing a progressive lactate removal. Also via the reactivation of the TCA cycle and decarboxylases activities, CO_2 production is increased and can be converted to bicarbonate, increasing the buffering capacities. Its ability to reduce lactate and H+ within the tumor microenvironment can explain action of DCA on tumor size (Kankotia, 2014).

However, anticancer effects of DCA may involve other mechanisms. DCA may also target fatty acid β-oxidation. The underlying mechanism is still unknown but disruption of the balance between fatty acid β-oxidation and glucose oxidation may play a role in the overall effects of DCA in vivo (Sutendra, 2013). Also some groups reported that DCA impacted cell growth without apoptosis induction (Stockwin, 2010) (De Preter, 2016) or showed apoptotic response at concentrations that were too high to be clinically relevant (Papandreou, 2011) (Abildgaard, 2014) (Delaney, 2015). The anticancer effects of DCA appear to rely on multiple mechanisms depending on the drug concentration and cell type.

The first data available from the clinical trials indicate that DCA appears to be safe, tolerable, feasible and efficient for chronic administration in adults with brain tumor (Dunbar, 2014) and advanced solid tumors (Chu, 2015) but no firm conclusions stand out in advanced non-small cell lung cancer (Garon, 2014). Sensory and motor peripheral neuropathies are potential side effects of DCA that appear to be largely reversible. The risk may depend on whether cancer patients have prior or concurrent neurotoxic therapy (taxane, platinum, vinca-alkaloide chemotherapies) (Michelakis, 2008). Fatigue and nausea were also reported. To potentiate therapeutic effect (Garon, 2014) and limit toxicity (Dunbar, 2014), GSTZ1/MAAI (enzyme that metabolizes DCA) genotyping has been suggested to reach adequate systemic drug levels (van der Mijn, 2016). Known for decades as an efficient drug to reduce lactate levels, further investigations will elucidate if DCA could represent a novel anticancer strategy, especially in association with conventional therapy.

2.3. Disruption of mitochondrial metabolism

As previously described (see Introduction section 1.2.), enhanced glycolysis is not a common feature of all cancer cells. While some tumors strongly rely on OXPHOS, some glycolytic tumors still retain mitochondrial functions, including respiration (Zong, 2016). Given the key role of mitochondria in many cellular processes like metabolism, redox balance and cell cycle and apoptosis regulation (**Figure 9**), various mitochondria-targeted approaches have emerged as potential cancer therapies. Some compounds that preferentially target mitochondria in cancer cells directly or preferentially interfere with cancer metabolism have been investigated and may have potential utility in cancer treatment. Still, targeting mitochondria remains a

challenge. Indeed, enzymes of the TCA cycle reside in the mitochondrial matrix and the electron transfer chain and ATP-synthase/-ase are located on the inner mitochondrial membrane. Whereas drug accumulation in the tumor mass is already a limiting factor in cancer therapy, mitochondria-specific accumulation requires specific physicochemical properties. Therefore drug discovery studies must include strategies aimed at conferring selective accumulation of molecules with promising selective action (D'Souza, 2011).

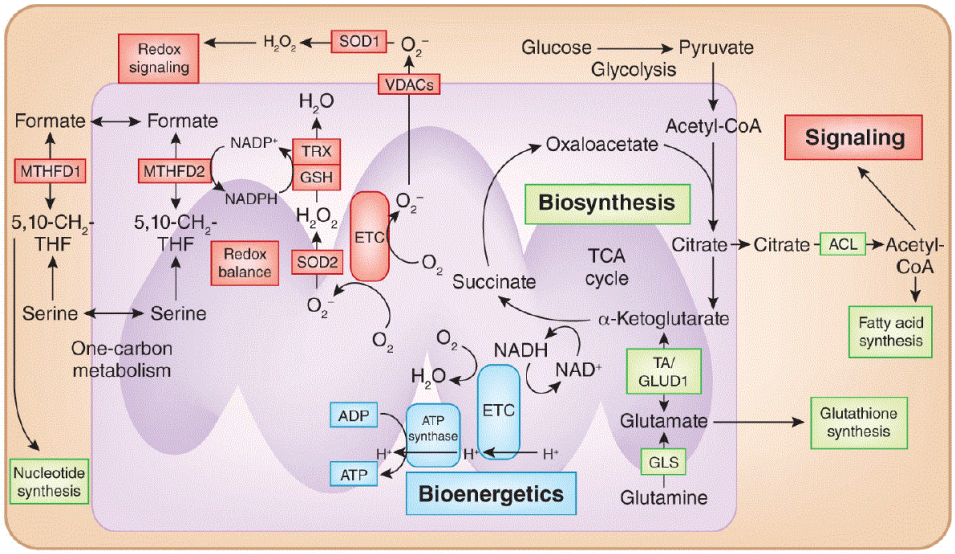

Figure 9: Mitochondrial functions as potential targets for cancer therapy (Weinberg, 2015)

One strategy is to target mitochondrial respiration. Through the inhibition of mitochondrial electron transfer chain (ETC) complex, mitochondrial ATP production is limited, inducing a bioenergetic stress in oxidative cancer cells. The first drug that was described to inhibit oxygen consumption in tumors was metaiodobenzylguanidine (MIBG), which causes an inhibition of the complex I (Biaglow, 1998). Numerous treatments have already been presented as potent treatments altering ETC and oxygen consumption in tumor cells. Glucocorticoids, insulin, non-steroidal and anti-inflammatory drugs have been described to improve tumor oxygenation leading to the enhancement of radiotherapy efficacy (Jordan, 2012) Arsenic trioxide, vitamin E and resveratrol are in clinical use for various cancer types (Wang, 2010). Also, metformin has become the focus of intense research as a potential anticancer agent (Leone, 2014). Prescribed as first line of treatment for patients with type II diabetes, several retrospective epidemiological reports have highlighted that the use of metformin in diabetic patients correlated with a reduced cancer risk, leading to further investigations about the mechanisms involved. Metformin exerts its antitumor effects by insulin-dependent and insulin-independent mechanisms. Metformin can suppress cell growth by inactivation of AKT–mTOR pathway and by the inhibition of the complex I of the mitochondrial ETC, resulting in activation of AMPK (Leone, 2014) (Choi, 2013). As metformin showed encouraging results in combination with radiotherapy in preclinical studies (Zannella, 2013) (Koritzinsky, 2015), numerous clinical trial studies were initiated to test this well-known molecule in association with various treatments.

Another strategy would be to target biosynthetic pathways occurring in the mitochondria. TCA cycle enzymes like isocitrate dehydrogenase (IDH), fumarase, pyruvate carboxylate and succinate dehydrogenase were reported as mutated in various cancers making them novel interesting therapeutic modalities (Weinberg, 2015) (Zong, 2016).

Compounds that target mitochondrial DNA (mtDNA) have also demonstrated significant impact on cellular energy metabolism and cell viability (Wang, 2010). In this category, we can mention the following drugs:

- cisplatin, that preferentially bind to mtDNA (~50 times more than to nuclear DNA);
- topoisomerase inhibitors (mechanism affecting mtDNA unclear):
- ditercalinium, an intercaling agent which accumulates in the mitochondria;
- vitamin K3 (menadione), a specific inhibitor of DNA polymerase γ (the mitochondrial enzyme responsible for mtDNA replication).

Other therapeutic strategies targeting the mitochondrial membrane potential and membrane permeability or redox status and mitochondrial OXPHOS uncouplers can indirectly affect mitochondrial function. In this category, drugs, such as rhodamine-123, MKT-077 and Bcl-2 inhibitors, have entered clinical trials (Pathania, 2009) (Weinberg, 2015) (Wang, 2010).

Nevertheless, a combination of mitochondria-targeted agents with glycolytic inhibitors should be preferred to avoid a metabolic shift in favor of glycolysis and combination with other chemotherapeutic drugs may be required to achieve maximum efficacy.

3. Cancer phenotyping in vivo and molecular imaging biomarkers

A specific description of biochemical pathways and metabolic alterations is crucial to understand the metabolic features of cancer. Also the characterization of malignant tissues should allow the identification of key metabolic activities, making them effective target for the development of anticancer treatment.

Identification of the peculiarities of a given cancer can be derived from in vitro phenotyping. The study of metabolic gene expression, metabolomics and even metabolic fluxes in various cancer cell lines represents an easy and fast approach which can define distinct metabolic profiles. Despite the high specificity and reproducibility of in vitro studies, but also the availability of various models (well-established tumor cell lines, biopsies derived cell lines and modified cell lines), this approach does not recapitulate the complexity of cancer metabolic systems. Indeed, heterogeneity represents a key challenge in tumor characterization and single cell cultures totally avoid this aspect. Also, even if the culture conditions can be easily manipulated, in vitro context does not truly model the impact of the microenvironment or even the entire physiological context. Moreover, the impact of vascularization, cell density, metabolic competition and cooperation with host cells, is missing. Tissue biopsies, also known as the ex-vivo approach that can better represent patient heterogeneity, are readily available and can be rapidly frozen for fixation. In parallel with immunohistochemistry staining, novel techniques allow the generation of maps of metabolites distribution in cryosections and can relate local metabolite concentrations to a specific tissue region. ATP, glucose or lactate can be imaged quantitatively in cryosections using bioluminescence (Walenta, 2002) while

mass spectroscopy imaging was reported to detect more than 30 metabolites which included nucleotides, cofactors, phosphorylated sugars, amino acids, lipids, and carboxylic acids (Lin, 2014). However, a biopsy only represents a snapshot of the tumor at a specific time (Sengupta, 2016) and is unsuitable to study metabolic changes over time. The detection of molecules also relies on the preservation conditions of the samples. Additionally, a biopsy is not a representation of the whole tumor and multiple biopsies is not feasible in routine clinical practice (Lin, 2014). Given these limitations, in vivo cancer models should also be considered in order to study metabolism of cells interacting with their microenvironment and identify relevant metabolic alterations.

The characterization of tumor metabolic profiles should rely on non invasive techniques providing accurate and reproducible biomarkers, feasible over time, able to detect early metabolic changes and spatially map the heterogeneity of metabolism within a tumor (Smith, 2003) (Lin, 2014). Molecular imaging techniques represent relevant tool for tumor phenotyping in vivo. While anatomical imaging plays a crucial role in cancer detection, staging and assessment of treatment response, molecular imaging allows the in vivo characterization and measurement of key biomolecules and molecularly based events involved in the malignant process (Kircher, 2012). Molecular imaging in oncology relies on various technologies currently available in preclinical but also in clinical practice, exploiting endogenous information or exogenous probes. These include positron emission tomography (PET), single photon emission computed tomography (SPECT), computed tomography (CT), magnetic resonance imaging (MRI), magnetic resonance spectroscopy (MRS) and optical imaging. Beyond the phenotypic

characterization, molecular imaging is also a powerful tool in oncology for diagnosis and staging, for treatment guidance, follow-up and restaging. Molecular imaging also provides a strong basis for the development and optimization of new therapies and can document the effectiveness of new class of drugs. Playing an important role for accurate preoperative diagnostics, some molecular imaging techniques are now investigated as powerful intraoperative tools for image guided surgery (Kircher, 2012) (Serkova, 2011) (Figueiras, 2011). In the clinic, the characterization of metabolic features within a tumor is largely based on PET and MRI or MRS presenting respectively a high sensibility and specificity. While numerous imaging techniques are available to directly study metabolic processes in tissues, powerful methods are also currently used to study physiologic conditions such as hypoxia, extracellular pH, interstitial pressure and redox status (Jordan, 2010a). As tumor microenvironment is largely influenced by the tumor cell metabolism, non-invasive imaging of the tumor microenvironment also represents an indirect way to study tumor metabolism. In this chapter, direct in vivo phenotyping techniques of glucose metabolism, currently used in clinical practice will be discussed. Also emerging technologies having potential clinical application will be presented.

3.1. ^{18}F-FDG PET scan

Developed in the seventies, positron emission tomography (PET) is a well established molecular imaging technique for preclinical and clinical researches but is also used in current clinical practice. PET measures and visualizes the distribution of positron-emitting radiotracers in vivo. Depending on the radiolabeled tracer used, PET can measure various

physiological, biochemical and pathological processes in the fields of neurology or cardiology, but the major utilization of PET clinically is in oncology to study glucose metabolism, cell proliferation and hypoxia (Rohren, 2004) (Avril, 2007) (Farwell, 2014).

3.1.1. Principles of PET

Unstable proton-rich radionuclides can return to stability by either electron capture or positron (β^+) emission. PET is based on the detection of two annihilation photons produced when a β^+ is emitted from positron-emitting tracer. Fluorine 18 (^{18}F) is the most widely used radionuclide, with an half-life of 110 min, and is principally used as an hydrogen substitute. Other positron emitters such as Carbon 11, Nitrogen 13, Oxygen 15 or Rubidium 85, Copper 62, Copper 64, Potassium 38, Gallium 68 and Iodine 124, presenting various half-lives, have been used in PET. For some nuclei, short half-lives limit the biochemical and physiological processes that can be imaged (Rhoren, 2004) (Phelps, 2000) (Jadvar, 2005).

During radiotracer decay, β^+ are emitted. Produced β^+ leave the decay site and gradually lose their kinetic energy through ionizations and excitations of nearby atoms. When energy is lost, β^+ annihilate with nearby electrons (e^-). When the annihilation occurs, two photons (γ) are produced with an energy of 511 kev: $\beta^+ + e^- \rightarrow \gamma + \gamma$. The photons leave the annihilation site in opposite direction and hit two detectors surrounding the body. Simultaneous detection of two 511 kev photons in a detector pair, called coincidence, indicates that an annihilation occurred somewhere in the axis connecting those detectors. When a positron-emitting tracer is injected intravenously, PET scan provides measures of tracer concentration in the

tissues over time. By using multiple detector pairs in a complete ring around the patient, each coincidence is recorded and after correction for photon attenuation and tomographic images of the distribution of radiotracer in the body are reconstructed (Rhoren, 2004) (Phelps, 2000). The principle of PET is illustrated in **Figure 10**.

PET is sensitive to detect small concentrations (picomolar) of tracer in the body, but some limitations are technically inherent (Rhoren, 2004) (Phelps, 2000) (Hutchins, 2008):

- Limited spatial resolution linked to the geometry of the individual detector elements;
- Low detection efficiency;
- Partial volume effects with small objects;
- Lack of anatomical reference;
- Motion artifacts;
- On site production required for short half-life positron emitters;
- Radioactive exposure.

However, since the first PET scanners, the technology and instrumentation in PET has considerably progressed. Improvements in detectors, hardware and image processing, or combination of PET with anatomical imaging such as MRI or CT, have majorly enhanced the spatial resolution, sensitivity and image quality. For example, current generation of time-of-flight PET scanners use the relative time difference between the detection of the two annihilation photons to determine the location of the annihilation site and operate in fully-3D mode. These whole-body PET systems present a high sensitivity, high spatial resolution and reduced total imaging, leading to a

combination of improved lesion detectability, reduced scan time or injected dose and precise lesion uptake measurement (Surti, 2015). Also, combined PET/CT devices are increasingly used in the clinic, offering a better attenuation correction, and providing anatomical and molecular information in a shorter imaging time for the patient. Initially developed for preclinical research, hybrid PET/MRI scanners are now available for clinical use and offer interesting opportunities but clinical significance need to be defined.

(A) Annihilation reaction

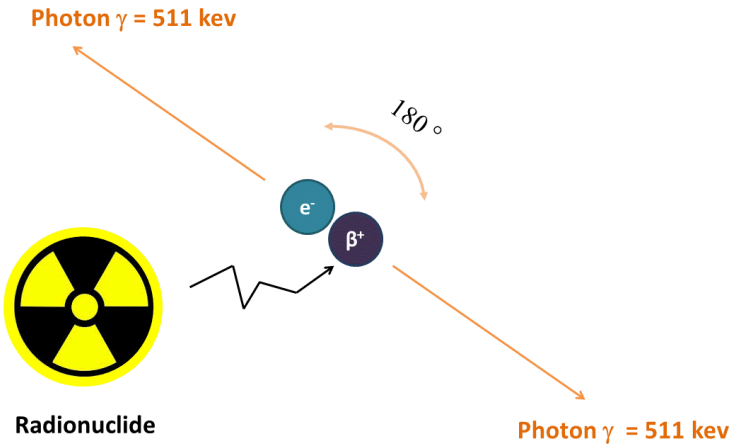

(B) PET detection

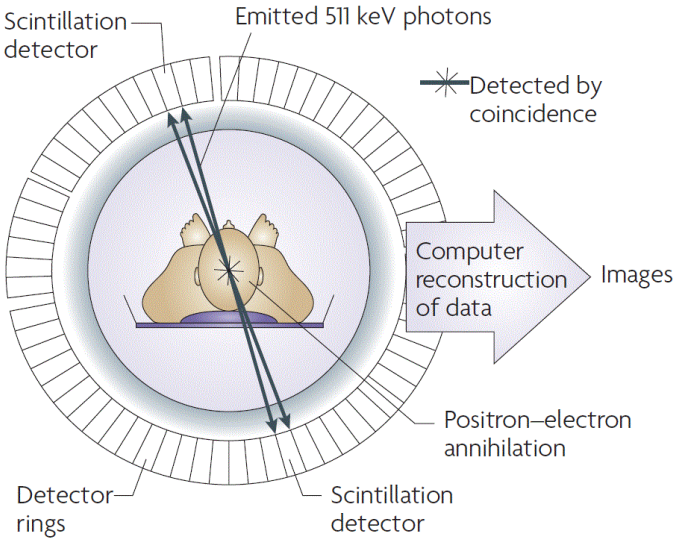

Figure 10: Principle of PET: detection of 2 annihilation photons produced when a positron is emitted from a radionuclide. (A) Adapted from (Phelps, 2000) (Rohren, 2004) (Hutchins, 2008). (B) (Brindle, 2008)

3.1.2. ^{18}F-FDG as metabolic tracer

First described in the late 1970s, 18-Fluorodeoxyglucose (^{18}F-FDG) is the radiotracer that has had the most impact on clinical PET imaging and is a widespread technology to study glucose metabolism, especially in oncology. ^{18}F-FDG is a glucose analogue that is metabolized similarly to glucose (**Figure 11**). ^{18}F-FDG enters in the cell via glucose transporters (GLUT) and is phosphorylated by hexokinase to form ^{18}F-FDG-6-phosphate. Due to the lack of the hydroxyl group in position 2, ^{18}F-FDG-6-phosphate is metabolically trapped and cannot go through glycolysis. ^{18}F-FDG-6-phosphate will accumulate in cells in proportion to the rate of glycolysis (Avril, 2007) (Pauwels, 2000) (Phelps, 2000). The mechanisms of ^{18}F-FDG uptake and accumulation are presented in **Figure 12**.

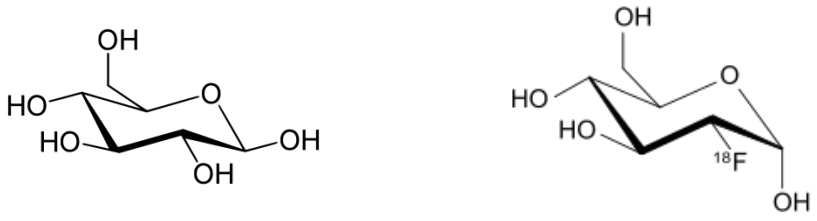

D-Glucose ***18-Fluorodeoxyglucose***

Figure 11: Structures of D-Glucose and 18-Fluorodeoxyglucose

The transport into cells and the intracellular phosphorylation are key steps for the cellular accumulation of ^{18}F-FDG. As cancer cells generally present an increased glycolytic flux compared to normal non proliferating cells, ^{18}F-FDG PET scan became rapidly a standard imaging procedure for the

detection of many types of cancer and is often presented as the gold standard to image tumor metabolism in patients (**Figure 12**). Supported by the overexpression of GLUT and the increased HK activity, ^{18}F-FDG mainly accumulates in cancer cells. Also the dephosphorylation is limited due to the low levels of glucose-6-phosphatase in cancer cells (Avril, 2007) (Pauwels, 2000) (Phelps, 2000) (Rohren, 2004).

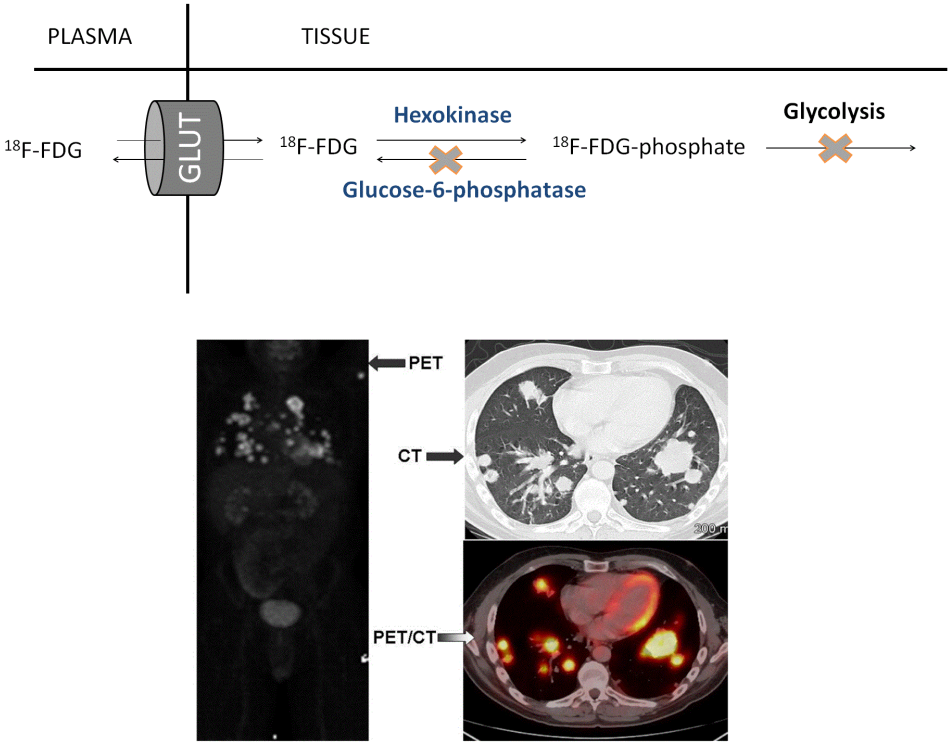

Figure 12: Mechanisms of 18-Fluorodeoxyglucose uptake and PET, CT and fused PET/CT images on a patient with colon cancer and multiple pulmonary metastasis. Adapted from (Phelps, 2000) (Serkova, 2011)

^{18}F-FDG PET scan can thus discriminate tumor lesions from normal tissues based on their altered metabolism. The standardized uptake value (SUV) is the most common parameter to assess ^{18}F-FDG accumulation. The SUV is a semiquantitative parameter measured by normalizing the radioactivity concentration of a region of interest (ROI), measured with PET, to the injected dose and the patient's body weight. SUV is a reliable method to assess tracer accumulation and allows a follow-up of the patients over time when repeated exams are performed. However, strict imaging protocol is required for reliable measurements (Avril, 2007) (Adams, 2010).

^{18}F-FDG PET scan is approved in clinical practice for cancer diagnosis, staging and treatment monitoring in various cancer including breast, esophageal, lung, head and neck and lymphoma. This technique has demonstrated efficacy by distinguishing viable residual tumor tissue and necrotic tissues and by determining tumor response early after the initiation of therapy, compared to conventional anatomical imaging modalities (Avril, 2007). ^{18}F-FDG PET has also been investigated for radiotherapy planning and for the delineation of tumor subvolumes for dose escalation, also called dose painting (Grégoire, 2007).

Beside biological factors such as glucose transporters expression and hexokinase activity, numerous parameters can impact ^{18}F-FDG uptake and could represent major issues in tumor localization or in response assessment with PET scan. Firstly, several normal tissues exhibit a high glucose metabolism. Tissues like brain, heart, muscle, liver, bone marrow, brown fat or the gastro-intestinal tract present a higher physiological tissue accumulation of ^{18}F-FDG that can hamper tumor localization (Pauwels, 2000) (Jadvar, 2005) (Tomasi, 2012). On the contrary, some tumors present

a low FDG uptake due to a slow glucose metabolism, like thyroid and neuroendocrine tumors (Tomasi, 2012), or even due to the expression of high levels of glucose-6-phosphatase, like hepatocellular carcinoma (Rohren, 2004). ^{18}F-FDG PET scan is thus not appropriate in all cancer types. Secondly, inflammation and infection can lead to false-positive diagnoses (Jadvar, 2005). Cellular inflammation and macrophage response elicited by chemotherapy or radiation-induced necrosis is frequently seen on ^{18}F-FDG PET images (Rohren, 2004) (Pauwels, 2000) (Tomasi, 2012). We can note that, as inflammatory cells and more particularly macrophages utilize glucose, ^{18}F-FDG has been explored as a new tracer to image inflammation. Thirdly, vascularization and plasma clearance can mainly impact the uptake. As both can be affected by treatments, changes in the uptake may be due to variations in tracer administration and clearance rather than in tumor uptake. Finally, hyperglycemia can limit ^{18}F-FDG uptake as ^{18}F-FDG competes with glucose for uptake and phosphorylation (Pauwels, 2000) (Jadvar, 2005). In order to limit variations in tracer uptake, fasting and complete rest is generally prescribed to patients.

^{18}F-FDG PET scan is a modality of choice for cancer imaging. The development of combined PET/CT scanner has improved the ability to monitor cancer treatments. Nevertheless, even if ^{18}F-FDG has become increasingly popular in oncology, this tracer may be not suitable for all cancer types and for the monitoring of all treatments.

3.2. Nuclear magnetic resonance spectroscopy

Nuclear magnetic resonance spectroscopy (MRS) is an analytical technique that enables noninvasive exploration of the molecular composition of tissue. MRS is based on nuclei that possess magnetic properties, called nuclear spin, such as ^{1}H, ^{31}P or ^{13}C.

For a defined volume of tissue, the nuclear spins are randomly oriented in all directions leading to no net magnetization in the tissue. If the tissue is placed inside a magnetic field (B_0), the individual spins precess around the magnetic field and will distribute between various possible energy levels: the lowest energy state (parallel to B_0) and the highest energy state (antiparallel to B_0) (**Figure 13.A**). The difference in energy between the two configurations is proportional to the magnetic field and the corresponding precession frequency (ω_0). Since the levels are not equal in energy, the distribution of spin will be unequal between the levels. As described by the Boltzmann equation, a larger number of spins will be in the state of lower energy, leading to a net magnetization M_0 in the tissue parallel to B_0 (**Figure 13.B**). When energy is applied to the sample at the precession frequency (rf pulse), this energy is absorbed and will cause the spin to go from one energy level to another one through a process called resonance absorption, affecting the net magnetization M_0. When the system returns to equilibrium, energy emission occurs in the form of a radio wave. The response of the net magnetization M_0 to an rf pulse constitutes the magnetic resonance signal (Salibi, 1998).

(A) Precession of nuclear spin

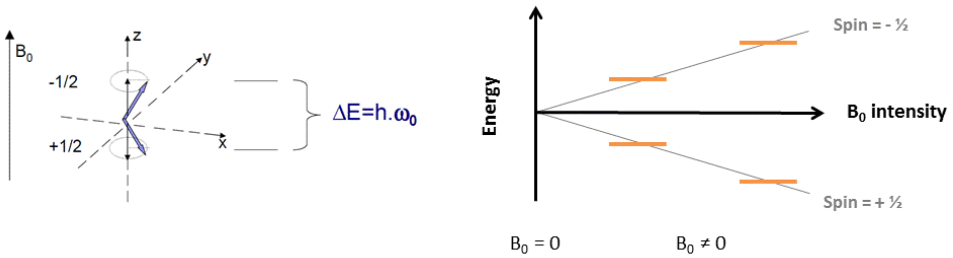

(B) Net magnetization in presence of B0

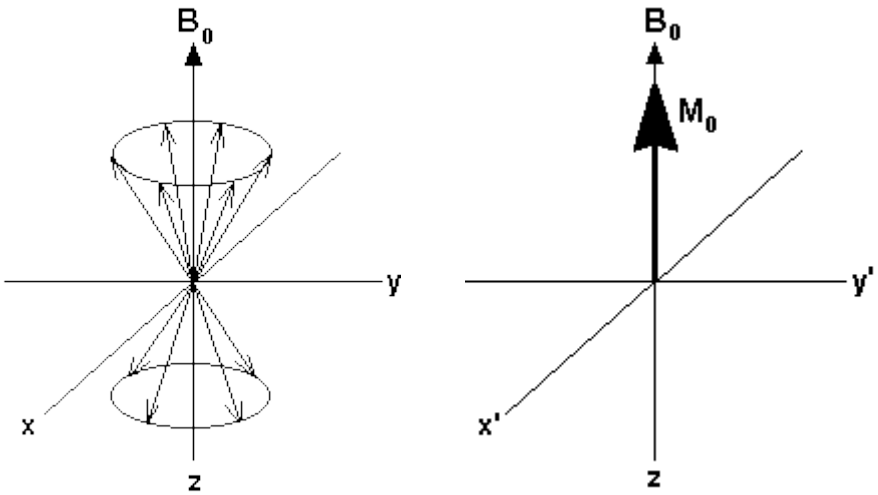

Figure 13: Basic principles of magnetic resonance.

(A) When placed in a strong magnetic field (B_0) nuclear spins precess around B_0. The spins aligned parallel to B_0 (+½) correspond to a lower energy level, while spins aligned antiparallel to B_0 (-½) correspond to a higher energy level. Precession frequency, also called Larmor frequency, is proportional to the field strength and gyromagnetic constant: $\omega_0 = \gamma B_0$. Adapted from (Hashemi, 2004) (Reiser, 2008).

(B) In a sample, there will be a small excess of spins in the lower energy state (parallel to B_0) compared to the higher energy state (antiparallel to B_0). This unequal number of spins in each energy level will lead to a net magnetization in the sample parallel to the magnetic field. Adapted from (Salibi, 1998).

NMR active nuclei resonate at different frequencies which depend on the nucleus type and on the chemical and electronic environment of that nucleus. The presence of an electron around a nucleus constitutes an electronic shield and modifies the effective field to which the nucleus would normally be subjected. As the electron density around each nucleus in a molecule varies according to the types of nuclei and bonds in the molecule, individual nuclei will resonate at slightly different frequencies. This difference in frequency is known as the chemical shift (**Figure 14**) and enables identification of nuclei or functional groups within molecules (Hashemi, 2004) (de Graaf, 2007).

Nuclear magnetic resonance spectra can be obtained from different nuclei but ^{1}H MRS is the most used for clinical application due to the higher sensitivity and abundance of protons (Castillo, 1996). In oncology, MRS is a non invasive and powerful tool to reveal tumor metabolites in vivo. ^{1}H MRS, ^{31}P MRS or ^{13}C MRS measurements can identify a wide range of metabolic and functional tumor information and also detect changes after treatment (Brindle, 2008). Nevertheless, MRS is a rather insensitive technique (de Graaf, 2007), especially for nuclei with lower concentrations such as ^{13}C and ^{31}P and thus requires much longer acquisition times. Also, complex data processing and the absence of standardized procedure for

analysis are factors limiting the actual impact of MRS in the clinical setting (Lin, 2014).

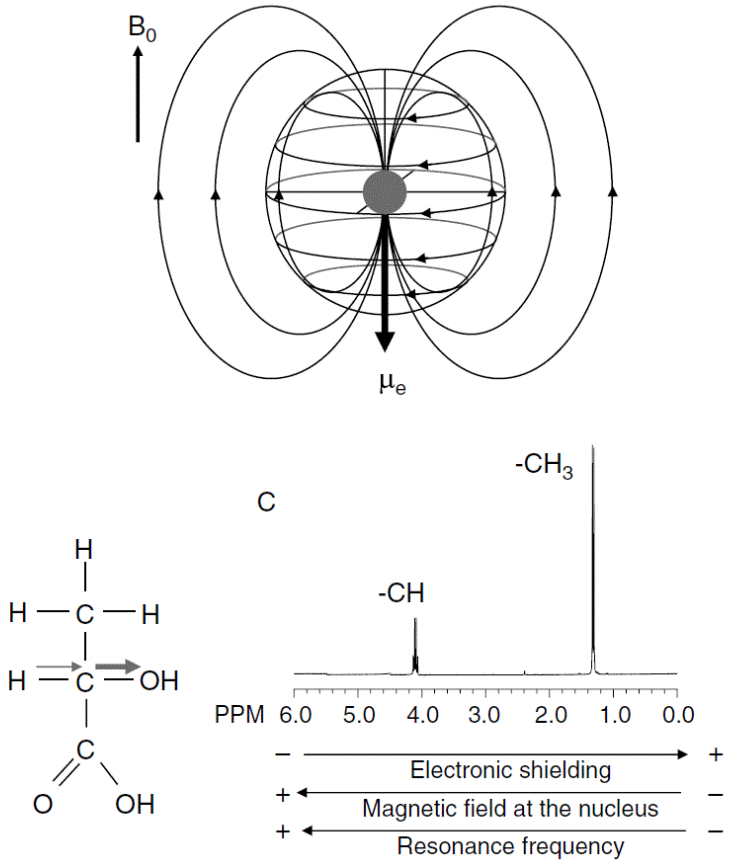

Figure 14: Chemical shift.

The electrons surrounding a nucleus can produce a shield opposing the external magnetic field. The effective magnetic field at the nucleus is modified, thereby leading to a different precession frequency and hence a different chemical shift. As the electron density and electron shielding depends on the atoms and bounds in a molecule, different functional groups within a molecule will present different chemical shifts such as in lactate molecule (de Graaf, 2007).

3.2.1. ^{1}H MRS

Due to the natural abundance of protons in the body, ^{1}H MRS can detect a large number of endogenous metabolites. This technique is highly used to detect changes in concentrations of metabolites characterized to be biomarkers of disease. In cancer, detection of high levels of choline and choline-containing compounds is actually used as the main diagnostic value in brain, breast, prostate, liver and other cancer types. Low choline levels are generally seen in normal tissues and high levels are shown in tumors and are associated with high rate of proliferation (García-Figueiras, 2016) (Lynch, 2014). Lactate, the final product of aerobic and anaerobic glycolysis, is the metabolite of interest to study high glycolytic rate in tumors. Beside a characteristic doublet located at 1.31 ppm, lactate is generally difficult to observe due to contaminations and an overlap with the resonance from lipids and macromolecules (García-Figueiras, 2016). Other metabolites related to glucose metabolism have also demonstrated their usefulness in the MRS evaluation of tumors in vivo, including:

- High levels of 2-hydroxyglutarate, associated with the presence of isocitrate dehydrogenase mutations (Li, 2015) (Andronesi, 2013);
- Elevated creatine levels, related to an increased metabolic rate of the tumor (Li, 2015) (García-Figueiras, 2016);
- Decreased citrate levels, especially in prostate cancers (Lin, 2014);
- Increased levels of alanine (García-Figueiras, 2016).

The variations in concentrations of these metabolites have been used for localizing the tumor, determining tumor grades, planning treatment, and evaluating response to therapy (Li, 2015).

3.2.2. ^{31}P MRS

^{31}P MRS has been used since the 1970s to study energy metabolism in various tissues. Due to the high natural abundance of the phosphorus 31 isotope (^{31}P), key endogenous markers can be monitored to assess bioenergetic as well as metabolic changes associated with aging, diet or diseases such as myopathy, mitochondrial dysfunction, diabetes and also cancer (Li, 2015) (Hwang, 2015). Phosphocreatine, ATP and Pi are the main metabolite markers but NAD+ and G6P can also be detected in vivo. pHi, pHe and pHe gradient can also be monitored non invasively by this technique using endogenous peak such as Pi or using pH reporters such as 3-aminopropyl phosphonate (Lin, 2014) (Gillies, 1994). Using magnetization transfer ^{31}P MRS experiments, the activity of ATP synthase and phosphocreatine kinase can be studied to assess mitochondrial function of tissues (Hwang, 2015). However, ^{31}P MRS generally suffers from low signal-to-noise ratio (SNR), low spatial and temporal resolution and limited spectral dispersion. Detection sensibility and quantification precision can be improved by using high field scanners (Li, 2015).

3.2.3. ^{13}C MRS

^{13}C MRS relies on the only stable carbon isotope that is NMR detectible, carbon 13 (^{13}C), and is used to study organic molecules (Hwang, 2015). Due to the low natural abundance of ^{13}C (1%) and a low gyromagnetic ratio, only a few endogenous molecules are easily detectable in vivo. Carbons from fatty acids chains and triglycerides are observed in most tissues and glycogen carbons are detectable in the liver or muscles in vivo (Rodrigues, 2005). While the detection of endogenous compounds presents a low

sensitivity, the signal coming from exogenous labeled ^{13}C substrates can be easily detected, without background signal interference (by replacing a ^{12}C atom by a ^{13}C atom at a specific position in a molecule of interest) (Kurhanewicz, 2008). After the administration of ^{13}C-labelled tracers, ^{13}C MRS can detect the tracer biotransformation and can follow metabolic pathways in real-time. Exogenous labeled substrates such as [1-^{13}C]glucose, [2-^{13}C]glucose, [1-^{13}C]acetate or [2-^{13}C]acetate were administered to study TCA cycle intermediates or glutamate/glutamine metabolism, especially in the brain (de Graaf, 2003). In 2001, the effects of oxygen supply on tumor glycolytic rate were assessed in a murine mammary carcinoma model by monitoring the rate of conversion of [1-^{13}C]glucose into [3-^{13}C]lactate (Nielsen, 2001). Unfortunately, the low sensitivity of ^{13}C MRS has limited the applications of this technique in the clinic. Indirect detection of ^{13}C signals by ^{1}H-[^{13}C]-NMR spectroscopy has been proposed to provide a higher sensitivity (de Graaf, 2011) but the recent development of dynamic nuclear polarization (DNP) has revolutionized the field of metabolic imaging and provides signal enhancements of over 10,000-folds of magnitude for ^{13}C enriched compounds. DNP technology and hyperpolarized ^{13}C MRS is described hereafter (see Introduction section 3.3.1.).

3.3. Emerging technologies

3.3.1. Hyperpolarized ^{13}C magnetic resonance using dynamic nuclear polarization

The use of ^{13}C MRI or ^{13}C MRS has been limited in vivo due to the lack of sensitivity. Given the low natural abundance and low gyromagnetic ratio of ^{13}C compared to ^{1}H, low SNR induces long measurements time and poor image resolution. In order to increase the SNR, enhancement of nuclear spin polarization has been investigated to increase the sensitivity of MRI and MRS, especially for nuclei with low gyromagnetic ratio. The polarization is the difference in populations of spins that occupies the parallel and antiparallel orientations when ½ spins are placed in an external magnetic field (**Figure 13.A**). The conventional approach could be to increase the magnetic field and lowering temperature but presents limited effects in conventional NMR and MRI (Ardenkjaer-Larsen, 2016). In the 1950's (Overhauser, 1953), solid state experiments performed at low temperature showed that the high polarization of electrons could be transferred to nuclear spins by microwave irradiation, at frequencies close to the resonance frequency of the electron spins (**Figure 15.A**) (Keshari, 2014). It's only in 2003 that this principle was successfully applied for in vivo studies, using a process called dissolution-DNP, allowing the production of labeled-tracer solutions suitable for in vivo magnetic resonance studies (Ardenkjaer-Larsen, 2003). DNP can increase the detection sensitivity by more than 10.000-fold, increase the SNR and reduce the acquisition time (**Figure 15.B**). The technique has been used to hyperpolarize different nuclei such as ^{1}H, ^{6}Li, ^{15}N, and ^{89}Y in a large variety of molecules or nanoparticles but ^{13}C MRI studies remain the main field of application.

DNP, associated with proper MRI detection, allows to image the location of a molecule of interest but also allows to follow in real time its metabolic conversion into other metabolites (Golman, 2006a).

Dissolution-DNP is a multistep process (Keshari, 2014) (Brindle, 2012) (Ardenkjaer-Larsen, 2016):

- First, hyperpolarization of the ^{13}C-tracer at solid state occurs in a dedicated polarizer. The tracer is mixed with a free radical (containing unpaired electron) and is rapidly frozen to form a glass and is then placed in a magnetic field (up to 5T). The DNP sample, containing the ^{13}C-tracer and the radical, needs to form an amorphous solid when frozen to ensure homogeneous distribution of the radical. At low temperature (~1K), the electron spins become practically completely polarized. The electron spin polarization can then be transferred to the nuclear spins by irradiating the sample with a microwave at the electron resonance frequency. Nuclear spin populations start to slowly redistribute and the solid-state polarization reaches a plateau at 1–2 hours depending on the tracer.
- Secondly, polarized material need to be dissolved and warmed rapidly to room temperature with minimal loss of polarization, in a process called dissolution. This is achieved by rapidly dissolving the frozen sample in pressurised superheated buffer solution at 180 C°.
- Finally, the polarized tracer can be injected and imaged. Due to rapid signal loss, typically 10-30s for hyperpolarized ^{13}C-labeled tracers, fast injection is required and imaging must be accomplished within a few minutes using specific sequences.

The principle of hyperpolarization is summarized in **Figure 15**.

(A)

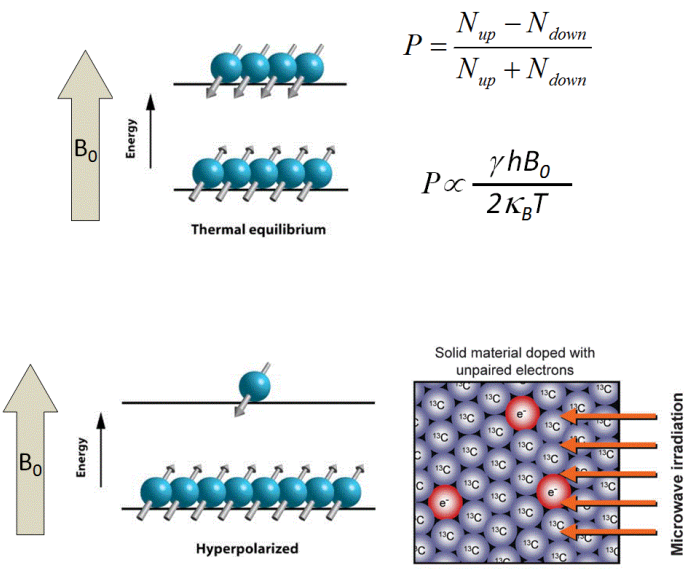

(B)

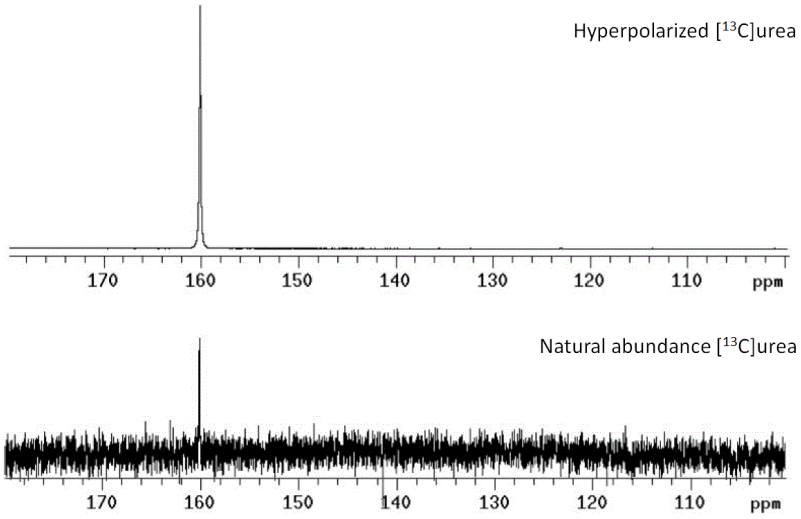

Figure 15: Principle of DNP.

(A) Nuclear spin polarization and description of the orientation of the nuclear spins when placed in an external magnetic field. At thermal equilibrium, nuclear spins exhibit a small population difference between the two states (low degree of polarization). During the dynamic nuclear polarization process, polarization is transferred from the electrons of the doping material to the ^{13}C nuclei by means of microwave irradiation, increasing the polarization. Adapted from (Golman, 2003)
(B) ^{13}C spectrum of urea (natural abundance ^{13}C) hyperpolarized by the DNP method. The concentration of urea was 59.6mM, and the polarization was 20%. This spectrum is acquired in 1 sec. Thermal equilibrium spectrum of the same sample at 9.4 T and room temperature. The signal is averaged during 65 hours. Adapted from (Ardenkjaer-Larsen, 2003)

Hyperpolarized ^{13}C-labeled tracers have revolutionized the field of molecular imaging and more specifically metabolic imaging. As the polarization lifetime is critical in DNP experiments, numerous criteria are required for successful detection in vivo such as (Brindle, 2011) (Dutta, 2013):

- High aqueous solubility required for the dissolution;
- Low toxicity regarding the high doses required;
- Ability to form a glass in the solid state;
- Long T_1 relaxation time in the liquid state as the rapid decay of polarization is caused by T_1 processes;
- Rapid plasma membrane transport;
- Rapid metabolism such as catabolic reactions;
- Sufficient chemical shift difference between the resonance of the substrate and its metabolites;

- Fast imaging approaches are required.

Nevertheless, despite these limitations, there are now numerous examples of hyperpolarised ^{13}C-labelled tracers whose metabolism has been detected in vivo using MRI or MRS.

[1-^{13}C]pyruvate has been the most widely studied substrate to date and has been the first to be translated to the clinic (Nelson, 2013). Pyruvate is a tracer of choice regarding its key role in several major metabolic pathways. After the injection hyperpolarized [1-^{13}C]pyruvate to animals, the appearance of signals from pyruvate, lactate, alanine and bicarbonate revealed the pyruvate metabolism in various tissues (**Figure 16.A**) (Golman, 2006b). The first in vivo study that examined the metabolism of tumor-bearing rats after i.v. injection of hyperpolarized ^{13}C-pyruvate revealed an increased lactate production in the tumors (Golman, 2006c), highlighting the characteristic glycolytic rate of tumors. Since then hyperpolarized [1-^{13}C]pyruvate has been used in various cancer models for detection of tumor response to treatments, including chemotherapies and radiation therapy (as reviewed by Tee, 2015). The first Phase I clinical trial has been successfully completed in patients with prostate cancer demonstrating no dose-limiting toxicities or adverse effects, and high [1-^{13}C]lactate signal in tumor regions (**Figure 16.B**) (Nelson, 2013). At present, 5 clinical trials are ongoing to judge the safety and reproducibility of the technique (Phase I, malignant solid tumors and prostate cancer) but also to evaluate the ability of the imaging to reflect a metabolic response to treatment (Phase I, androgen deprivation therapy in prostate cancer, NCT02450201).

(A)

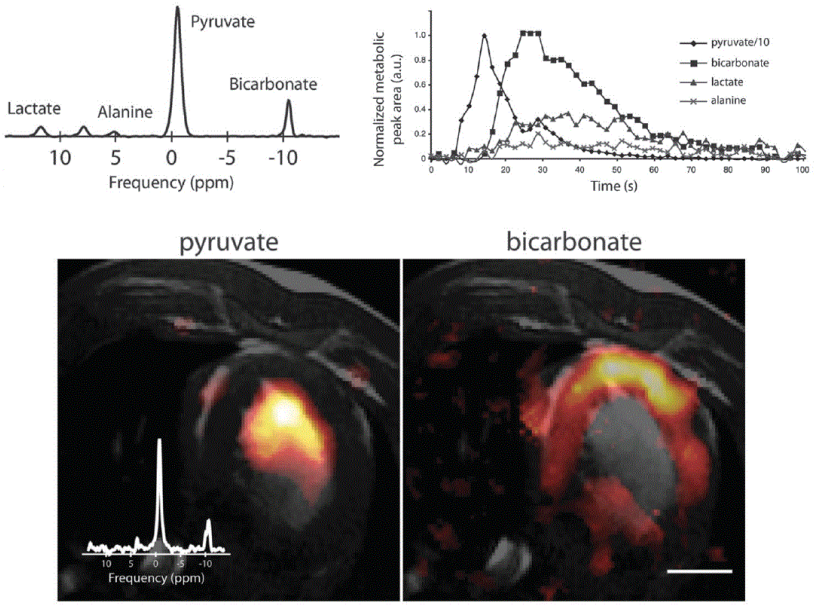

(B)

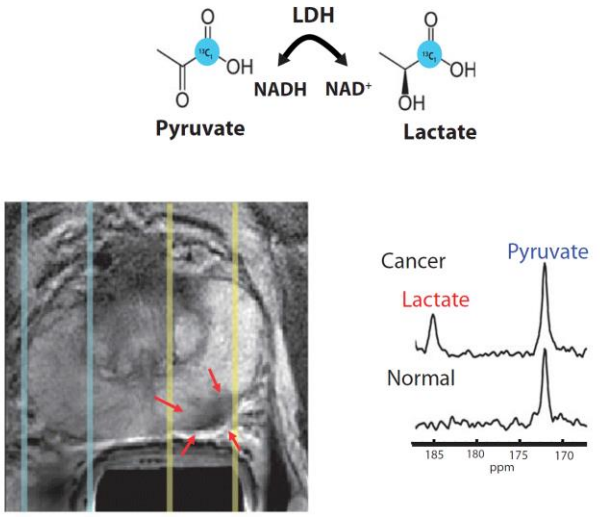

Figure 16: Hyperpolarized [1-^{13}C]pyruvate and its metabolic products such as [1-^{13}C]lactate, [1-^{13}C] alanine and [1-^{13}C]bicarbonate.

(A) Single ^{13}C spectrum acquired following injection of hyperpolarized [1-^{13}C]pyruvate in a porcine heart. The peak height plot demonstrates the time course of pyruvate delivery and lactate, alanine and bicarbonate labeling. Corresponding ^{13}C images demonstrate the spatial distribution of pyruvate and bicarbonate. (Keshari, 2014).
(B) Dynamic ^{13}C spectra obtained from a prostate cancer patient after injection of hyperpolarized [1-^{13}C]pyruvate. The cancer spectrum demonstrated a high flux of hyperpolarized [1-^{13}C]pyruvate to [1-^{13}C]lactate. Spectra from the contralateral side of the prostate demonstrated only [1-^{13}C]pyruvate (Nelson, 2013).

Hyperpolarized [1-^{13}C]pyruvate has become a key tracer to study lactate production in tumors. However, many parameters can affect the rate of hyperpolarized ^{13}C label exchange such as the rate of pyruvate delivery, the rate of pyruvate and lactate transport across the cell plasma membrane (mediated by the MCTs), the LDH activity, the NAD^+ and NADH coenzyme pool or cell loss. Lactate labeling could also result both from exchange of the hyperpolarized ^{13}C label between the injected hyperpolarized [1-^{13}C]pyruvate and the endogenous lactate pool and from net conversion of pyruvate into lactate. Any drug that affects one of these aspects will have an effect on the kinetics of lactate labeling by hyperpolarized [1-^{13}C]pyruvate (Brindle, 2015). As an example, the effects of dichloroacetate, known as a lactate lowering drug, have been investigated in cancer using this tracer. Seth and coworkers monitored metabolic changes induced by DCA in A549 xenograft tumors (Seth, 2011). They identified a reduction in lactate signal in tumors treated during 24 hours with DCA compared to untreated tumors. In another study, Park and colleagues

followed the metabolic response of glioma to DCA in tumor-bearing rats using hyperpolarized ^{13}C-pyruvate magnetic resonance spectroscopic imaging (Park, 2013a). In C6 glioma model, DCA induced after 45 min a drop in lactate production, an increase in bicarbonate production and a reduced lactate to bicarbonate ratio. Also, a stronger response to dichloroacetate was observed in glioma compared to normal brain. Both these studies present hyperpolarized [1-^{13}C]pyruvate MRS as an attractive tool to monitor treatment affecting tumor metabolism.

Another pyruvate tracer has been recently investigated in cancer. Labeled at the ketone position, hyperpolarized [2-^{13}C] pyruvate can detect both lactate production and downstream metabolites in the mitochondria (**Figure 17**). High rate of oxidative phosphorylation and the conversion of hyperpolarized [2-^{13}C]pyruvate to [1-^{13}C]citrate and [5-^{13}C]glutamate were observed in isolated perfused heart (Schroeder, 2009). This tracer has also been successfully validated in glioma-bearing rat brains tumor imaging hyperpolarized [2-^{13}C]pyruvate and the downstream products [2-^{13}C]lactate, [5-^{13}C]glutamate but also demonstrating changes in mitochondrial metabolism with dichloroacetate (Park, 2016). This tracer may be particularly useful for cancer studies through the simultaneous assessments of glycolytic and TCA cycle activity.

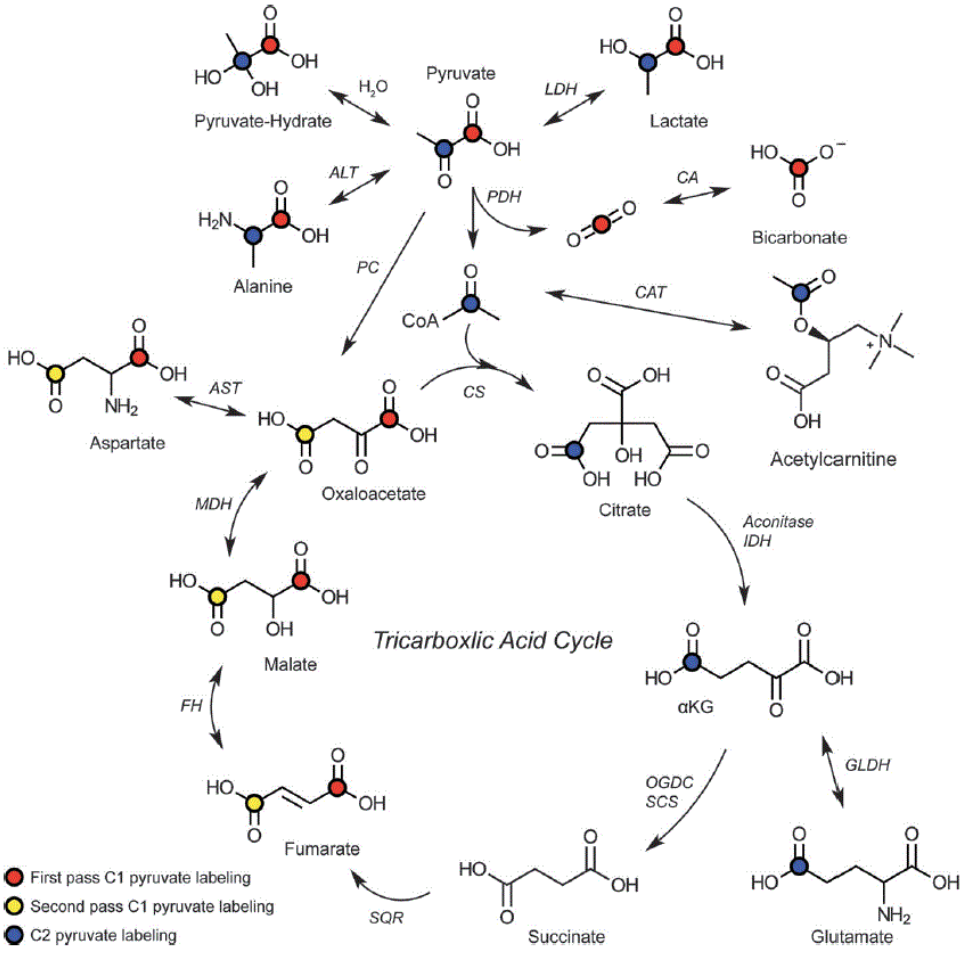

Figure 17: Biochemical scheme of labeling resulting from the injection of hyperpolarized [1-^{13}C]pyruvate and [2-^{13}C]pyruvate. (Keshari, 2014)

Other interesting tracers were developed and investigated to study glucose metabolism in vivo:

- Hyperpolarized [1-^{13}C]lactate can reflect pyruvate, alanine or bicarbonate pool when injected at physiological doses, while [1-^{13}C]pyruvate is injected at subphysiological concentrations (Chen, 2008);
- Conversion of hyperpolarized [U-^{2}H,U-^{13}C]glucose, a glucose tracer, to lactate and to 6-phosphogluconate (generated by PPP activity) was observed in a preclinical lymphoma model (Rodrigues, 2014);
- Conversion of hyperpolarized [2-^{13}C]-fructose to fructose-6-phosphate was able to reflect hexokinase activity and flux through the pentose phosphate pathway in a preclinical prostate cancer model (Keshari, 2009);
- Hyperpolarized [1-^{13}C]bicarbonate has been used to probe the extracellular pH in tumors (Gallagher, 2008);
- Hyperpolarized [1-^{13}C]α-ketoglutarate can serve as a metabolic imaging agent for non-invasive, real-time, in vivo monitoring of mutant IDH1 activity, and can inform on tumor IDH1 status (Chaumeil, 2013).

Given the preclinical results obtained so far, metabolic imaging with hyperpolarized ^{13}C label has proven its usefulness in oncology, especially for tumor detection and monitoring tumor response. While PET technology only visualizes the distribution of the radioactive nuclei, DNP-MRS is capable of distinguishing signal from the tracer but also tracer-derived metabolites. Also DNP-MRS is a non-ionizing radiation technique, suitable for repeated measurements and treatment follow-up in patients. Also, due to

the absence of background signal, ^{13}C-labeled tracers could be an alternative technique to image tissues with a higher physiological accumulation of ^{18}F-FDG. However, the short lifetime of polarization mainly restricts the field of view during DNP-MRS experiments, making impossible to simultaneously monitor a primary tumor and distant metastases. Also the high doses of ^{13}C-labeled tracer required for DNP-MRS experiments could impact the solubility and create toxicity. To become a routine clinical practice, DNP-MRS, progress has to be made to develop and standardize data analysis methods, design high-resolution fast imaging sequences, develop robust, automated and safe polarizer and to find methods that could extend the relatively short polarization lifetime (Brindle, 2011) (Brindle, 2012) (Ardenkjaer-Larsen, 2016). Current clinical trials involving [1-^{13}C]pyruvate should determine the impact of DNP-MRS in clinical practice.

3.3.2. ^{17}O nuclear magnetic resonance

Even if oxygen consumption is a key factor in cell metabolim, the assessment of O_2 consumption in tumors remains critical as current technologies generally display poor specificity. In the 1990's, the possibility of using oxygen-17 nuclear magnetic resonance (^{17}O NMR) to monitor O_2 consumption in the brain has been introduced. By breathing a ^{17}O-enriched gas ($^{17}O_2$), the oxygen consumption could be monitored by following the transfer of the ^{17}O atom from oxygen gas to the water molecule, the end product of oxidative metabolism. After the administration of $^{17}O_2$ gas, the metabolically produced ^{17}O-labeled water ($H_2{}^{17}O$) was detected using MRI in the brain of small animals (Arai, 1990) (Arai, 1991). Promising preclinical studies and attempts in human have been reported but high cost of ^{17}O isotope and the low sensitivity of the technique have limited the use

of ^{17}O NMR to study cerebral metabolic rate of oxygen ($CMRO_2$) (as reviewed by Zhu, 2011). ^{17}O, the only NMR-active isotope of oxygen, presents a low natural abundance (0.037%) and a low gyromagnetic ratio and thus presents a low inherent NMR sensitivity. In the 2000's, Zhu and co-workers investigated the relaxations properties and the SNR of $H_2{}^{17}O$ at different magnetic fields and showed that the relaxation times of $H_2{}^{17}O$ were field-independent and that the ^{17}O NMR sensitivity was increased by fourfold at 9.4T compared to 4.7T field strength, indicating that ^{17}O NMR approach at high field could offer significant advantages for monitoring oxygen metabolism (Zhu, 2001). This concept was rapidly validated using fast imaging for $CMRO_2$ assessment in rats at high magnetic field (Zhu, 2002). Since then, numerous efforts have been made by the Center for Magnetic Resonance Research group at the University of Minnesota (Minneapolis, USA) to develop the methodology, validate methods for $CMRO_2$ calculation and perform the applicability assessments (as reviewed by Zhu, 2011). Given the encouraging results obtained in preclinical models, a few groups successfully applied ^{17}O NMR for mapping $CMRO_2$ in the human brain (Zhu, 2011) (Atkinson, 2010) (Hoffmann, 2011).

$^{17}O_2$ is used in the same way that $^{16}O_2$ in the body (**Figure 18**). After gas exchange in the lung, the inhaled O_2 molecules quickly bind to hemoglobin (Hb) in the blood, forming O_2–hemoglobin complexes (HbO_2). The HbO_2 complex enters the tissues via feeding vessels, where the O_2 molecules dissociate, cross the membranes in the form of free dissolved gas, diffuse into the tissue, and finally enter mitochondria where they are converted to the metabolic water via oxidative metabolism. As $H_2{}^{17}O$ can be specifically detected using NMR, the amount of ^{17}O-labeled water metabolically

generated from the inhaled $^{17}O_2$ gas will reflect the rate of oxygen consumption in the tissue under study (Zhu, 2005) (Zhu, 2011).

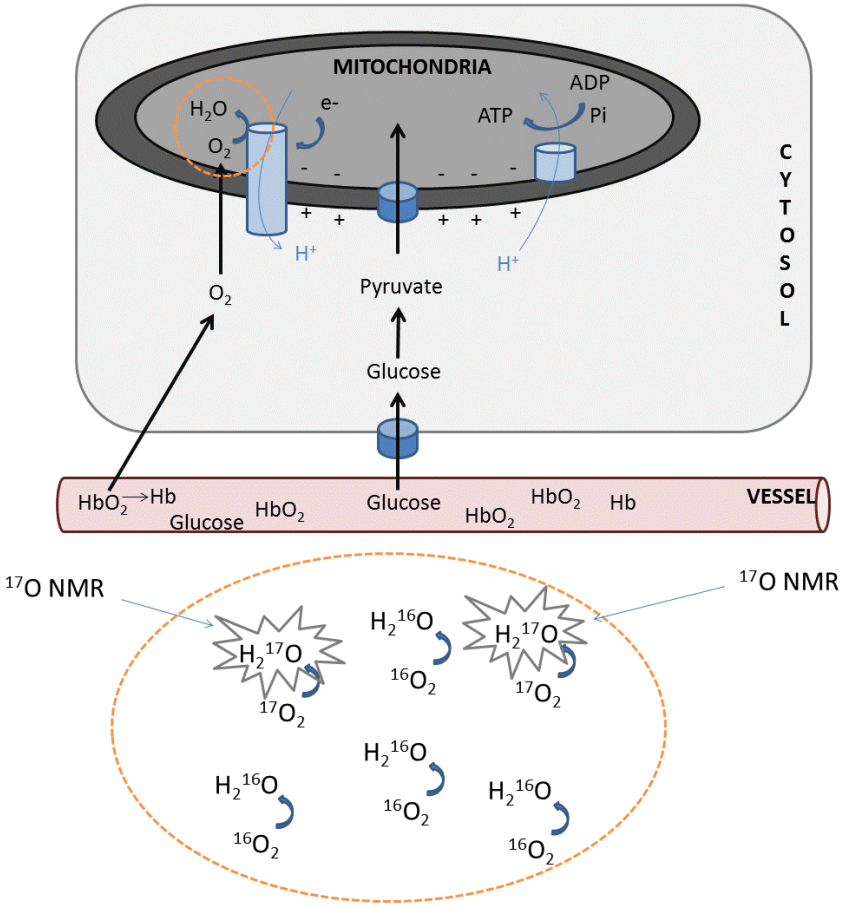

Figure 18: Transportation and metabolic processes of oxygen molecules in tissues. Due to the specific detection by NMR, $H_2{}^{17}O$ signal can be used to monitor oxygen consumption in tissues after $^{17}O_2$ inhalation. Adapted from (Zhu, 2005)

During in vivo ^{17}O NMR experiments, dynamic changes of $H_2{}^{17}O$ signal is monitored before, during and after a brief inhalation of ^{17}O-enriched oxygen gas and is generally characterized by 3 phases (**Figure 19.A**): (i) stability of $H_2{}^{17}O$ signal before $^{17}O_2$ inhalation; (ii) increase in $H_2{}^{17}O$ signal during the $^{17}O_2$ inhalation and (iii) new steady state during the post-inhalation period (Zhu, 2005). The linear increase of $H_2{}^{17}O$ signal during the $^{17}O_2$ inhalation is tightly coupled to the oxygen consumption rate (**Figure 19.B**) (Zhu, 2011).

(A)

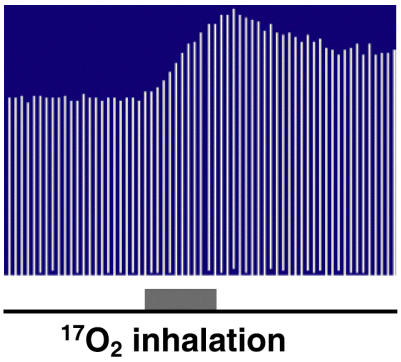

(B)

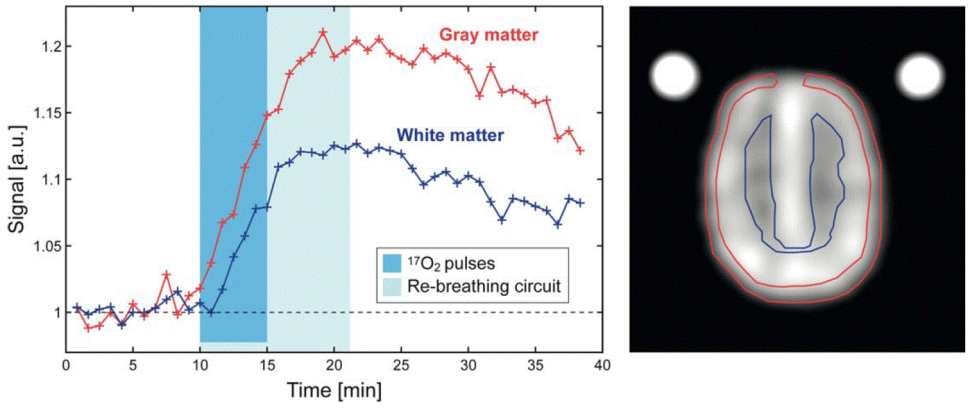

Figure 19: In vivo ^{17}O NMR experiments

(A) Dynamic changes of $H_2{}^{17}O$ signal is monitored before, during and after a brief inhalation of ^{17}O-enriched oxygen gas and presents 3 characteristic phases. (Zhu, 2011)
(B) Evolution of $H_2{}^{17}O$ signal in the human brain during $^{17}O_2$ delivery. The gray matter and the white matter present differences in oxygen consumption rate (Hoffmann, 2011).

By monitoring the metabolism of inhaled $^{17}O_2$ gas, this NMR technique provides a robust, direct and non-invasive way to appraise oxygen consumption in vivo. The single and well defined $H_2{}^{17}O$ signal allows specific detection, simple and reliable quantification and data analysis. Indeed, $^{17}O_2$ bound to the hemoglobin or $^{17}O_2$ in gas phase or dissolved in water are undetectable by conventional in vivo MRI scanner. Detection of small dynamic changes of metabolic $H_2{}^{17}O$ is feasible at high magnetic field and the technique is suitable for repeated measurements over time.

Conventional techniques currently used to study oxygen metabolism, such as ^{15}O PET, ^{19}F MRI, BOLD MRI or electron paramagnetic resonance, generally rely on indirect measurements and do not provide specific detection or quantitative measurements. On the contrary, ^{17}O MRI approach may be a promising tool to study oxidative metabolism in vivo. But before routine applications, further methodology development is required. Fast imaging sequences are mandatory regarding the short relaxation times of $H_2{}^{17}O$ and models for oxygen consumption quantification need to be developed.

This technique has been used to study O_2 metabolism in the brain (as previously presented) and in the heart (Lu, 2012) (Zhu, 2010) and could potentially be applied to numerous tissues. Recent studies have investigated the use of direct ^{17}O MRI to measure oxygen metabolism in tumors. In the study of Narazaki and colleagues, increase in the signal intensity in ^{17}O images of tumor bearing mice was detected after the $^{17}O_2$ gas inhalation (Narazaki, 2013). Hoffmann and colleagues recently attempted to determine the $CMRO_2$ in a glioblastoma patient by direct ^{17}O MRI (Hoffmann, 2014). Large differences in the signal increase during $^{17}O_2$ inhalation were obtained for the white matter, the gray matter and different tumor zones of the patient. These studies presented encouraging data, highlighting the potential of ^{17}O NMR to evaluate oxygen consumption in tumor patients.

3.4. Assessment of tumor oxygenation by electron paramagnetic resonance

Oxygen plays a key role in cellular metabolism. Changes in oxygen level will force cells to adapt their metabolism and critical oxygenation status will affect tumor response to therapies. Consequently, evaluation of tumor oxygenation in parallel to tumor metabolism studies would mainly improve tumor phenotyping research. Numerous techniques are available for the assessment of tumor oxygenation in vivo including MR-based methods such as ^{19}F MRI, BOLD MRI, T_1-based method MRI, Overhauser MRI, and non-MR based techniques such as oxygen electrodes and near infrared spectroscopy (Gallez, 2004). The application of electron paramagnetic resonance (EPR), a spectrometric technique used to detect impaired electron species (or paramagnetic species) and their interaction with the environment, as an oximetric method will be presented in this chapter.

Molecular oxygen is a triplet radical that possesses two unpaired electrons. In the gas phase, at very low oxygen partial pressure (i.e. 0.1 mmHg), it is possible to record an EPR spectrum with conventional EPR spectrometers. However, no EPR spectra have been reported from oxygen dissolved in fluids near room temperature, due to fast relaxation of electron spins. However, indirect methods exist. Most of these methods rely on the paramagnetic properties of molecular oxygen, which acts as an efficient relaxer for other paramagnetic species. Bimolecular collisions between oxygen and free radicals alter the resonance characteristics of the radical and consequently its EPR spectrum. The enhancement of relaxation times scales linearly with the concentration of oxygen over a wide range of oxygen tensions (**Figure 20.A**).

EPR measurements of an oxygen sensor with paramagnetic properties can thus provide a direct indication of the concentration of oxygen. After the injection of the paramagnetic probe, the spectra line width (the peak to peak splitting along the magnetic field axis) is generally measured and converted to pO_2 or $[O_2]$ using an appropriate calibration curve (**Figure 20.B**). Two classes of stable paramagnetic materials are useful for oximetry purposes. There are a variety of oxygen-sensitive soluble paramagnetic molecules available, especially nitroxide and trityl radicals, that vary in structure and chemical properties but can present lack in sensitivity and are susceptible to bioreduction/oxidation by the cells in vivo, resulting in instability of the probe. On the contrary, many of the particulate paramagnetic materials such as inks, charcoal or lithium crystals, are very inert in biological system that makes them especially useful for studies in vivo. Once placed into tissues, they can be used to obtain repeated measurements of pO_2 from the same site

and generally present a very large sensitivity over a large range of pO_2 (Gallez, 2004) (Swartz, 2004).

EPR spectroscopy has been successfully used in several tumor models to monitor changes in oxygenation levels induced pharmacological modulators (Karroum, 2012) (Jordan, 2010b) but also to predict tumor response to radiotherapy (Hou, 2013). However, current EPR scanner operating at 1GHz or less can only measure a single point in the tumor and only allows the penetration of microwaves up to a 10 mm maximum depth into the tissue, and is thus unable to map pO_2 tumor heterogeneity. Using EPR imaging techniques, the spatial distribution of free radicals can be performed utilizing magnetic field gradients in a manner similar to MRI (**Figure 20.C**). For this purpose, the use of soluble EPR materials such as trityl radicals is more convenient as they can diffuse in the whole tissue (Krishna, 2012). While EPR systems for use in laboratory animals have been fairly well developed, EPR is not currently used in clinical routine. Nevertheless, clinical EPR systems are under development, facing some challenges with respect to instrumentation, probe administration, and regulatory issues but measurements underway in patients with superficial tumors already demonstrated that oxygen measurements can be made in human subjects using India ink (Swartz, 2014).

(A)

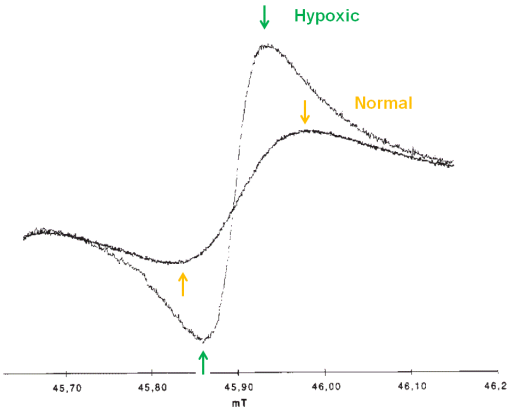

(B)

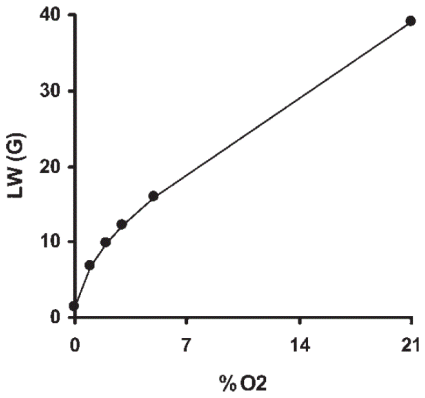

(C)

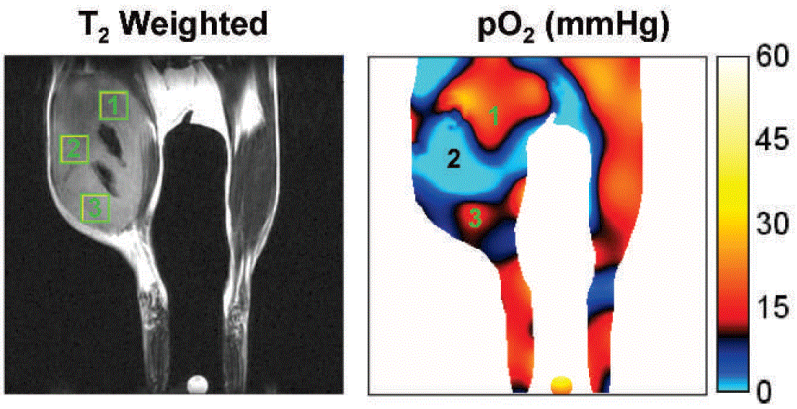

Figure 20: Effects of oxygen on the EPR spectra of oxygen probes.

(A) EPR spectrum of charchoal particules. Spectra line width is indicated by arrows. Adapted from (Gallez, 2004).

(B) Charcoal calibration curves: linewidth as a function of pO_2 (Gallez, 2004).

(C) Image of pO_2 distribution in a tumor and corresponding anatomical image (Krishna, 2012).

AIMS OF THE THESIS

Upregulated glycolysis being presented as a hallmark of various cancers (Hanahan, 2011), reverting glycolytic metabolism may represent an attractive strategy for cancer therapy. Dichloroacetate (DCA), long used to treat lactic acidosis in various pathologies, has recently emerged as a promising anticancer drug. By inhibiting the pyruvate dehydrogenase kinase, DCA actually reactivates the mitochondrial function and decreases the glycolytic flux in tumor cells resulting in cell cycle arrest and apoptosis (see Introduction section 2.2.).

Recently, our group investigated the link between glycolysis inhibition and tumor progression impairment by examining the effects of DCA treatment in tumor cell lines presenting different metabolic profiles (De Preter, 2016). We found that 5 mM DCA was more effective in glycolytic-phenotype cancer cells, while oxidative cells remained less sensitive. Also, the reduction in cell proliferation observed in glycolytic cells was mediated by a reactivation of mitochondrial function and a decrease in glycolytic and pentose phosphate pathway fluxes. Clear effects on oxygen consumption, glucose consumption and lactate production were identified in glycolytic MDA-MB-231 human breast cancer cells treated with DCA compared to oxidative SiHa human cervical cancer cells. By preferentially inducing a metabolic shift in glycolytic cancer cells, DCA may potentially limit cancer progression in patients with highly glycolytic tumors.

To validate the relevance of these findings, we aimed to determine in vivo the response to DCA in MDA-MB-231 and SiHa cancer models presenting distinct metabolic profiles in vitro. The influence of DCA treatment on critical bioenergetic parameters was explored using a multi-modality

imaging project. The metabolic markers investigated were the oxygen consumption, the glucose consumption as well as the lactate production.

Firstly, we assessed the feasibility of an innovative technology, namely direct ^{17}O MRS, to assess oxygen metabolism in tumors and its modulations. While only a few techniques are described to assess oxygen consumption in vivo, such as ^{15}O PET, ^{19}F MRI, BOLD MRI, ^{13}C NMR or EPR approaches, there is still a critical need of sensitive methods to measure the oxygen consumption of tumors non-invasively. ^{17}O MRS approach has demonstrated potential as a novel technology to appraise oxygen consumption in the brain and in the heart (see Introduction section 3.3.2.). By using mild hypothermia to modulate oxygen metabolism in tumors, we evidenced the ability of ^{17}O MRS to assess subtle variations in O_2 consumption rate in tumors.

Secondly, we explored the metabolic effects of DCA on glycolytic MDA-MB-231 and oxidative SiHa tumors using advanced imaging technologies. Oxygen consumption, studied by ^{17}O MRS, glucose uptake, evaluated by ^{18}F-FDG PET and pyruvate transformation into lactate, measured using hyperpolarized ^{13}C-MRI, were monitored before and 24 hours after DCA treatment. Using these imagings, no clear metabolic shift was observed in both tumor models highlighting a dramatically different response to DCA between in vitro and in vivo conditions.

Given this observation that tumor cells exhibit distinct metabolic preferences according to their in vitro versus in vivo growth, **we studied the metabolic behavior of the glycolytic MDA-MB-231 and the oxidative SiHa tumor models under different oxic conditions.** Impact of hypoxic

and oxygenated conditions on glucose metabolism were tested in vitro and in vivo. **As a first approach, we evaluated the impact of carbogen breathing on tumor oxygenation status, measured by EPR, and on tumor glucose uptake, assessed by ^{18}F-FDG PET, in vivo.** We identified a rapid metabolic adaptation to the oxygen environment in both MDA-MB-231 and SiHa tumor models, independently of the metabolic discrepancies previously identified in vitro. **Finally, a global metabolic study with advanced imaging techniques including PET, EPR oximetry and ^{13}C-hyperpolarizated MRI was achieved to evaluate the nature and the extent of the metabolic discrepancies observed between the in vitro and in vivo models.**

RESULTS

1. ^{17}O MRS as an innovative tool to investigate O_2 consumption in tumors

^{17}O MRS assesses the effect of mild hypothermia on oxygen consumption rate in tumors

Marie-Aline Neveu†, Nicolas Joudiou†, Géraldine De Preter, Jean-Paul Dehoux, Bénédicte F. Jordan and Bernard Gallez

† These authors contributed equally to this work.

Manuscript submitted as a research article to NMR in Biomedicine

(In revision)

^{17}O MRS assesses the effect of mild hypothermia on oxygen consumption rate in tumors

Marie-Aline Neveu[a†], Nicolas Joudiou[a†], Géraldine De Preter[a], Jean-Paul Dehoux[b], Bénédicte F. Jordan[a] and Bernard Gallez[a]

[a] Biomedical Magnetic Resonance Research Group, Louvain Drug Research Institute (LDRI), Université catholique de Louvain (UCL), Belgium

[b] Experimental Surgery Unit, Medical School, Institute of Experimental and Clinical Research (IREC), Université catholique de Louvain (UCL), Belgium

[†] These authors contributed equally to this work.

Corresponding author:

Bernard Gallez, Biomedical Magnetic Resonance Unit – REMA, Louvain Drug Research Institute (LDRI), Université catholique de Louvain, Avenue Mounier, 73.08, B-1200 Brussels, BELGIUM

bernard.gallez@uclouvain.be

Phone: +32 2 7647391

Fax : +32 2 7647390

Total number of pages: 13

Tables/Figures: 4

Abstract: 176/300 words

Body text: 4033/6000 words

Keywords: oxygen consumption, EPR, direct ^{17}O MRS, tumor hypoxia

Abbreviation list:

$CMRO_2$: cerebral metabolic rate of oxygen

$^{17}O_2$: ^{17}O-enriched oxygen gas

$H_2{}^{17}O$: ^{17}O-labeled water

Manuscript submitted as a research article to NMR in Biomedicine

Abstract

Even if oxygen consumption is a key factor in metabolic phenotyping, the assessment of O_2 consumption in tumors remains critical as current technologies generally display poor specificity. Recently, the possibility of using ^{17}O NMR spectroscopy to monitor O_2 consumption in tissues has been introduced. To assess the value of direct ^{17}O NMR spectroscopy in depicting variation in O_2 consumption rate in tumors, normothermic and hypothermic tumor bearing mice were studied. Tumor pO_2 was monitored using EPR oximetry during 2 hours in animals kept under normothermic (37°C) and hypothermic (32°C) conditions. To measure oxygen consumption rate in tumors, dynamic changes in $H_2{}^{17}O$ signal were monitored by NMR spectroscopy before, during and after a 2 min inhalation period of $^{17}O_2$-renriched gas. Hypothermic animals showed an increase in tumor pO_2 after 2 hours contrarily to normothermic animals. This pO_2 change was related to a decrease in oxygen consumption rate measured by direct ^{17}O MRS in hypothermic animals. This study highlights the ability of direct ^{17}O MRS to measure oxygen metabolism in tumors and modulations of tumor oxygen consumption rate.

Introduction

Direct ^{17}O NMR spectroscopy is an advanced tool to study oxygen metabolism in various tissues at high magnetic field (1-5). During oxidative metabolism, molecular oxygen is converted into water at a rate dependent on the metabolic activity in tissues. This conversion can be monitored using ^{17}O MRS. During the inhalation of ^{17}O-enriched oxygen gas ($^{17}O_2$), the metabolic inclusion of the ^{17}O atom in water molecules and the appearance of the water peak ($H_2{}^{17}O$) reflect the local oxygen consumption (6,7). Due to specific detection of $H_2{}^{17}O$ using direct ^{17}O MRS in vivo (6,8,9), this non-invasive technique allows the measurement and quantification of subtle dynamic changes in metabolic $H_2{}^{17}O$ and oxygen consumption rate.

Oxygen plays a key role in cellular metabolism. Like glucose, amino acids, lipids or other nutrients, O_2 is a major fuel to produce energy and O_2 metabolism is highly regulated to ensure normal tissue function. Direct ^{17}O NMR in vivo has been used to study O_2 metabolism in the brain (1,3,7,10,11) and in the heart (12,13). These organs strongly rely on oxygen to produce energy and many brain or heart diseases have been linked to abnormal O_2 metabolism. Recently, tumor oxygen consumption rate has also been appraised using this technique (14,15). For a long time, tumor cells have been considered defective in mitochondrial oxygen consumption due to their dominant glycolytic metabolism (16,17). However, new evidences of oxidative activities in tumor cells have challenged this paradigm (18-20). Metabolic characterization in vivo could change the understanding of tumor metabolism and could allow the identification of new targets for innovative anti-cancer strategies.

The objectives of the present study were to explore the feasibility of direct ^{17}O MRS to assess oxygen metabolism in tumors and its modulations. To investigate the impact of hypometabolism induction in the murine fibrosarcoma FSAII tumor model, we monitored the oxygen consumption of normothermic (37°C) and hypothermic (32°C) tumor bearing mice. We first evaluated the effect of mild hypothermia on tumor oxygenation. Using Electron Paramagnetic Resonance (EPR), we observed an increase in pO_2 in FSAII tumors that was not observed under normothermic condition. Then we studied oxygen consumption in FSAII tumors using direct ^{17}O MRS approach. We showed that the induction of mild hypothermia had a profound effect on tumor oxygen consumption in the tumor model. This study highlights the ability of direct ^{17}O MRS to quantitatively assess oxygen metabolism in tumors.

Experimental

Animal preparation

Animal studies were undertaken in accordance with Belgian and the Université catholique de Louvain ethical committee regulations (agreements number UCL/2010/MD/001 and UCL/2014/MD/026).

A total of 10^6 FSAII murine fibrosarcoma cells were inoculated subcutaneously into the hind thigh of C3H/HeOuJIco male mice (Janvier, Le Genest-Saint-Isle, France). The experiments were performed when tumors reached 8 ± 1.0 mm in diameter. During experiments, animals were anesthetized by inhalation of isoflurane (Forene, Abbot, England) mixed with air in a continuous flow (2 L/min), as this form of anesthesia has been shown to have negligible effect on tissue hemodynamics (21). Anesthesia

was induced using 3% isoflurane. 1.5-2% of isoflurane was then used to maintain a respiration at a rate of 80 ± 10 breaths per minute during experiments. A pressure cushion was used to monitor respiration during the experiments (SA Instruments Inc., Stony Brook, NY, USA). A circulating water system was used to regulate body temperature and animal temperature was monitored using a rectal temperature probe (Bioseb, Vitrolles, France). For normothermic condition, animal temperature was kept at 37°C during the experiments. For hypothermic condition, water pump temperature was reduced to maintain the body.

Electron paramagnetic resonance (EPR) measurements

In vivo tumor pO_2 was monitored by EPR spectroscopy using charcoal as the oxygen-sensitive probe (22,23). EPR spectra were recorded using a 1.1 GHz EPR spectrometer (Magnettech, Berlin, Germany). According to calibration curves made by measuring the EPR line width as a function of the pO_2 (24), the EPR spectra line width was converted to pO_2. A charcoal suspension (100 mg/mL) was injected intratumorally (60 µl) 24h before experiments. For EPR reading, the tumor under study was placed in the center of the extended loop resonator whose sensitive volume extends 1 cm into the tumor mass. The pO_2 measurements correspond to an average of pO_2 values in the tumor volume.

After the induction of mild hypothermia, pO_2 measurements were started when the body temperature of the mice reached 32°C. For normothermic condition, measurements were performed after a 10 min equilibration period. For each condition, EPR spectra were recorded every 30 minutes during 2 hours.

Gas delivery system

The gas delivery system for $^{17}O_2$ inhalation experiments is presented in Figure 1. The animal was placed in a home-made system containing a nose cone, a circulating water system for body temperature regulation, a breathing monitoring system and space for the RF coil. The nose cone was attached to a breathing line connected to the main anesthesia line and to a $^{17}O_2$ delivery line controlled by a valve. Prefilled syringes were used to manually deliver the $^{17}O_2$ gas and ensure continuous delivery. $^{17}O_2$ gas (70% enriched, NUKEM Isotopes GmbH, Alzenau, Germany) and isoflurane/N_2 gas mixture were stored in separate gas reservoirs (Tedlar® bag). 40 ml of $^{17}O_2$ gas were mixed with 160 ml of isoflurane/N_2 mixture. The final mixture was loaded into 100 ml syringes connected to the breathing line. To deliver the mixture, the breathing line was manually switched to the $^{17}O_2$ line. By applying pressure on the prefilled syringes, the $^{17}O_2$ mixture was delivered as a continuous flow during 2 min. Then gas was switch back to the main anesthesia line. The valve and syringes connected to the $^{17}O_2$ line were placed as close to the outside of the magnet to limit dead volume. Also, the home-made system holding the animal was closed during the experiments to limit gas dispersion.

^{17}O MRS measurements

For oxygen consumption experiments, direct ^{17}O MRS was performed on an 11.7 T (Bruker, Biospec) controlled by Paravision 6.0 (Bruker, Ettlingen, Germany). Experiments were carried out using a $^{1}H/^{17}O$ Bruker surface coil system (2 cm in diameter) positioned over the tumor mass. Anatomical images were firstly acquired using a T_2-weighted axial turbo RARE

sequence (TR = 2500ms; TE = 30ms; rare factor = 8; NA = 2; FOV = 25x25mm²; resolution: 98 x 98 µm²; 1 mm slice thickness). ^{17}O MRS measurements were carried out using a nonlocalized, single-pulse sequence (TR = 16.5 ms; NA = 600; repetition: 120; T_{acq} = 20 min; Acq BW = 5000 Hz; FA = 20°). For ^{17}O MRS sequence, the 90° reference pulse was optimized previously on natural abundance $H_2{}^{17}O$ samples (Supplementary Figure 1).

To measure tumor oxygen consumption during the $^{17}O_2$ delivery, a total of 120 ^{17}O-spectra were collected in about 20 min, before, during and after a 2 min inhalation period of the $^{17}O_2$ mixture. The integrals of the $H_2{}^{17}O$ peaks over time were measured to follow using a home-made program written in Matlab (The MathWorks Inc., Natick, MA, USA). $H_2{}^{17}O$ signal was then expressed as relative to the mean baseline signal before $^{17}O_2$ delivery. The mean signal of the final steady state (s_{final}) during the post-inhalation period was calculated between 1100 and 1200 sec. We considered that the steady state was reached when the signal stood between s_{final} ± 5 % of signal variation. For each experiment, the slope during the linear incorporation phase was measured between 600 sec and the time point when steady state was reached.

We randomly separated mice into two distinct cohorts to undergo normothermic or hypothermic conditions. For normothermic condition, basal measurements were performed. For mild hypothermic condition, experiments were started 2 hours after the mice reached 32°C.

Statistical analysis

Analysis was performed using the Graphpad software. Results were expressed as mean value of parameter ± SEM. Paired t-test was used to compare mean changes of pO_2 values for each conditions (32°C or 37°C), and unpaired t-test was used to compare mean changes of $H_2{}^{17}O$ signal between the two conditions. For all tests, results with P <0.05 (*), <0.01 (**), or <0.001 (***) were considered significant.

Results

Effect of mild hypothermia on the tumor oxygenation

Using EPR oximetry, pO_2 levels of FSAII tumors were monitored after the induction of mild hypothermia (32°C), as presented in Figure 2. Basal measured pO_2 (mean ± SEM) was 3.6 ± 0.3 mmHg. The tumors displayed a systematic increase in their oxygenation level 30 min after hypothermia induction. The maximal pO_2 was reached after ~90 min, with a mean pO_2 of 5.9 ± 0.3 mmHg. This value was significantly higher than the baseline (n = 5, P = 0.0005). No oxygenation changes were observed for mice kept under normothermic (37°C) conditions during 2 hours (n = 4, P = 0.1028 after 2 hours)

Effect of mild hypothermia on the tumor oxygen consumption

In figure 3, a typical evolution of $H_2{}^{17}O$ signal is presented for FSAII tumors under normothermic (Fig 3.A) and hypothermic (Fig 3.B) conditions during ^{17}O MRS experiments. Before $^{17}O_2$ inhalation, the natural abundance $H_2{}^{17}O$ signal was detected (SNR = 42). $H_2{}^{17}O$ signal increased during the $^{17}O_2$ inhalation and reached a new steady state during the post-inhalation

period. This scheme was consistent with previous studies performed in brain (1) and heart tissues (13).

A total of 11 tumors under normothermic conditions and 6 tumors under hypothermia were scanned. Pooled stacked plots of tumor $H_2{}^{17}O$ spectra are presented in Figure 4. The results were highly reproducible under the same thermic condition (Fig 4.A). For mice kept under mild hypothermia for 2 hours, the rate of increase in $H_2{}^{17}O$ signal was lower compared to animals kept under normothermic condition ($P = 0.0011$) (Fig 4.B). Under hypothermia, FSAII tumors exhibited a slope of $2.295\ 10^{-4} \pm 0.26\ 10^{-4}\ s^{-1}$. Under normothermic condition, the slope was $6.619\ 10^{-4} \pm 0.767\ 10^{-4}\ s^{-1}$.

Discussion

In this study, we evaluated the impact of hypothermia on oxygen consumption rate in tumor using direct ^{17}O MRS. Mild hypothermia is currently used in intensive care unit and provides protective effects in traumatic brain injury, cardiopulmonary resuscitation, stroke, and various other disorders (25). Likewise, mild hypothermia has been presented as an attractive tool to modulate oxygen metabolism in tumor. By inducing a hypometabolism, oxygen consumption rate drops leading to an improvement in tumor oxygenation and a reduction in the hypoxic fraction (26). Here, we observed an increased in pO_2 values (measured by EPR oximetry) in FSAII tumors 2 hours after the induction of mild hypothermia. This increase in tumor oxygenation coincided with a drop in tumor oxygen consumption (assessed by direct ^{17}O MRS) for mice kept under hypothermic condition. These data were consistent with a previous study attesting the effects of hypothermia on cerebral metabolic rate of oxygen ($CMRO_2$) using

direct ^{17}O MRI in rat brain (27) and validate the ability of direct ^{17}O MRS to assess subtle variations in O_2 consumption rate in tumors.

The ability of cancer cells to remodel the biochemical pathways and their amassed metabolic flexibility have become major features of cancer (28). For long, oxygen consumption has been considered as a minor actor in tumor metabolism (29). However, recent findings indicated the key role of oxidative pathways in cancer for the maintenance of tumorigenic potential (18,21,30). Oxygen consumption can also contribute to the hypoxic microenvironment in tumors (31). Indeed, imbalance between consumption rates and oxygen delivery will result in tumor hypoxia and will affect tumor response to therapies. Likewise, pharmacological modulators of oxygen consumption have been described to improve tumor oxygenation leading to the enhancement of radiotherapy efficacy (32-39). Consequently, there is a critical need of sensitive methods to measure the oxygen consumption of tumors non-invasively. Highly sensitive methods are used for determining cellular oxygen consumption in vitro (40). Nevertheless, techniques described to assess oxygen consumption in vivo, such as ^{15}O PET, ^{19}F MRI, BOLD MRI, ^{13}C NMR or EPR approaches (41-46) generally lack specificity, do not provide a direct measurement of O_2 consumption and cannot always provide quantitative information. For some of them, long measurement time and extensive modeling are required. The potential of following $H_2{}^{17}O$ by ^{17}O MRS/MRI as a tracer for oxygen consumption has been explored using different approaches. Detection of $H_2{}^{17}O$ distribution by indirect ^{1}H–(^{17}O) methods (47-49), exploiting the impact of ^{17}O on ^{1}H relaxation properties, has the advantage to rely on the high sensitivity of the proton signal and can be apply using conventional MRI scanners systems.

However, difficulties of quantitatively correlating the ^{1}H signal changes to the $H_2{}^{17}O$ concentration and the impact of many physiological parameters on the indirect measurements represent major challenges for absolute quantification of the $H_2{}^{17}O$ concentration (as reviewed by Zhu and Chen (4)). On the contrary, direct ^{17}O MRS/MRI consists on the specific detection of $H_2{}^{17}O$ and can detect small dynamic changes of metabolic $H_2{}^{17}O$, especially at high magnetic field (8), but required dedicated RF coils and ultra-fast MR sequences. However, this NMR technique provides a robust, direct, fast and non-invasive way to appraise oxygen consumption in vivo and could potentially be applied to numerous tissues. Recent studies have investigated the use of direct ^{17}O MRI to measure oxygen metabolism in tumors (14,15). In the study of Narazaki and colleagues (14), ^{17}O signal was measured by 10 min data accumulation before and 40 min after a brief inhalation of $^{17}O_2$ gas. They identified an increase in the signal intensity in ^{17}O images of tumor bearing mice after $^{17}O_2$ gas inhalation. Hoffmann and colleagues recently attempted to determine the $CMRO_2$ in a glioblastoma patient by ^{17}O MRI (15). Large differences in the signal increase during $^{17}O_2$ inhalation were obtained for the white matter, the gray matter and different tumor areas of the patient. While both studies presented a first attempt to evaluate oxygen consumption in preclinical tumor models and in a glioblastoma patient, our present adds to this study in several ways. First, we demonstrated the feasibility to non-invasively quantify oxygen consumption in tumors using direct ^{17}O MRS in vivo. Based on models previously described for quantification of $CMRO_2$ (2), we measured the slope during the linear incorporation phase to assess oxygen consumption. The oxygen consumption rates measured in tumors were highly reproducible within groups. Secondly, we assessed the value of the method

to highlight differences in oxygen consumption rate in tumors. As the technique was able to reveal the effect of a modulator of tumor oxygenation (hypothermia treatment), direct ^{17}O MRS could represent a relevant tool for tumor metabolic profiling in vivo and could potentially be translated into human patients to guide treatments targeting tumor metabolism.

In conclusion, our study demonstrated a new field of application for direct ^{17}O MRS in oncology. The technique was able to reveal subtle variations in O_2 consumption rate in tumors induced by hypothermic treatment. Therefore, the technique provides a unique way to study in vivo an important aspect of tumor metabolism non-invasively and could have a significant impact in oncology research.

Acknowledgement

This study was supported by grants from Belgian National Fund for Scientific Research (FNRS) - Grant PDR T.0107.13, the Televie (7.4578.13), the Action de Recherches Concertées 14/19-058. Marie-Aline Neveu and Bénédicte F. Jordan are respectively research fellow and senior research associate of the FNRS. The authors would like to thank Drs. Xiao-Hong Zhu and Michiko Narazaki for helpful discussion.

References

1. Zhu XH, Zhang Y, Tian RX, Lei H, Zhang N, Zhang X, Merkle H, Ugurbil K, Chen W. Development of (17)O NMR approach for fast imaging of cerebral metabolic rate of oxygen in rat brain at high field. Proc. Natl. Acad. Sci. USA 2002;99(20):13194-13199.
2. Zhu XH, Zhang N, Zhang Y, Zhang X, Ugurbil K, Chen W. In vivo 17O NMR approaches for brain study at high field. NMR Biomed. 2005;18(2):83-103.
3. Atkinson IC, Thulborn KR. Feasibility of mapping the tissue mass corrected bioscale of cerebral metabolic rate of oxygen consumption using 17-oxygen and 23-sodium MR imaging in a human brain at 9.4 T. NeuroImage 2010;51(2):723-733.
4. Zhu XH, Chen W. In vivo oxygen-17 NMR for imaging brain oxygen metabolism at high field. Prog. Nucl. Magn. Reson. Spectrosc. 2011;59(4):319-335.
5. Cui W, Zhu XH, Vollmers ML, Colonna ET, Adriany G, Tramm B, Dubinsky JM, Oz G. Non-invasive measurement of cerebral oxygen metabolism in the mouse brain by ultra-high field (17)O MR spectroscopy. J. Cereb. Blood. Flow. Metab. 2013;33(12):1846-1849.
6. Arai T, Mori K, Nakao S, Watanabe K, Kito K, Aoki M, Mori H, Morikawa S, Inubushi T. In vivo oxygen-17 nuclear magnetic resonance for the estimation of cerebral blood flow and oxygen consumption. Biochem. Biophys. Res. Commun. 1991;179(2):954-961.
7. Pekar J, Ligeti L, Ruttner Z, Lyon RC, Sinnwell TM, van Gelderen P, Fiat D, Moonen CT, McLaughlin AC. In vivo measurement of cerebral oxygen consumption and blood flow using 17O magnetic resonance imaging. Magn. Reson. Med. 1991;21(2):313-319.
8. Zhu XH, Merkle H, Kwag JH, Ugurbil K, Chen W. 17O relaxation time and NMR sensitivity of cerebral water and their field dependence. Magn. Reson. Med. 2001;45(4):543-549.
9. Arai T, Nakao S, Mori K, Ishimori K, Morishima I, Miyazawa T, Fritz-Zieroth B. Cerebral oxygen utilization analyzed by the use of oxygen-17 and its nuclear magnetic resonance. Biochem. Biophys. Res. Commun. 1990;169(1):153-158.
10. Hoffmann SH, Begovatz P, Nagel AM, Umathum R, Schommer K, Bachert P, Bock M. A measurement setup for direct 17O MRI at 7 T. Magn. Reson. Med. 2011;66(4):1109-1115.
11. Zhu XH, Chen JM, Tu TW, Chen W, Song SK. Simultaneous and noninvasive imaging of cerebral oxygen metabolic rate, blood flow and oxygen extraction fraction in stroke mice. NeuroImage 2013;64:437-447.

12. Lu M, Atthe B, Mateescu GD, Flask CA, Yu X. Assessing mitochondrial respiration in isolated hearts using (17)O MRS. NMR Biomed. 2012;25(6):883-889.
13. Zhu XH, Zhang Y, Chen W. In vivo 17O MRS imaging for assessing myocardial oxygen metabolism in rat heart at 9.4 T. In Proceedings of International Society of Magnetic Resonance Medicine, Stockholm, 2010; 172.
14. Narazaki M, Kanazawa Y, Koike S, Ando K, Ikehira H. Quantitative 17O imaging towards oxygen consumption study in tumor bearing mice at 7 T. Magn. Reson. Imaging 2013;31(5):643-650.
15. Hoffmann SH, Radbruch A, Bock M, Semmler W, Nagel AM. Direct (17)O MRI with partial volume correction: first experiences in a glioblastoma patient. Magma 2014;27(6):579-587.
16. Warburg O. Uber den Stoffwechsel der Carcinomzelle. Klinische Wochenschrift 1925;4: 534–536.
17. Gatenby RA, Gillies RJ. Why do cancers have high aerobic glycolysis? Nat. Rev. Cancer 2004;4(11):891-899.
18. Moreno-Sanchez R, Rodriguez-Enriquez S, Marin-Hernandez A, Saavedra E. Energy metabolism in tumor cells. FEBS J 2007;274(6):1393-1418.
19. Jose C, Bellance N, Rossignol R. Choosing between glycolysis and oxidative phosphorylation: a tumor's dilemma? Biochim. Biophys. Acta 2011;1807(6):552-561.
20. Viale A, Corti D, Draetta GF. Tumors and mitochondrial respiration: a neglected connection. Cancer Res. 2015;75(18):3685-3686.
21. Baudelet C, Gallez B. Effect of anesthesia on the signal intensity in tumors using BOLD-MRI: comparison with flow measurements by Laser Doppler flowmetry and oxygen measurements by luminescence-based probes. Magn. Reson. Imaging 2004;22(7):905-912.
22. Gallez B, Jordan BF, Baudelet C, Misson PD. Pharmacological modifications of the partial pressure of oxygen in murine tumors: evaluation using in vivo EPR oximetry. Magn. Reson. Med. 1999;42(4):627-630.
23. Jordan BF, Baudelet C, Gallez B. Carbon-centered radicals as oxygen sensors for in vivo electron paramagnetic resonance: screening for an optimal probe among commercially available charcoals. Magma 1998;7(2):121-129.
24. Gallez B, Baudelet C, Jordan BF. Assessment of tumor oxygenation by electron paramagnetic resonance: principles and applications. NMR Biomed. 2004;17(5):240-262.
25. Polderman KH. Application of therapeutic hypothermia in the ICU: opportunities and pitfalls of a promising treatment modality. Part 1: Indications and evidence. Intensive care medicine 2004;30(4):556-575.

26. Kelleher DK, Nauth C, Thews O, Krueger W, Vaupel P. Localized hypothermia: impact on oxygenation, microregional perfusion, metabolic and bioenergetic status of subcutaneous rat tumours. Br. J. Cancer 1998;78(1):56-61.
27. Zhu XH, Zhang Y, Zhang N, Ugurbil K, Chen W. Noninvasive and three-dimensional imaging of CMRO(2) in rats at 9.4 T: reproducibility test and normothermia/hypothermia comparison study. J. Cereb. Blood. Flow. Metab. 2007;27(6):1225-1234.
28. Hanahan D, Weinberg RA. Hallmarks of cancer: the next generation. Cell 2011;144(5):646-674.
29. Warburg O. On respiratory impairment in cancer cells. Science 1956;124(3215):269-270.
30. Moreno-Sanchez R, Marin-Hernandez A, Saavedra E, Pardo JP, Ralph SJ, Rodriguez-Enriquez S. Who controls the ATP supply in cancer cells? Biochemistry lessons to understand cancer energy metabolism. Int. J. Biochem. Cell. Biol. 2014;50:10-23.
31. Höckel M, Vaupel P, Tumor hypoxia: definitions and current clinical, biologic, and molecular aspects, J. Natl. Cancer Inst. 2001;93(4):266-276.
32. Jordan BF, Grégoire V, Demeure RJ, Sonveaux P, Feron O, O'Hara J, Vanhulle VP, Delzenne N, Gallez B. Insulin increases the sensitivity of tumors to irradiation: involvement of an increase in tumor oxygenation mediated by a nitric oxide-dependent decrease of the tumor cells oxygen consumption. Cancer Res. 2002;62(12):3555-3561.
33. Crokart N, Radermacher K, Jordan BF, Baudelet C, Cron GO, Gregoire V, Beghein N, Bouzin C, Feron O, Gallez B. Tumor radiosensitization by antiinflammatory drugs: evidence for a new mechanism involving the oxygen effect. Cancer Res. 2005;65(17):7911-7916.
34. Crokart N, Jordan BF, Baudelet C, Cron GO, Hotton J, Radermacher K, Gregoire V, Beghein N, Martinive P, Bouzin C, Feron O, Gallez B. Glucocorticoids modulate tumor radiation response through a decrease in tumor oxygen consumption. Clins Cancer Res. 2007;13(2 Pt 1):630-635.
35. Jordan BF, Sonveaux P, Feron O, Gregoire V, Beghein N, Dessy C, Gallez B. Nitric oxide as a radiosensitizer: evidence for an intrinsic role in addition to its effect on oxygen delivery and consumption. Int. J. Cancer 2004;109(5):768-773.
36. Jordan BF, Peeterbroeck J, Karroum O, Diepart C, Magat J, Gregoire V, Gallez B. Captopril and S-nitrosocaptopril as potent radiosensitizers: Comparative study and underlying mechanisms. Cancer Lett. 2010;293(2):213-219.
37. Diepart C, Karroum O, Magat J, Feron O, Verrax J, Calderon PB, Gregoire V, Leveque P, Stockis J, Dauguet N, Jordan BF, Gallez B. Arsenic trioxide

treatment decreases the oxygen consumption rate of tumor cells and radiosensitizes solid tumors. Cancer Res. 2012;72(2):482-490.

38. Ansiaux R, Dewever J, Gregoire V, Feron O, Jordan BF, Gallez B. Decrease in tumor cell oxygen consumption after treatment with vandetanib (ZACTIMA; ZD6474) and its effect on response to radiotherapy. Radiat. Res. 2009;172(5):584-591.
39. Jordan BF, Christian N, Crokart N, Grégoire V, Feron O, Gallez B. Thyroid status is a key modulator of tumor oxygenation: implication for radiation therapy. Radiat. Res. 2007;168(4):428-432.
40. Diepart C, Verrax J, Calderon PB, Feron O, Jordan BF, Gallez B. Comparison of methods for measuring oxygen consumption in tumor cells in vitro. Anal. Biochem. 2010;396(2):250-256.
41. Diepart C, Jordan BF, Gallez B. A New EPR oximetry protocol to estimate the tissue oxygen consumption in vivo. Radiat. Res. 2009;172(2):220-225.
42. Baron JC, Jones T. Oxygen metabolism, oxygen extraction and positron emission tomography: Historical perspective and impact on basic and clinical neuroscience. NeuroImage 2012;61(2):492-504.
43. Diepart C, Magat J, Jordan BF, Gallez B. In vivo mapping of tumor oxygen consumption using (19)F MRI relaxometry. NMR Biomed. 2011;24(5):458-463.
44. Zhao D, Ran S, Constantinescu A, Hahn EW, Mason RP. Tumor oxygen dynamics: correlation of in vivo MRI with histological findings. Neoplasia. 2003;5(4):308-318.
45. Coquery N, Francois O, Lemasson B, Debacker C, Farion R, Remy C, Barbier EL. Microvascular MRI and unsupervised clustering yields histology-resembling images in two rat models of glioma. J. Cereb. Blood. Flow. Metab. 2014;34(8):1354-1362.
46. Shestov AA, Lee SC, Nath K, Guo L, Nelson DS, Roman JC, Leeper DB, Wasik MA, Blair IA, Glickson JD. (13)C MRS and LC-MS Flux Analysis of Tumor Intermediary Metabolism. Front. Oncol. 2016;6:135.
47. Mellon EA, Beesam RS, Elliott MA, Reddy R. Mapping of cerebral oxidative metabolism with MRI. Proc. Natl. Acad. Sci. USA 2010;107(26):11787-11792.
48. Mellon EA, Beesam RS, Baumgardner JE, Borthakur A, Witschey WR, 2nd, Reddy R. Estimation of the regional cerebral metabolic rate of oxygen consumption with proton detected 17O MRI during precision 17O2 inhalation in swine. J. Neurosci. Methods 2009;179(1):29-39.
49. Tailor DR, Baumgardner JE, Regatte RR, Leigh JS, Reddy R. Proton MRI of metabolically produced H2 17O using an efficient 17O2 delivery system. NeuroImage 2004;22(2):611-618.

Figures Captions

Fig 1

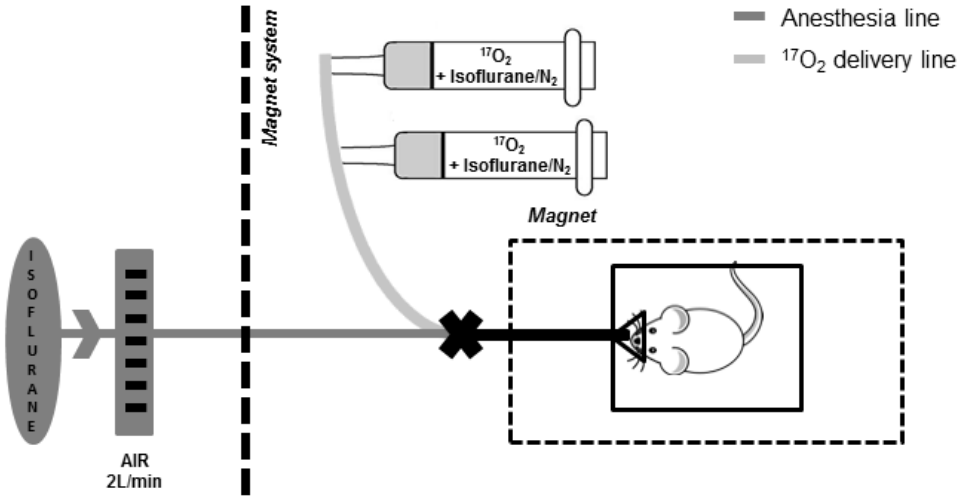

Fig 1: Gas delivery system

Fig 2

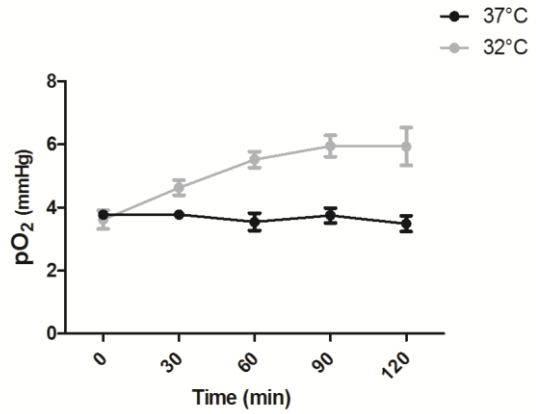

Fig 2: Evolution of pO_2 in tumors under normothermic (37°C) and hypothermic (32°C) condition, monitored by EPR oximetry. Data are expressed as means ± SEM.

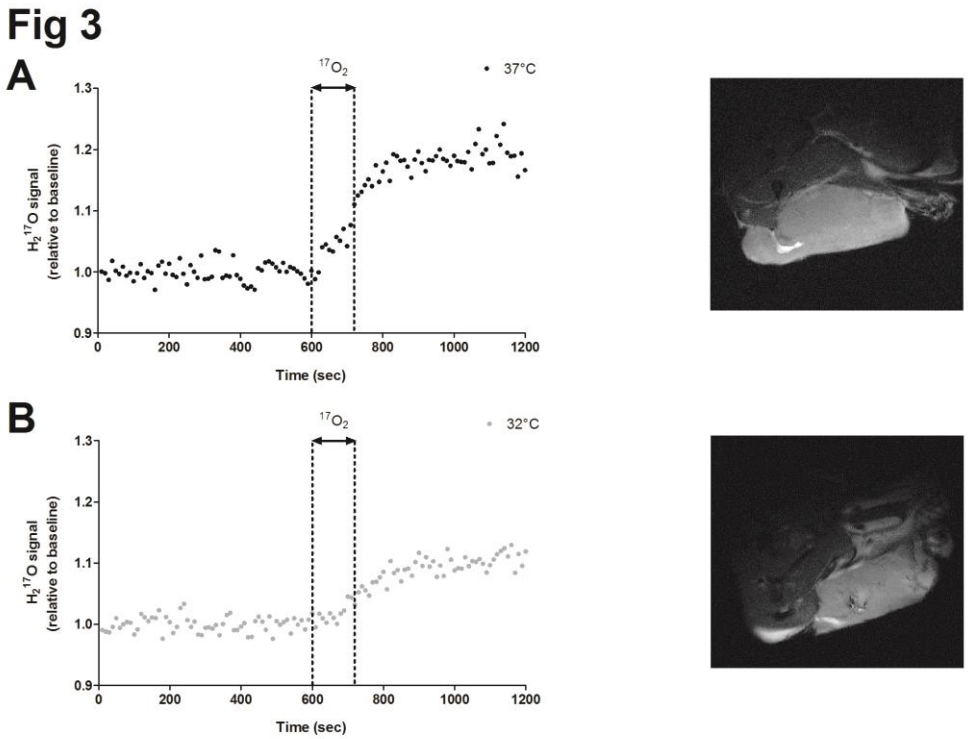

Fig 3: $H_2{}^{17}O$ signal from representative tumors under normothermic **(A)** and hypothermic **(B)** condition acquired before, during and after a 2 min inhalation period of the $^{17}O_2$ gas and corresponding ^{1}H anatomical images. $H_2{}^{17}O$ signal is expressed as relative to the mean baseline signal before $^{17}O_2$ delivery.

Fig 4

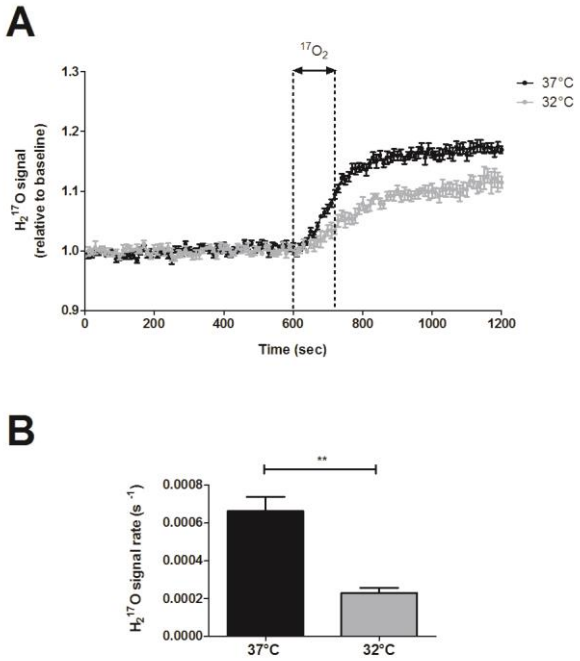

Fig 4: Comparison of oxygen consumption in tumors under normothermic (37°C) and hypothermic (32°C) conditions. **(A)** Pooled stacked plots of tumor $H_2{}^{17}O$ signal during $^{17}O_2$ delivery experiments. $H_2{}^{17}O$ signal is expressed as relative to the mean baseline signal before $^{17}O_2$ delivery **(B)** Comparison of the rate of $H_2{}^{17}O$ signal after $^{17}O_2$ delivery in tumors.

Data are expressed as means ± SEM. Unpaired tests were two-sided.

Supplementary Fig 1

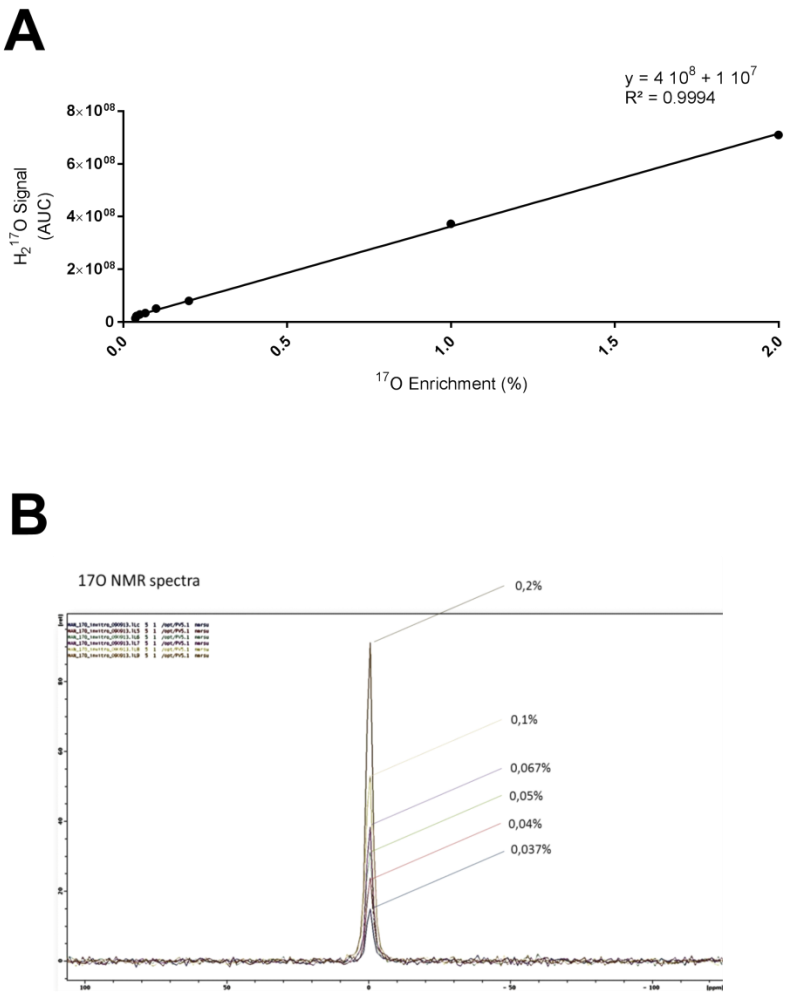

Supplementary Fig 1: Feasibility assessment of ^{17}O MRS. Phantoms with 0,037% (natural abundance), 0,04%, 0,05%, 0,067%, 0,1%, 0,2%, 1%, 2 % enrichment were used for calibration (A). ^{17}O spectra of $H_2{}^{17}O$ phantoms (B). The signal to noise ratio of natural abundance phantom (0.037%) at 11.7T was 9.

2. In vivo assessment of the response to dichloroacetate using multi-modality imaging technologies

Multi-modality imaging to assess metabolic response to dichloroacetate treatment in tumor models

Marie-Aline Neveu, Géraldine De Preter, Nicolas Joudiou, Anne Bol, Jeffery R. Brender, Keita Saito, Shun Kishimoto, Vincent Grégoire, Bénédicte F. Jordan, Murali C. Krishna, Olivier Feron, and Bernard Gallez

Manuscript accepted for publication in Oncotarget

(epub ahead of print)

www.impactjournals.com/oncotarget/ Oncotarget, Advance Publications 2016

Multi-modality imaging to assess metabolic response to dichloroacetate treatment in tumor models

Marie-Aline Neveu[1], Géraldine De Preter[1], Nicolas Joudiou[1], Anne Bol[2], Jeffery R. Brender[3], Keita Saito[3], Shun Kishimoto[3], Vincent Grégoire[2], Bénédicte F. Jordan[1], Murali C. Krishna[3], Olivier Feron[4], Bernard Gallez[1]

[1]Biomedical Magnetic Resonance Research Group, Louvain Drug Research Institute, Université catholique de Louvain, Brussels, Belgium

[2]Radiation Oncology Department & Center for Molecular Imaging, Radiotherapy & Oncology, Institute of Experimental and Clinical Research, Université catholique de Louvain, Brussels, Belgium

[3]Radiation Biology Branch, National Cancer Institute, NIH, Bethesda, USA

[4]Pole of Pharmacology and Therapeutics, Institute of Experimental and Clinical Research, Université catholique de Louvain, Brussels, Belgium

Correspondence to: *Bernard Gallez,* ***email:*** *bernard.gallez@uclouvain.be*

Keywords: *tumor metabolism, DCA, ^{17}O MRS, hyperpolarized ^{13}C-MRI, ^{18}F-FDG PET*

Received: *September 08, 2016* ***Accepted:*** *October 19, 2016* ***Published:*** *November 07, 2016*

ABSTRACT

Reverting glycolytic metabolism is an attractive strategy for cancer therapy as upregulated glycolysis is a hallmark in various cancers. Dichloroacetate (DCA), long used to treat lactic acidosis in various pathologies, has emerged as a promising anti-cancer drug. By inhibiting the pyruvate dehydrogenase kinase, DCA reactivates the mitochondrial function and decreases the glycolytic flux in tumor cells resulting in cell cycle arrest and apoptosis. We recently documented that DCA was able to induce a metabolic switch preferentially in glycolytic cancer cells, leading to a more oxidative phenotype and decreasing proliferation, while oxidative cells remained less sensitive to DCA treatment. To evaluate the relevance of this observation in vivo, the aim of the present study was to characterize the effect of DCA in glycolytic MDA-MB-231 tumors and in oxidative SiHa tumors using advanced pharmacodynamic metabolic biomarkers. Oxygen consumption, studied by ^{17}O magnetic resonance spectroscopy, glucose uptake, evaluated by ^{18}F-FDG PET and pyruvate transformation into lactate, measured using hyperpolarized ^{13}C-magnetic resonance spectroscopy, were monitored before and 24 hours after DCA treatment in tumor bearing mice. In both tumor models, no clear metabolic shift was observed. Surprisingly, all these imaging parameters concur to the conclusion that both glycolytic tumors and oxidative tumors presented a similar response to DCA. These results highlight a major discordance in metabolic cancer cell bioenergetics between in vitro and in vivo setups, indicating critical role of the local microenvironment in tumor metabolic behaviors.

INTRODUCTION

Warburg metabolism (enhanced glycolysis in the presence of oxygen) is a common feature of several malignant tumors and is associated with cancer aggressiveness, invasiveness and poor prognosis [1–3]. Because of this high glycolytic rate in various cancers, targeting glucose metabolism is presented as an attractive anticancer approach endowed with a high specificity and limited undesirable side effects [4, 5]. Indeed, conventional treatments rely on the rapid proliferation process present in cancer cells but also in healthy cells. Treatments targeting glycolytic metabolism should instead specifically alter metabolic adaptations that support the Warburg malignant phenotype, adaptations that are not shared by normal cells. To support drug development and assessment in clinical trials, there is a critical need for dedicated criteria evaluating tumor response to these

emerging therapies. Moreover, for new cytostatic agents targeting tumor metabolism, the use of conventional anatomical imaging techniques is not optimal for treatment response assessment [4] and only functional and molecular imaging techniques may offer the possibility of an early assessment of the tumor response [6–8].

Recently, we have investigated the effects of dichloroacetate (DCA) in tumor cell lines presenting different metabolic profiles [9]. DCA is a promising molecule that promotes glucose oxidation over glycolysis by inhibiting the mitochondrial pyruvate dehydrogenase kinase (PDK) and has successfully reached clinical trials [10]. We found that 5 mM DCA was more effective in glycolytic-phenotype cancer cells, where reduction in cell proliferation was mediated by a reactivation of mitochondrial function and a decrease in glycolytic and pentose phosphate pathway fluxes. Our data suggested that DCA may benefit to patients with highly glycolytic tumors. Therefore, the objective of the present study was to assess the effect of DCA in these prototypical tumor models in vivo, namely the glycolytic MDA-MB-231 human breast cancer model and the oxidative SiHa human cervical cancer model. For this purpose, we used a multi-modality molecular imaging approach using several pharmacodynamic metabolic biomarkers. Oxygen consumption, studied by ^{17}O magnetic resonance spectroscopy (^{17}O MRS), glucose uptake, evaluated by ^{18}F-fluorodeoxyglucose positron emission tomography (^{18}F-FDG PET) and pyruvate transformation into lactate, measured during hyperpolarized ^{13}C-magnetic resonance imaging (hyperpolarized ^{13}C-MRI), were monitored before and after DCA treatment in tumor bearing mice. Surprisingly, in vivo models did not recapitulate the previously observed in vitro behavior.

RESULTS

To assess the impact of DCA treatment on the metabolism of the models in vivo, oxygen consumption (Figure 1), glucose uptake (Figure 2) and lactate flux (Figure 3) were measured in MDA-MB-231 and SiHa tumors before and 24 hours after DCA treatment.

In Figure 1, tumor $H_2{}^{17}O$ spectra are presented for representative MDA-MB-231 (Figure 1A) and SiHa tumors (Figure 1B) during ^{17}O MRS experiments. The results were highly reproducible under the same conditions tested. The evolution of $H_2{}^{17}O$ signal, demonstrating the $^{17}O_2$ metabolism in tumors, was similar before and after DCA treatment in MDA-MB-231 tumors (Figure 1A) and in SiHa tumors (Figure 1B). In both tumors models, we found that DCA treatment did not majorly impact oxygen consumption, as assessed by the rate of increase in $H_2{}^{17}O$ signal (Figure 1C). MDA-MB-231 tumors exhibited a slope of 1.02 $10^{-3} \pm 0.16$ 10^{-3} s^{-1} and 0.91 $10^{-3} \pm 0.09$ 10^{-3} s^{-}

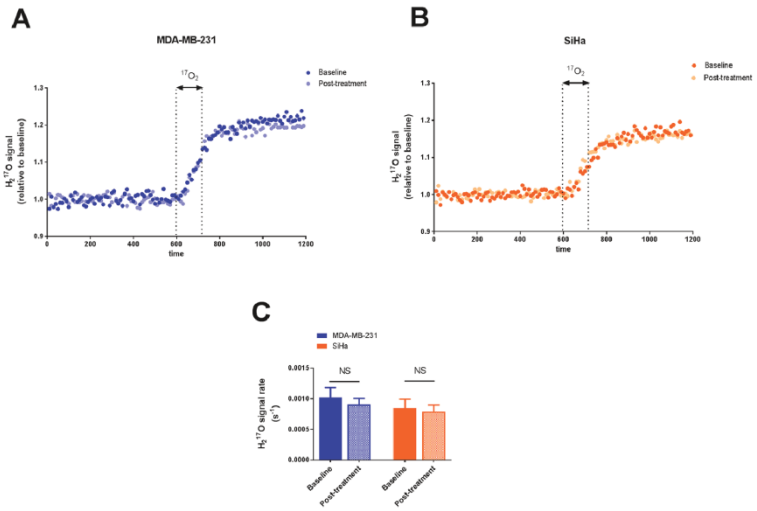

Figure 1: Effect of dichloroacetate on tumor oxygen consumption in vivo. Tumor $H_2{}^{17}O$ signal from representative MDA-MB-231 tumors **A.** and SiHa tumors **B.** acquired before, during and after a 2 min inhalation period of the $^{17}O_2$ gas. $H_2{}^{17}O$ signal is expressed as relative to the mean baseline signal before $^{17}O_2$ delivery. $^{17}O_2$ metabolismis not modified by DCA treatment. **C.** Comparison of the rate of $H_2{}^{17}O$ signal after $^{17}O_2$ delivery in tumors pre and post-treatment. Data are expressed as means ± SEM. Paired tests were two-sided.

^{1} before and after treatment respectively (n=5, P=0.5366). For SiHa tumors, the slopes were 0.85 $10^{-3} \pm 0.14\ 10^{-3}\ s^{-1}$ under baseline condition and 0.79 $10^{-3} \pm 0.11\ 10^{-3}\ s^{-1}$ post-treatment (n =5, P=0.2892).

^{18}F-FDG uptake (%ID/g) measured in both tumor models under baseline and post-treatment conditions are presented in Figure 2. In both tumor models, we found that DCA treatment did not lead to a significant change in the uptake of ^{18}F-FDG (Figure 2A-2D), assessing a limited impact of DCA on glucose uptake (Figure 2E). %ID/g measured on PET images (mean ± SEM) were 1.88 ± 0.12 under baseline condition and 1.78 ± 0.11 after treatment for MDA-MB-231 tumors (n=7, P=0.2120) and 1.79 ± 0.21 under baseline condition and 1.89 ± 0.19 after treatment for SiHa tumors (n=7, P=0.0813).

The influence of DCA treatment on pyruvate transformation into lactate was measured after hyperpolarized 1-^{13}C pyruvate injection during hyperpolarized ^{13}C-MRS studies (Figure 3). Representative pyruvate and lactate peak intensities over time of MDA-MB-231 tumors and SiHa tumors captured before and 24 hours after DCA treatment are shown in Figure 3A-3D. Lactate production was reduced after DCA treatment only in SiHa tumors (Figure 3E). Lactate/pyruvate ratio (Lac/

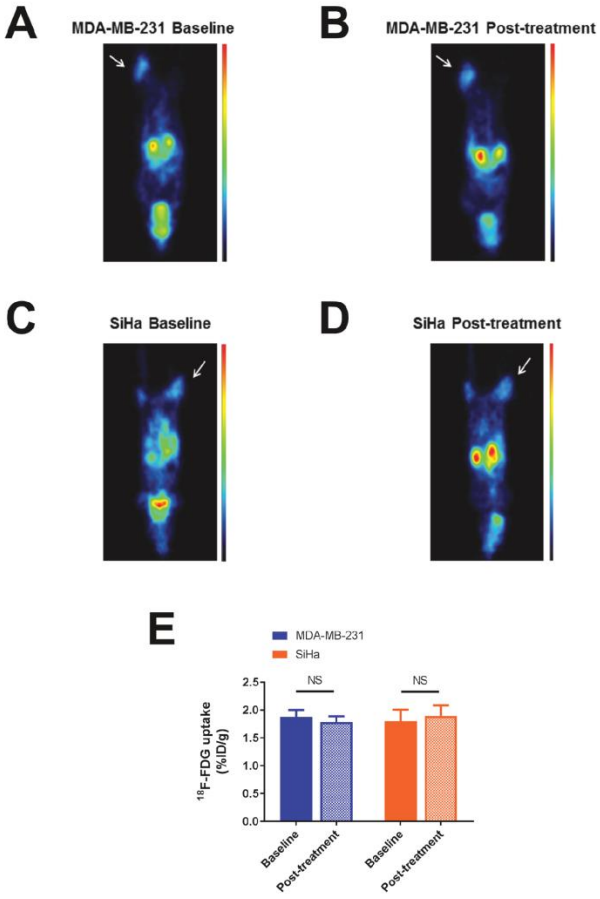

Figure 2: Effect of dichloroacetate on tumor glucose uptake in vivo. Representative ^{18}F-FDG PET images showing MDA-MB-231 **A-B.** and SiHa **C-D.** tumor-bearing mouse imaged before and 24 hours after DCA treatment. Tumors are indicated by thin arrows. ^{18}F-FDG uptake is expressed in %ID/g. Images were normalized. DCA does not alter ^{18}F-FDG uptake in MDA-MB-231 and SiHa tumors. **E.** Comparison of ^{18}F-FDG uptake before and after treatment. Data are expressed as means ± SEM. Paired tests were two-sided.

Pyr) shifted from 0.55 ± 0.05 to 0.48 ± 0.04 in MDA-MB-231 tumors (n=7, P=0.3105) and from 0.82 ± 0.05 to 0.63 ± 0.07 in SiHa tumors (n=7, P=0.0348).

We also evaluated the magnitude of response to the treatment by measuring the variation within the above biomarkers between baseline and post-treatment conditions (Figure 4). No differences in oxygen consumption and lactate flux measurements were observed between MDA-MB-231 and SiHa tumors during the treatment (P>0.05) (Figure 4A, 4C). Only a small but significant difference in behavior was observed for ^{18}F-FDG uptake measurements (P=0.0240) (Figure 4B). MDA-MB-231 tumors decreased their ^{18}F-FDG uptake after treatment (n=7, -5.4 ± 3.5 %) compared to SiHa tumors (n=7, +6.7 ± 3.1 %).

DISCUSSION

In this study, the impact of DCA on tumors presenting different metabolic profiles was evaluated using molecular imaging in vivo. Recent findings identified that DCA preferentially impairs glycolytic cells compared to oxidative cells. The purpose of the present study was to establish the relevance of these findings in vivo using the same prototypical tumor models as in our in vitro study [9], namely the MDA-MB-231 human breast cancer model reported as glycolytic [1, 11] and the SiHa human cervical cancer model documented as oxidative [11, 12]. The dose and administration scheme were selected based on

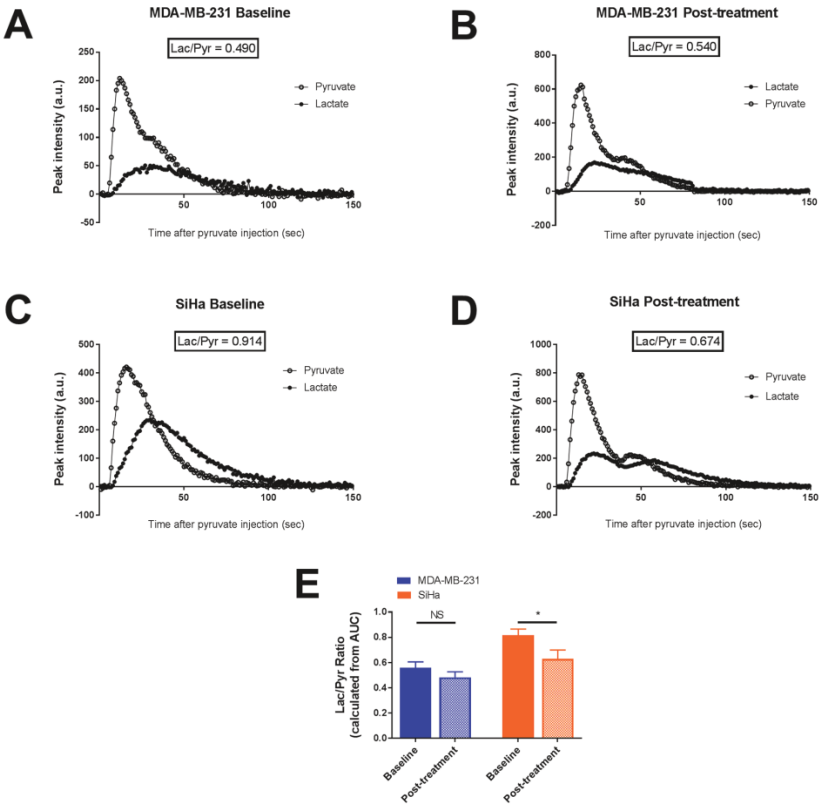

Figure 3: Effect of dichloroacetate on tumor lactate production in vivo. Tumor lactate and pyruvate peak intensities after i.v. injection of hyperpolarized 1-^{13}C pyruvate from representative MDA-MB-231 tumors **A-B.** and SiHa tumors **C-D.** Lactate production, measured by the Lac/Pyr ratio, in MDA-MB-231 and SiHa tumors before and after treatment **E.** Data are expressed as means ± SEM. Paired tests were two-sided.

previous reports attesting the efficacy of DCA in tumors [13–15].

In vitro, we previously identified clear effects of DCA treatment on oxygen consumption, glucose consumption and lactate uptake in glycolytic MDA-MB-231 human breast cancer cells. On the other hand, the metabolic activity of oxidative SiHa human cervical cancer cells was not altered by DCA treatment. Using a multi-modality imaging project, we were not able to recapitulate these findings in vivo. Pre-treatment, MDA-MB-231 and SiHa tumors exhibit the same metabolic profile. As MDA-MB-231 and SiHa tumors were previously described as hypoxic under baseline condition [16], we highlighted here that both tumor models exhibit a glycolytic phenotype under anaerobic condition. Post-treatment, glycolytic MDA-MB-231 tumors do not appear more impacted than oxidative SiHa tumors (Figure 1-4). Also, some marginal metabolic changes were identified such as a significant decreased lactate production in SiHa tumors (Figure 3E) or a decreased ^{18}F-FDG uptake in MDA-MB-231 tumors (Figure 4B). Together, those findings did not highlight a clear metabolic shift in MDA-MB-231 tumors or in SiHa tumors treated with DCA during 24 hours (Supplementary Figure S1). This inability to observe any treatment response in vivo could not be attributed to any differences in growth rate between the tumor models under study (Supplementary Figure S2). Also, the measurement repeatability was formerly established using the same tumor models [16]. Our study demonstrated that the tumor metabolic response to DCA was dramatically different between in vitro and in vivo conditions.

Because of its good tolerability and safety, DCA has been universally exploited to lower lactate levels in acquired or congenital forms of lactic acidosis [17]. In 2007, Bonnet and colleagues investigated the effects of DCA in cancer and discovered that DCA was promoting apoptosis in vitro and decreasing tumor growth in vivo [18]. Since then, this orally available and cheap molecule has been further investigated in vitro, in vivo and successfully reached clinical trials. The first data available from the clinical trials indicate that DCA appears to be efficient in adults in solid and brain tumors [19, 20]. However, no firm conclusions stand out in advanced non-small cell lung cancer [21]. In another recent study of Feuerecker and co-workers, promotion of tumor growth was even observed after DCA treatment in neuroblastoma tumors [22]. These studies indicate that response to DCA treatment may drastically vary among tumor types.

The redirection of glucose metabolism from glycolysis to oxidation leading to the inhibition of proliferation and the induction of caspase-mediated apoptosis was initially proposed as the generic mechanism of action of DCA. In a recent phase I study in patients with advanced solid tumors, decreased ^{18}F-FDG uptake was observed after DCA therapy, supporting the use of ^{18}F-FDG uptake as a potential biomarker of response to DCA [20]. Also, hyperpolarized ^{13}C-pyruvate MRI has already been used in several preclinical studies to monitor DCA effect in solid tumors [13–15], but also in cardiac [23, 24] and brain studies [25, 26]. In the present study, ^{18}F-FDG uptake was unchanged after DCA treatment (Figure 2E). This suggests that DCA treatment does not impair glucose uptake and phosphorylation but could potentially impact downstream transformation of glucose. However, no effects on bicarbonate production were detected that could demonstrate changes in energy metabolism from glycolysis to oxidative phosphorylation (Supplementary Figure S3). Recent findings suggested that DCA may also act by other mechanisms. While a possible disruption of the balance between fatty acid β-oxidation and glucose oxidation has already been suggested as an additional mechanism involved in the overall effects of DCA in vivo (as reviewed by [27]), PDK inhibitors may potentially induce other compensatory mechanisms that could limit the impact of such drugs on global tumor metabolism. The anti-cancer effects of DCA appear to rely on multiple mechanisms depending on the drug

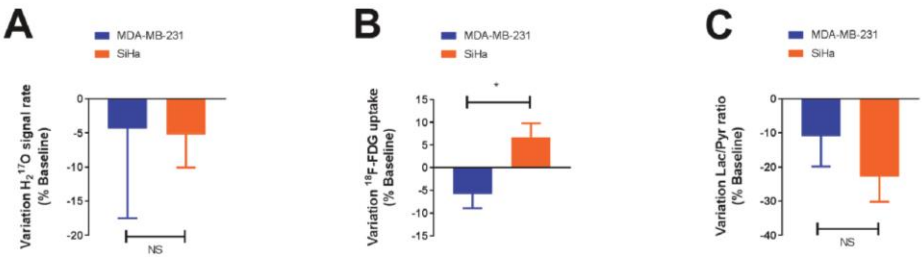

Figure 4: DCA does not significantly influence the metabolism of glycolytic tumors compared to oxidative tumors, as assessed by $^{17}O_2$ metabolism A., ^{18}F-FDG uptake B. and pyruvate transformation into lactate C. measurements in vivo. The magnitude of response to dichloroacetate (variation) is identical in both models, only a small difference in behavior is observed for ^{18}F-FDG uptake. Data are expressed as means ± SEM. Unpaired tests were two-sided.

concentration, drug administration scheme [28] and cell type [29]. Also, a change in PDK isoform expression between in vitro and in vivo model could also greatly influence the effect of DCA on tumor metabolism in vivo. Indeed, oncogene regulation and tumor microenvironment, like extracellular acidosis, can affect PDK isoform expression [30], possibly leading to the expression of a PDK isoform less sensitive to DCA effects. Our findings are consistent with a recent study highlighting that tumor microenvironment could be as important as the (epi) genetic profile to shape the tumor phenotype [31]. Further investigations using relevant isogenic cell clones with ability to form tumors in vivo should be considered to determine the effects of DCA on energy metabolism in vivo.

In conclusion, our multi-modality imaging study identified major discordances between in vitro and in vivo metabolic responses to DCA treatment, in cancer models presenting distinct metabolic profiles. Results suggest preferring implanted tumors and spontaneous cancer models to study DCA treatment within the milieu of the tumor microenvironment. Overall, further investigations are required to elucidate the impact of different tumor microenvironments on metabolic effects of DCA and its impact for clinical use.

MATERIALS AND METHODS

Cell culture

MDA-MB-231 (human breast cancer) and SiHa (human cervix squamous cell carcinoma) cell lines (American Type Culture Collection [ATCC]), were routinely cultured in Dulbecco's modified Eagle's medium containing 4.5g/l glucose supplemented with 10% fetal bovine serum and 1% penicillin-streptomycin.

Animal housing

Animal studies were undertaken in accordance with Belgian and the Université catholique de Louvain ethical committee regulations (agreements number UCL/2010/MD/001 and UCL/2014/MD/026). Hyperpolarized ^{13}C-MRI experiments were carried out in compliance with the Guide for the Care and Use of Laboratory Animal Resources (National Research Council, 1996) and approved by the National Cancer Institute (NCI) Animal Care and Use Committee.

Tumor implantation and animal experiments

A total of 10^7 MDA-MB-231 cells or 10^7 SiHa cells, amplified in vitro, were collected by trypsinization, washed three times with Hanks balanced salt solution and resuspended in 200 µL of a 1:1 mixture of Matrigel (BD Biosciences) and Hanks balanced salt solution. For ^{17}O MRS and PET scan experiments, the tumor cells were inoculated subcutaneously into the hind thigh of nude NMRI female mice (Janvier Le Genest-Saint-Isle, France). For hyperpolarized ^{13}C-MRI experiments, the tumor cells were inoculated subcutaneously into the hind thigh of athymic nude female mice (Frederick Cancer Research Center, Animal Production, Frederick, MD, USA). The experiments were performed when tumors reached 7 mm (at this tumor size, necrosis was less than 5% as characterized by Hematoxylin Eosin staining).

To assess the effects of DCA on tumor metabolism using biomarkers, all animals have undergone imaging before and after treatment, with one day between each measurement. Dichloroacetate sodium (Sigma-Aldrich) was administered intraperitoneally (200 mg/kg) after baseline measurements to the mouse. Another dose was given 24 hours after the first dose injection. Post-treatment measurements were initiated 1 hour after treatment administration. This administration scheme is consistent with previous studies attesting the effects of DCA in tumors using hyperpolarized ^{13}C-MRI [13, 15]. The imaging protocol is summarized in Figure 5.

Mice were anesthetized by isoflurane inhalation (Forene, Abbot, England) mixed with air in a continuous flow (2 L/min). Animals were warmed (approximately 35°C) throughout the anesthesia period.

^{17}O MRS experiments

For oxygen consumption experiments, ^{17}O MRS was performed on an 11.7 T (Bruker, Biospec) controlled by Paravision 6.0 (Bruker, Ettlingen, Germany). Experiments were carried out using a ^{1}H/^{17}O Bruker surface coil system positioned over the tumor mass. Anatomical images were firstly acquired using a T_2-weighted axial turbo RARE sequence (TR = 2500ms; TE = 30ms; rare factor = 8; NA = 2; FOV = 25x25mm^2; resolution: 98 x 98 µm^2; 1 mm slice thickness). ^{17}O MRS measurements were carried out using a nonlocalized, single-pulse sequence (TR = 16.5 ms; NA = 600; repetition: 120; T_{acq} = 20 min; Acq BW = 5000 Hz; FA = 20°). For ^{17}O MRS sequence, the

Figure 5: Experimental protocol.

90° reference pulse was optimized previously on natural abundance $H_2{}^{17}O$ samples.

To measure tumor oxygen consumption during the $^{17}O_2$ delivery, a total of 120 ^{17}O-spectra were collected in about 20 min, before, during and after a 2 min inhalation period of the $^{17}O_2$ mixture. The integrals of the $H_2{}^{17}O$ peaks over time were measured using a home-made program written in Matlab (The MathWorks Inc., Natick, MA, USA). $H_2{}^{17}O$ signal was then expressed as relative to the mean baseline signal before $^{17}O_2$ delivery. The mean signal of the final steady state (s_{final}) during the post-inhalation period was calculated between 1100 and 1200 s. We considered that the steady state was reached when the signal stood between s_{final} ± 5 % of signal variation. The slope during the linear incorporation phase was measured between 600 sec and the time point when steady state was reached.

PET/CT imaging

Whole-body PET imaging was performed on a dedicated small-animal PET scanner (Mosaic, Philips Medical Systems, Cleveland, USA) with a spatial resolution of 2.5 mm (FWHM). The PET scans were followed by whole-body acquisitions using a helical CT scanner (NanoSPECT/CT Small Animal Imager, Bioscan Inc., DC, USA). For each breathing condition, anesthetized mice were injected 120 µl intraperitoneally with 11.1-14.8 MBq of ^{18}F-FDG (Betaplus Pharma, Brussels, Belgium). A 10 min transmission scan was first obtained in a single mode using a 370 MBq ^{137}Cs source for attenuation correction. A 10 min static PET acquisition was then performed after a 60 min resting period. After the correction with attenuation factors obtained from the transmission scan, images were reconstructed using a fully 3D iterative algorithm (3D-RAMLA) in a 128 x 128 x 120 matrix, with a voxel size of 1 mm^3. After PET acquisition, anesthetized animals were transferred on the same bed from the PET scanner to the CT scanner (x-ray tube voltage: 55 kVp; number of projections: 180; exposure time 1000 ms) for anatomical reference. The CT projections were reconstructed with a voxel size of 0.221 x 0.221 x 0.221 mm^3. Regions of Interest (ROIs) were delineated on PET images using PMOD software (PMOD™, version 3.403, PMOD technologies Ltd, Zurich, Switzerland). 2D ROIs were established on consecutive transversal slices using a 50% isocontour tool (ROI including the pixel values larger than 50% of the maximum pixel) that semi-automatically defined a 3D Volume of Interest (VOI) around the tissue of interest. To avoid overestimation of the uptake within the VOI, PET/CT fused images where used to discriminate hot pixels coming from the neighboring tissues like urinary bladder. Using the mean uptake within this VOI, the global tracer uptake was assessed in tumors and expressed as percentage of injected dose per gram of tissue (%ID/g).

Hyperpolarized ^{13}C-MRI studies

1-^{13}C pyruvic acid (30 µL), containing 15 mM OXO63 and 2.5 mM gadolinium chelate ProHance (Bracco Diagnostics, Milano, Italy), was hyperpolarized at 3.35T and 1.4K using the Hypersense DNP polarizer (Oxford Instruments, Abingdon, UK) according to the manufacturer's instructions. After 60-90 min, the hyperpolarized sample was rapidly dissolved in 4.5 mL of a superheated alkaline buffer that consisted of 50 mM Tris(hydroxymethyl)aminomethane, 75 mM NaOH, and 100 mg/L ethylenediaminetetraacetic acid. The hyperpolarized 1-^{13}C pyruvate solution (96 mM) was intravenously injected through a catheter placed in the tail vein of the mouse (12 µL/g body weight). Hyperpolarized ^{13}C MRI studies were performed on a 3T scanner (MR Solutions, Guildford, UK) using a home-built ^{13}C solenoid leg coil. After the rapid injection of hyperpolarized 1-^{13}C pyruvate, spectra were acquired every second for 240 seconds using a single pulse sequence. Data were analyzed in a model free approach using the lactate/pyruvate ratio, calculated from the areas under the curves of the 1-^{13}C lactate peak and the 1-^{13}C pyruvate peak [15].

Statistical analysis

Analysis was performed using the GraphPad Prism 7 software. Results are expressed as means value of parameter ± SEM. All statistical tests were two-sided. Paired t-test was used to compare mean changes between groups (baseline vs. post-treatment) for each tumor model, and unpaired t-test was used to compare mean changes between the two tumor models. Results with $P < 0.05$ (*), <0.01 (**), or <0.001 (***) were considered to be statistically significant.

ACKNOWLEDGMENTS

This work was supported by grants from the Belgian National Fund for Scientific Research (F.S.R.-FNRS; PDR T.0107.13); the Action de Recherches Concertées ARC 14/19-058; Belgian Science Policy Office Interuniversity Attraction Pole IUAP #P7/03; and intramural National Institute of Health (NIH) funds.

CONFLICTS OF INTEREST

The authors have no conflicts of interest to declare.

REFERENCES

1. Gatenby RA, Gillies RJ. Why do cancers have high aerobic glycolysis? Nature reviews Cancer. 2004; 4:891-899.
2. López-Lázaro M. The Warburg Effect: why and how do cancer cells activate glycolysis in the presence of oxygen? Anticancer Agents Med Chem. 2008; 8:305-312.

3. Upadhyay M, Samal J, Kandpal M, Singh OV, Vivekanandan P. The Warburg effect: insights from the past decade. Pharmacology & therapeutics. 2013; 137:318-330.
4. Tennant DA, Duran RV, Gottlieb E. Targeting metabolic transformation for cancer therapy. Nature reviews Cancer. 2010; 10:267-277.
5. Porporato PE, Dhup S, Dadhich RK, Copetti T, Sonveaux P. Anticancer targets in the glycolytic metabolism of tumors: a comprehensive review. Frontiers in pharmacology. 2011; 2:49.
6. Figueiras RG, Padhani AR, Goh VJ, Vilanova JC, Gonzalez SB, Martin CV, Caamano AG, Naveira AB, Choyke PL. Novel oncologic drugs: what they do and how they affect images. Radiographics: a review publication of the Radiological Society of North America, Inc. 2011; 31:2059-2091.
7. Serkova NJ. Translational imaging endpoints to predict treatment response to novel targeted anticancer agents. Drug resistance updates: reviews and commentaries in antimicrobial and anticancer chemotherapy. 2011; 14:224-235.
8. Vander Heiden MG. Targeting cancer metabolism: a therapeutic window opens. Nature reviews Drug discovery. 2011; 10:671-684.
9. De Preter G, Neveu MA, Danhier P, Brisson L, Payen VL, Porporato PE, Jordan BF, Sonveaux P, Gallez B. Inhibition of the pentose phosphate pathway by dichloroacetate unravels a missing link between aerobic glycolysis and cancer cell proliferation. Oncotarget. 2016; 7:2910-2920. doi: 10.18632/oncotarget.6272.
10. Kankotia S, Stacpoole PW. Dichloroacetate and cancer: new home for an orphan drug? Biochimica et biophysica acta. 2014; 1846:617-629.
11. De Preter G, Danhier P, Porporato PE, Payen VL, Jordan BF, Sonveaux P, Gallez B. Direct Evidence of the Link Between Energetic Metabolism and Proliferation Capacity of Cancer Cells In Vitro. Advances in experimental medicine and biology. 2016; 876:209-214.
12. Sonveaux P, Vegran F, Schroeder T, Wergin MC, Verrax J, Rabbani ZN, De Saedeleer CJ, Kennedy KM, Diepart C, Jordan BF, Kelley MJ, Gallez B, Wahl ML, Feron O, Dewhirst MW. Targeting lactate-fueled respiration selectively kills hypoxic tumor cells in mice. The Journal of clinical investigation. 2008; 118:3930-3942.
13. Seth P, Grant A, Tang J, Vinogradov E, Wang X, Lenkinski R, Sukhatme VP. On-target Inhibition of Tumor Fermentative Glycolysis as Visualized by Hyperpolarized Pyruvate. Neoplasia. 2011; 13:60-71.
14. Park JM, Recht LD, Josan S, Merchant M, Jang T, Yen YF, Hurd RE, Spielman DM, Mayer D. Metabolic response of glioma to dichloroacetate measured in vivo by hyperpolarized (13)C magnetic resonance spectroscopic imaging. Neuro-oncology. 2013; 15:433-441.
15. Hill DK, Orton MR, Mariotti E, Boult JK, Panek R, Jafar M, Parkes HG, Jamin Y, Miniotis MF, Al-Saffar NM, Beloueche-Babari M, Robinson SP, Leach MO, Chung YL, Eykyn TR. Model Free Approach to Kinetic Analysis of Real-Time Hyperpolarized 13C Magnetic Resonance Spectroscopy Data. PLoS ONE. 2013; 8:e71996.
16. Neveu MA, Bol V, Bol A, Bouzin C, Gregoire V, Feron O, Jordan BF, Gallez B. The increase in tumor oxygenation under carbogen breathing induces a decrease in the uptake of [(18)F]-fluoro-deoxy-glucose. Radiotherapy and oncology: journal of the European Society for Therapeutic Radiology and Oncology. 2015; 116:400-403.
17. Stacpoole PW, Nagaraja NV, Hutson AD. Efficacy of Dichloroacetate as a Lactate-Lowering Drug. The Journal of Clinical Pharmacology. 2003; 43:683-691.
18. Bonnet S, Archer SL, Allalunis-Turner J, Haromy A, Beaulieu C, Thompson R, Lee CT, Lopaschuk GD, Puttagunta L, Bonnet S, Harry G, Hashimoto K, Porter CJ, Andrade MA, Thebaud B, Michelakis ED. A mitochondria-K+ channel axis is suppressed in cancer and its normalization promotes apoptosis and inhibits cancer growth. Cancer cell. 2007; 11:37-51.
19. Dunbar EM, Coats BS, Shroads AL, Langaee T, Lew A, Forder JR, Shuster JJ, Wagner DA, Stacpoole PW. Phase 1 trial of dichloroacetate (DCA) in adults with recurrent malignant brain tumors. Investigational new drugs. 2014; 32:452-464.
20. Chu QS, Sangha R, Spratlin J, Vos LJ, Mackey JR, McEwan AJ, Venner P, Michelakis ED. A phase I open-labeled, single-arm, dose-escalation, study of dichloroacetate (DCA) in patients with advanced solid tumors. Investigational new drugs. 2015; 33:603-610.
21. Garon EB, Christofk HR, Hosmer W, Britten CD, Bahng A, Crabtree MJ, Hong CS, Kamranpour N, Pitts S, Kabbinavar F, Patel C, von Euw E, Black A, Michelakis ED, Dubinett SM, Slamon DJ. Dichloroacetate should be considered with platinum-based chemotherapy in hypoxic tumors rather than as a single agent in advanced non-small cell lung cancer. Journal of cancer research and clinical oncology. 2014; 140:443-452.
22. Feuerecker B, Seidl C, Pirsig S, Bruchelt G, Senekowitsch-Schmidtke R. DCA promotes progression of neuroblastoma tumors in nude mice. Am J Cancer Res. 2015; 5:812-820.
23. Josan S, Park JM, Hurd R, Yen YF, Pfefferbaum A, Spielman D, Mayer D. In vivo investigation of cardiac metabolism in the rat using MRS of hyperpolarized [1-13C] and [2-13C]pyruvate. NMR in biomedicine. 2013; 26:1680-1687.
24. Dodd MS, Ball V, Bray R, Ashrafian H, Watkins H, Clarke K, Tyler DJ. In vivo mouse cardiac hyperpolarized magnetic resonance spectroscopy. Journal of cardiovascular magnetic resonance: official journal of the Society for Cardiovascular Magnetic Resonance. 2013; 15:19.

25. Hu S, Yoshihara HA, Bok R, Zhou J, Zhu M, Kurhanewicz J, Vigneron DB. Use of hyperpolarized [1-13C]pyruvate and [2-13C]pyruvate to probe the effects of the anticancer agent dichloroacetate on mitochondrial metabolism in vivo in the normal rat. Magnetic resonance imaging. 2012; 30:1367-1372.

26. Park JM, Josan S, Grafendorfer T, Yen YF, Hurd RE, Spielman DM, Mayer D. Measuring mitochondrial metabolism in rat brain in vivo using MR Spectroscopy of hyperpolarized [2-(1)(3)C]pyruvate. NMR in biomedicine. 2013; 26:1197-1203.

27. Sutendra G, Michelakis ED. Pyruvate dehydrogenase kinase as a novel therapeutic target in oncology. Frontiers in oncology. 2013; 3:38.

28. Fedorchuk AG, Pyaskovskaya ON, Gorbik GV, Prokhorova IV, Kolesnik DL, Solyanik GI. Effectiveness of sodium dichloroacetate against glioma C6 depends on administration schedule and dosage. Exp Oncol. 2016; 38:80-83.

29. Stockwin LH, Yu SX, Borgel S, Hancock C, Wolfe TL, Phillips LR, Hollingshead MG, Newton DL. Sodium dichloroacetate selectively targets cells with defects in the mitochondrial ETC. International Journal of Cancer. 2010; 127:2510-2519.

30. Papandreou I, Goliasova T, Denko NC. Anticancer drugs that target metabolism: Is dichloroacetate the new paradigm? International journal of cancer. 2011; 128:1001-1008.

31. Neveu MA, De Preter G, Marchand V, Bol A, Brender JR, Saito K, Kishimoto S, Porporato PE, Sonveaux P, Grégoire V, Feron O, Jordan BF, Krishna MC, Gallez B. Multimodality imaging identifies distinct metabolic profiles in vitro and in vivo. Neoplasia. In press.

www.impactjournals.com/oncotarget/ Oncotarget, Supplementary Materials 2016

Multi-modality imaging to assess metabolic response to dichloroacetate treatment in tumor models

SUPPLEMENTARY FIGURES

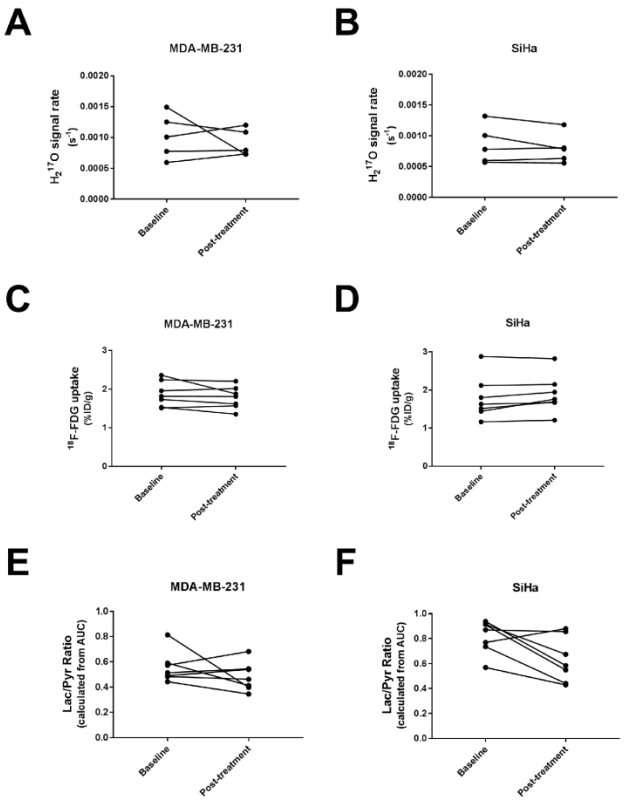

Supplementary Figure S1: Individual tumor responses to DCA treatment in MDA-MB-231 tumors (left side) and SiHa tumors (right side), assessed by $^{17}O_2$ metabolism A-B., ^{18}F-FDG uptake C-D. and pyruvate transformation into lactate E-F.

www.impactjournals.com/oncotarget/ Oncotarget, Supplementary Materials 2016

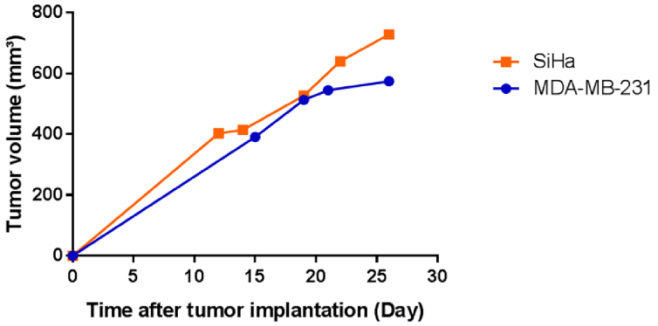

Supplementary Figure S2: Growth curves of MDA-MB-231 and SiHa tumors. Data are expressed as mean values, n = 8 per tumor models.

www.impactjournals.com/oncotarget/ Oncotarget, Supplementary Materials 2016

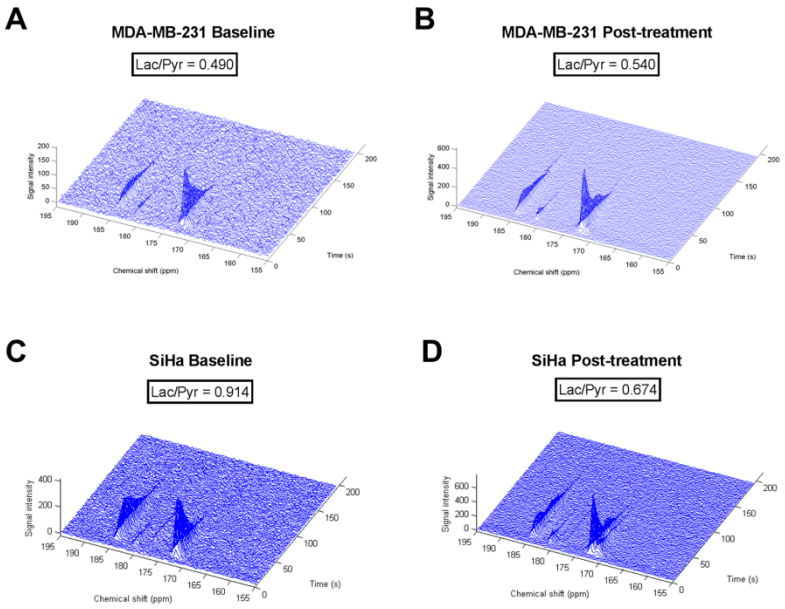

Supplementary Figure S3: Typical ^{13}C-MRS spectra from representative MDA-MB-231 tumors A-B. and SiHa tumors C-D.: pyruvate (173 ppm), lactate (185 ppm) peaks and pyruvate hydrate (181 ppm). Bicarbonate (162 ppm) was not observed before or after treatment, in both tumor models.

3. Characterization of metabolic behavior in tumors using imaging biomarkers

3.1. Impact of oxygenation status on ^{18}F-FDG uptake in tumors

The increase in tumor oxygenation under carbogen breathing induces a decrease in the uptake of [^{18}F]-fluoro-deoxy-glucose

Marie-Aline Neveu, Vanesa Bol, Anne Bol, Caroline Bouzin, Vincent Grégoire, Olivier Feron, Benedicte F. Jordan and Bernard Gallez

Radiotherapy and Oncology 2015 Sep; 116(3): 400-403

Radiotherapy and Oncology 116 (2015) 400–403

Contents lists available at ScienceDirect

Radiotherapy and Oncology

journal homepage: www.thegreenjournal.com

Hypoxia

The increase in tumor oxygenation under carbogen breathing induces a decrease in the uptake of [^{18}F]-fluoro-deoxy-glucose ☆

Marie-Aline Neveu [a], Vanesa Bol [b], Anne Bol [b], Caroline Bouzin [c], Vincent Grégoire [b], Olivier Feron [c], Benedicte F. Jordan [a], Bernard Gallez [a,*]

[a] Biomedical Magnetic Resonance Research Group; [b] Radiation Oncology Department & Center for Molecular Imaging; and [c] Pole of Pharmacology and Therapeutics, Université catholique de Louvain (UCL), Belgium

ARTICLE INFO

Article history:
Received 6 February 2015
Received in revised form 14 April 2015
Accepted 29 April 2015
Available online 14 May 2015

Keywords:
^{18}F-FDG-PET
EPR
Tumor oxygenation
Carbogen

ABSTRACT

We investigated the impact of oxygenation status (measured by EPR oximetry) on the uptake of ^{18}F-FDG (measured by PET) in two different tumor models during a carbogen breathing challenge. We observed a significant drop in ^{18}F-FDG uptake under carbogen breathing that suggests a rapid metabolic adaptation to the oxygen environment.

Hypoxia is known as a major factor in tumor progression, metastasis and response to treatment, especially radiotherapy. It is well established that glucose transporters (GLUTs) are upregulated by chronic hypoxia [1]. As a consequence, it has been suggested that high [^{18}F]-fluoro-deoxy-glucose (^{18}F-FDG) uptake measured by Positron Emission Tomography (PET) may reflect the level of tumor hypoxia. Nevertheless conflicting results were reported and the debate is still ongoing [2]. Indeed, in tumors, high ^{18}F-FDG uptake can also arise under non-hypoxic condition through a process known as aerobic glycolysis or Warburg effect [2,3]. The objectives of the present study were twofold: (1) to assess the link between ^{18}F-FDG uptake and tumor oxygenation by comparing micro-PET data with Electron Paramagnetic Resonance (EPR) oximetry that provides absolute pO_2 measurements [4,5]; (2) to assess the influence of rapid changes in tumor oxygenation on the uptake of ^{18}F-FDG using different oxic conditions (carbogen or air breathing). The study was carried out in two different tumor xenografts, MDA-MB-231 and SiHa models selected according to their glycolytic [3] and oxidative [6] behavior respectively.

Materials and methods

Animal and tumor models

A total of 10^7 MDA-MB-231 cells (ATCC) or 10^7 SiHa cells (ATCC), amplified in vitro, were collected by trypsinization, washed three times with Hanks balanced salt solution and resuspended in 200 μL of a 1:1 mixture of Matrigel (BD Biosciences) and Hanks balanced salt solution. The tumor cells were inoculated subcutaneously into the hind thigh of nude NMRI female mice (Janvier). The experiments were performed when tumors reached 7 mm in diameter to limit partial volume effects (at this tumor size, necrosis was less than 5% at this stage of development as characterized by Hematoxylin Eosin staining). A total of 16 MDA-MB-231 tumors and 12 SiHa tumors were used in the study.

Experimental design

Mice were fasted overnight before the measurements. Animals were anesthetized by inhalation of isoflurane (Forene, Abbot, England) mixed with either air (21% oxygen) or carbogen (5% CO_2/95% oxygen), depending on the breathing condition tested, in a continuous flow (2 L/min). Animals were warmed (approximately 35 °C) throughout the anesthesia period. Mice were scanned twice for the breathing challenge, air versus carbogen breathing, with one day between each condition (crossed conditions tested). The protocol is summarized in Supplementary Fig. 1. For each breathing condition, EPR measurements were performed before PET imaging in the same animals.

☆ This work has been presented in part at the 42nd Meeting of the International Society on Oxygen Transport to Tissue (ISOTT), June 28–July 3, 2014, London, UK.

* Corresponding author at: Biomedical Magnetic Resonance Unit – REMA, Louvain Drug Research Institute (LDRI), Université catholique de Louvain, Avenue Mounier, 73.08, B-1200 Brussels, Belgium.
E-mail address: bernard.gallez@uclouvain.be (B. Gallez).

http://dx.doi.org/10.1016/j.radonc.2015.04.023
0167-8140/

EPR oximetry

In vivo tumor pO_2 was monitored by EPR spectroscopy using charcoal as the oxygen-sensitive probe [4,5]. EPR spectra were recorded using a 1.1 GHz EPR spectrometer (Magnettech, Berlin, Germany). According to calibration curves made by measuring the EPR line width as a function of the pO_2 [7], the EPR spectra line width was converted to pO_2. A charcoal suspension (100 mg/mL) was injected intratumorally (60 µl) 24 h before experiments. For EPR readings, the tumor under study was placed in the center of the extended loop resonator whose sensitive volume extends 1 cm into the tumor mass. The pO_2 measurements correspond to an average of pO_2 values in the tumor volume. For air condition, basal measurements were performed. For carbogen condition, pO_2 measurements were started after a 10 min inhalation period.

PET/CT imaging

Whole-body PET imaging was performed on a dedicated small-animal PET scanner (Mosaic, Philips Medical Systems, Cleveland, USA) with a spatial resolution of 2.5 mm (FWHM). The PET scans were followed by whole-body acquisitions using a helical CT scanner (NanoSPECT/CT Small Animal Imager, Bioscan Inc., DC, USA). For each breathing condition, anesthetized mice were injected 120 µl intraperitoneally with 300–400 µCi of ^{18}F-FDG (Betaplus Pharma, Brussels, Belgium). A 10 min transmission scan was first obtained in a single mode using a 370 MBq ^{137}Cs source for attenuation correction. A 10 min static PET acquisition was then performed after a 60 min resting period. After the correction with attenuation factors obtained from the transmission scan, images were reconstructed using a fully 3D iterative algorithm (3D-RAMLA) in a 128 × 128 × 120 matrix, with a voxel size of 1 mm^3. After PET acquisition, anesthetized animals were transferred on the same bed from the PET scanner to the CT scanner (X-ray tube voltage: 55 kVp; number of projections: 180; exposure time 1000 ms) for anatomical reference. The CT projections were reconstructed with a voxel size of 0.221 × 0.221 × 0.221 mm^3. Regions of Interest (ROIs) were delineated on PET images using PMOD software (PMOD™, version 3.403, PMOD technologies Ltd, Zurich, Switzerland). 2D ROIs were established on consecutive transversal slices using a 50% isocontour tool (ROI including the pixel values larger than 50% of the maximum pixel) that semi-automatically defined a 3D Volume of Interest (VOI) around the tissue of interest. To avoid overestimation of the uptake within the VOI, PET/CT fused images where used to discriminate hot pixels coming from the neighboring tissues like urinary bladder. Using the mean uptake within this VOI, the global tracer uptake was assessed in tumors and expressed as percentage of injected dose per gram of tissue (%ID/g).

Statistics analysis

Paired *t*-tests were used to compare mean changes between groups (air vs. carbogen) for each tumor model and non-paired *t*-tests were used to compare mean changes between the two tumor models. Analysis was performed using the Graphpad software. Results were expressed as mean value of parameter ± SEM. For all tests, results with $P < 0.05$ (*),<0.01 (**), or <0.001 (***) were considered significant. The scatter plots of measured pO_2 as a function of %ID/g were traced using data from all tumors of both groups. The process of finding the best fit was done by using CurveExpert software (version 1.4).

Results

The pO_2 values and the ^{18}F-FDG uptake (%ID/g) measured in both tumor models under both breathing conditions are presented in Fig. 1. In both tumor models, we found that carbogen breathing led to a significant increase in tumor oxygenation and a significant decrease in the uptake of ^{18}F-FDG. Basal measured pO_2 (mean ± SEM) were 3.8 ± 0.2 mmHg for MDA-MB-231 tumors and 4.9 ± 0.3 mmHg for SiHa tumors. Under carbogen breathing, MDA-MB-231 and SiHa tumors reached pO_2 around 9.9 ± 0.95 mmHg and 16.0 ± 2.3 mmHg respectively. %ID/g measured on PET images (mean ± SEM) were 2.47 ± 0.09 under air and 1.98 ± 0.07 under carbogen for MDA-MB-231 tumors (n = 16) and 2.52 ± 0.12 under air and 1.98 ± 0.08 under carbogen for SiHa

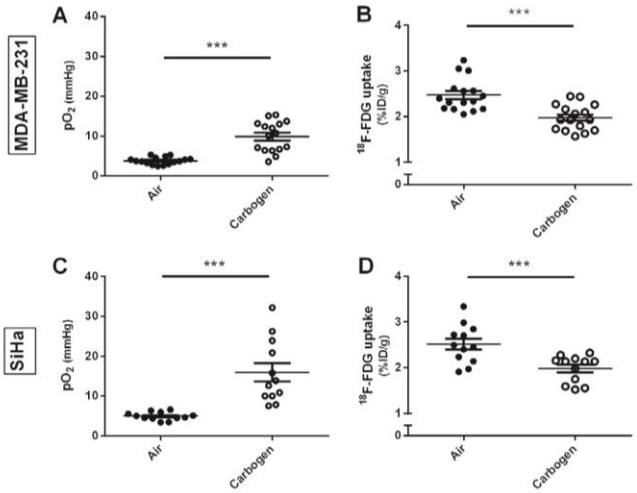

Fig. 1. pO_2 and ^{18}F-FDG uptake under air and carbogen breathing in MDA-MB-231 tumors (upper row) and SiHa tumors (lower row). A significant change of pO_2 was observed during the breathing challenge for each tumor model (A and C). A lower uptake of ^{18}F-FDG was observed under hyperoxic conditions compared to normoxic conditions in both tumor models (B and D).

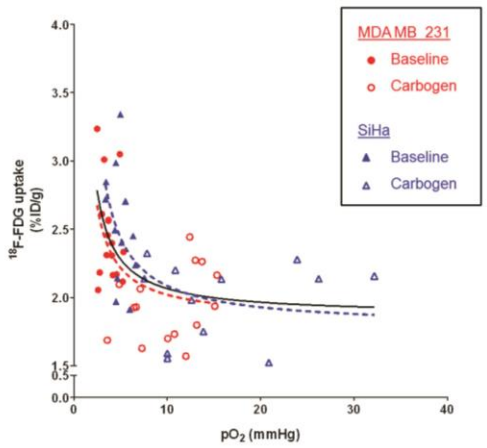

Fig. 2. Relationship between ^{18}F-FDG uptake and pO_2 values during air (filled symbol) and carbogen breathing (open symbol) presented as a non-linear fit for MDA-MB-231 (red line), SiHa (blue line), and pooled data (black line). The ^{18}F-FDG uptake was higher in hypoxic tumors compared to tumors with pO_2 larger than 10 mmHg. (For interpretation of the references to color in this figure legend, the reader is referred to the web version of this article.)

tumors ($n = 12$). Similar results were found by expressing the ^{18}F-FDG uptake as SUV. Fig. 2 shows the relationship between ^{18}F-FDG uptake and pO_2 measurements obtained from individual tumors (mice breathing air or carbogen). According to CurveExpert software, the best fit were $y = 1.84e^{0.93/x}$, $y = 1.78e^{1.56/x}$, $y = 1.87e^{0.99/x}$ for MDA-MB-231, SiHa, and pooled data, respectively. In both tumor models, the ^{18}F-FDG uptake was higher in tumors with a pO_2 value inferior to 10 mmHg.

Discussion

In this study, the experimental design was built as a dynamic follow-up of the tumors during a breathing challenge to determine the correlation between global ^{18}F-FDG PET uptake and pO_2 values for each tumor tested under different breathing conditions. Carbogen breathing influences several physiological parameters in tumors like oxygenation status, blood flow, extracellular pH, proliferation and energy status [8–11], changes described as tumor-dependent. In this study, carbogen has been investigated as a modulator of hypoxia in the two tumor models and pO_2 variation has been assessed by EPR oximetry. To our knowledge, it is the first time that EPR, a highly sensitive method to measure pO_2 values in vivo [7], has been associated to global ^{18}F-FDG uptake measurement in vivo. A higher ^{18}F-FDG uptake has been found in tumors with a pO_2 value inferior to 10 mmHg, a status encountered at the basal level (air breathing) in most tumors belonging to both tumor models. This observation could be consistent with the upregulation of the expression of glucose transporters and glycolytic enzymes that are associated with hypoxia. However, we also found that the uptake of ^{18}F-FDG was lower after a short period of carbogen breathing. This observation emphasizes that the tracer uptake is not only dependent on transcriptional changes (like glucose transporters GLUTs). It also most likely relies on the rapid adaptation of the tumor cell metabolism when oxygen became available, a phenomenon known as the Pasteur Effect. This was true for both tumor models although their metabolic phenotype characterized in vitro indicate that the MDA-MB-231 tumor model is highly glycolytic [3] compared to the SiHa model that possess an oxidative phenotype [6].

^{18}F-FDG PET is a widespread technology approved in clinical practice for cancer diagnosis, staging and treatment monitoring. Beyond these applications, it has been suggested in the literature that ^{18}F-FDG uptake could also indirectly reflect the oxygenation status of tumors, a major factor involved in resistance to radiation therapy. This assertion has already been discussed in several studies providing discordant results [12–21]. Here, we found in both tumor models an inverse relationship between ^{18}F-FDG uptake and pO_2 values, a behavior that is rather comparable to what has been found with several nitroimidazoles such as EF_3 [22] and ^{18}F-FAZA [23]. Our present findings are consistent with the study of Christian et al. that showed that the ^{18}F-FDG uptake was higher under severe hypoxia compared to normoxic conditions [21]. However, this trend was found only when considering results on the whole tumor. Indeed, Christian et al. also found that the correlation at the microscopic level was poor when considering the co-localization of ^{18}F-FDG uptake and of the nitroimidazole ^{14}C-EF3. Nevertheless, other studies have established a positive correlation between ^{18}F-FDG uptake and hypoxia using regional [24] or pixel by pixel analysis [25]. As commented by Pugachev and co-workers, the use of a thick section for autoradiography in Christian et al. study could explain the poor correlation reported [26].

Therefore, there is a need to take cautiously any relationship between oxygenation status and ^{18}F-FDG uptake, as the latter is dependent on other factors than oxygenation. Overall, our results highlight the rapid plasticity of the tumor cells to adapt their metabolism to the oxygen environment.

Conclusion

In conclusion, our longitudinal study demonstrates a rapid metabolic adaptation during the carbogen challenge in both tumor models investigated according to the significant drop of ^{18}F-FDG uptake under carbogen breathing compared to air breathing.

Research funding

This study was supported by grants from Belgian National Fund for Scientific Research (FNRS), the Fonds Joseph Maisin, the Action de Recherches Concertées.

Conflicts of interest

None.

Appendix A. Supplementary data

Supplementary data associated with this article can be found, in the online version, at http://dx.doi.org/10.1016/j.radonc.2015.04.023.

References

[1] Brahimi-Horn MC, Chiche J, Pouyssegur J. Hypoxia and cancer. Mol Med 2007;85:1301–7.
[2] Dierckx RA, Van de Wiele C. FDG uptake, a surrogate of tumour hypoxia? Eur J Nucl Med Mol Imag 2008;35:1544–9.
[3] Gatenby RA, Gillies RJ. Why do cancers have high aerobic glycolysis? Nat Rev Cancer 2004;4:891–9.
[4] Gallez B, Jordan BF, Baudelet C, Misson PD. Pharmacological modifications of the partial pressure of oxygen in murine tumors: evaluation using in vivo EPR oximetry. Magn Reson Med 1999;42:627–30.
[5] Jordan BF, Baudelet C, Gallez B. Carbon-centered radicals as oxygen sensors for in vivo electron paramagnetic resonance: screening for an optimal probe among commercially available charcoals. MAGMA 1998;7:121–9.

[6] Sonveaux P, Vegran F, Schroeder T, et al. Targeting lactate-fueled respiration selectively kills hypoxic tumor cells in mice. J Clin Invest 2008;118:3930–42.
[7] Gallez B, Baudelet C, Jordan BF. Assessment of tumor oxygenation by electron paramagnetic resonance: principles and applications. NMR Biomed 2004; 17:240–62.
[8] Bussink J, Kaanders JH, Rijken PF, et al. Vascular architecture and microenvironmental parameters in human squamous cell carcinoma xenografts: effects of carbogen and nicotinamide. Radiother Oncol 1999; 50:173–84.
[9] Secomb TW, Hsu R, Ong ET, Gross JF, Dewhirst MW. Analysis of the effects of oxygen supply and demand on hypoxic fraction in tumors. Acta Oncol 1995; 34:313–6.
[10] van der Sanden BP, Heerschap A, Hoofd L, et al. Effect of carbogen breathing on the physiological profile of human glioma xenografts. Magn Reson Med 1999;42:490–9.
[11] van Laarhoven HW, Bussink J, Lok J, Punt CJ, Heerschap A, van Der Kogel AJ. Effects of nicotinamide and carbogen in different murine colon carcinomas: immunohistochemical analysis of vascular architecture and microenvironmental parameters. Int J Radiat Oncol Biol Phys 2004;60:310–21.
[12] Busk M, Horsman MR, Kristjansen PE, van der Kogel AJ, Bussink J, Overgaard J. Aerobic glycolysis in cancers: implications for the usability of oxygen-responsive genes and fluorodeoxyglucose-PET as markers of tissue hypoxia. Int J Cancer 2008;122:2726–34.
[13] Busk M, Horsman MR, Jakobsen S, Bussink J, van der Kogel A, Overgaard J. Cellular uptake of PET tracers of glucose metabolism and hypoxia and their linkage. Eur J Nucl Med Mol Imag 2008;35:2294–303.
[14] Waki A, Fujibayashi Y, Yonekura Y, Sadato N, Ishii Y, Yokoyama A. Reassessment of FDG uptake in tumor cells: high FDG uptake as a reflection of oxygen-independent glycolysis dominant energy production. Nucl Med Biol 1997;24:665–70.
[15] Clavo AC, Brown RS, Wahl RL. Fluorodeoxyglucose uptake in human cancer cell lines is increased by hypoxia. J Nucl Med 1995;36:1625–32.
[16] Burgman P, Odonoghue JA, Humm JL, Ling CC. Hypoxia-Induced increase in FDG uptake in MCF7 cells. J Nucl Med 2001;42:170–5.
[17] Chan LW, Hapdey S, English S, et al. The influence of tumor oxygenation on (18)F-FDG (fluorine-18 deoxyglucose) uptake: a mouse study using positron emission tomography (PET). Radiat Oncol 2006;1:3.
[18] Gagel B, Piroth M, Pinkawa M, et al. pO polarography, contrast enhanced color duplex sonography (CDS), [18F] fluoromisonidazole and [18F] fluorodeoxyglucose positron emission tomography: validated methods for the evaluation of therapy-relevant tumor oxygenation or only bricks in the puzzle of tumor hypoxia? BMC Cancer 2007;7:113.
[19] de Geus-Oei LF, Kaanders JH, Pop LA, Corstens FH, Oyen WJ. Effects of hyperoxygenation on FDG-uptake in head-and-neck cancer. Radiother Oncol 2006;80:51–6.
[20] Li XF, Ma Y, Sun X, Humm JL, Ling CC, O'Donoghue JA. High 18F-FDG uptake in microscopic peritoneal tumors requires physiologic hypoxia. J Nucl Med 2010;51:632–8.
[21] Christian N, Deheneffe S, Bol A, et al. Is (18)F-FDG a surrogate tracer to measure tumor hypoxia? Comparison with the hypoxic tracer (14)C-EF3 in animal tumor models. Radiother Oncol 2010;97:183–8.
[22] Mahy P, De Bast M, Gallez B, et al. In vivo colocalization of 2-nitroimidazole EF5 fluorescence intensity and electron paramagnetic resonance oximetry in mouse tumors. Radiother Oncol 2003;67:53–61.
[23] Tran LBA, Bol A, Labar D, et al. Hypoxia imaging with the nitroimidazole 18F-FAZA PET tracer: a comparison with OxyLite, EPR oximetry and 19F-MRI relaxometry. Radiother Oncol 2012;105:29–35.
[24] Dearling JL, Flynn AA, Sutcliffe-Goulden J, et al. Analysis of the regional uptake of radiolabeled deoxyglucose analogs in human tumor xenografts. J Nucl Med 2004;45:101–7.
[25] Pugachev A, Ruan S, Carlin S, et al. Dependence of FDG uptake on tumor microenvironment. Int J Radiat Oncol Biol Phys 2005;62:545–53.
[26] Pugachev A, Axente M, Humm J. On autoradiographic studies comparing the distributions of ^{18}F- and ^{14}C-labeled compounds in tumor tissue specimens. Radiother Oncol 2010;97:609.

Supplementary Figure

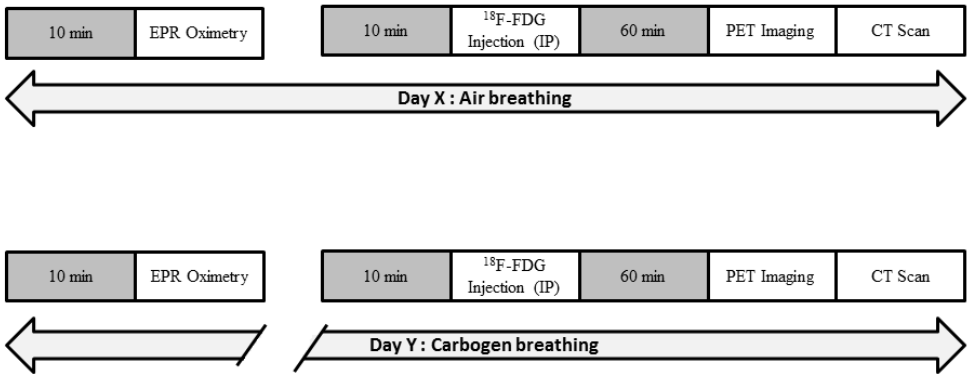

Supplementary Fig. 1: Experimental design built as a dynamic follow-up of the tumors during a breathing challenge. Mice were scanned twice for the breathing challenge, air versus carbogen breathing, with one day between each condition. Crossed conditions were tested for the breathing challenge and the animal cohort was divided in 2 groups. Condition Day 1 air/Day 2 carbogen was tested in 8 MDA-MB-231 and 6 SiHa tumors. Condition Day 1 carbogen/Day 2 air was tested in the remaining 8 MDA-MB-231 and 6 SiHa tumors.

3.2. Metabolic behavior of 2 well-established tumor models in vitro and in vivo

Multimodality imaging identifies distinct metabolic profiles in vitro and in vivo

Marie-Aline Neveu, Géraldine De Preter, Valérie Marchand, Anne Bol, Jeffery R. Brender, Keita Saito, Shun Kishimoto, Paolo E. Porporato, Pierre Sonveaux, Vincent Grégoire, Olivier Feron, Bénédicte F. Jordan, Murali C. Krishna, and Bernard Gallez

Neoplasia. 2016; 18: 742-752

NEOPLASIA
www.neoplasia.com

Volume 18 Number xx Month 2016 pp. 742–752 742

Multimodality Imaging Identifies Distinct Metabolic Profiles *In Vitro* and *In Vivo*[1]

Marie-Aline Neveu[*], Géraldine De Preter[*], Valérie Marchand[*], Anne Bol[†], Jeffery R. Brender[‡], Keita Saito[‡], Shun Kishimoto[‡], Paolo E. Porporato[§], Pierre Sonveaux[§], Vincent Grégoire[†], Olivier Feron[§], Bénédicte F. Jordan[*], Murali C. Krishna[‡] and Bernard Gallez[*]

[*]Biomedical Magnetic Resonance Research Group, Louvain Drug Research Institute (LDRI), Université catholique de Louvain, Brussels, Belgium; [†]Radiation Oncology Department & Center for Molecular Imaging, Radiotherapy & Oncology, Institute of Experimental and Clinical Research (IREC), Université catholique de Louvain, Brussels, Belgium; [‡]Radiation Biology Branch, National Cancer Institute, NIH, Bethesda, USA; [§]Pole of Pharmacology and Therapeutics, Institute of Experimental and Clinical Research (IREC), Université catholique de Louvain, Brussels, Belgium

Abstract

The study of alterations of tumor metabolism should allow the identification of new targets for innovative anticancer strategies. Metabolic alterations are generally established *in vitro*, and conclusions are often extrapolated to the *in vivo* situation without further tumor metabolic phenotyping. To highlight the key role of microenvironment on tumor metabolism, we studied the response of glycolytic and oxidative tumor models to metabolic modulations *in vitro* and *in vivo*. MDA-MB-231 and SiHa tumor models, characterized *in vitro* as glycolytic and oxidative, respectively, were studied. Theoretically, when passing from a hypoxic state to an oxygenated state, a Warburg phenotype should conserve a glycolytic metabolism, whereas an oxidative phenotype should switch from glycolytic to oxidative metabolism (Pasteur effect). This challenge was applied *in vitro* and *in vivo* to evaluate the impact of different oxic conditions on glucose metabolism. ^{18}F-fluorodeoxyglucose uptake, lactate production, tumor oxygenation, and metabolic fluxes were monitored *in vivo* using positron emission tomography, microdialysis, electron paramagnetic resonance imaging, and ^{13}C-hyperpolarizated magnetic resonance spectroscopy, respectively. *In vitro*, MDA-MB-231 cells were glycolytic under both hypoxic and oxygenated conditions, whereas SiHa cells underwent a metabolic shift after reoxygenation. On the contrary, *in vivo*, the increase in tumor oxygenation (induced by carbogen challenge) led to a similar metabolic shift in glucose metabolism in both tumor models. The major discordance in metabolic patterns observed *in vitro* and *in vivo* highlights that any extrapolation of *in vitro* metabolic profiling to the *in vivo* situation should be taken cautiously and that metabolic phenotyping using molecular imaging is mandatory *in vivo*.

Neoplasia (2016) 18, 742–752

Introduction

Enhanced glycolysis has for a long time been recognized as a common metabolic feature of cancer [1–3]. Otto Warburg identified in the 1920s the presence of a faster glycolytic flux in tumor cells [4], characterized by a high glucose uptake and increased lactate production even in the presence of oxygen. Despite a limited capacity for ATP production, aerobic glycolysis confers a major advantage to tumor cells by supporting proliferation and biomass production [3,5,6]. During decades, the loss of coupling between

Address all correspondence to: Bernard Gallez, Biomedical Magnetic Resonance Unit–REMA, Louvain Drug Research Institute (LDRI), Université catholique de Louvain, Avenue Mounier, 73.08, B-1200 Brussels.
E-mail: bernard.gallez@uclouvain.be

[1]This study was funded by grants from the Belgian National Fund for Scientific Research (F.S.R.-FNRS; PDR T.0107.13), the Fonds Joseph Maisin, the Action de Recherches Concertées ARC 14/19-058, Belgian Science Policy Office Interuniversity Attraction Pole IUAP #P7/03, and intramural National Institute of Health funds.
Received 7 September 2016; Revised 25 October 2016; Accepted 27 October 2016

1476-5586/16
http://dx.doi.org/10.1016/j.neo.2016.10.010

glycolysis and oxidative phosphorylation (OXPHOS) in tumor cells has been assigned to major mitochondrial dysfunctions [7]. However, new evidence of oxidative activities in tumor cells has challenged this paradigm [8–12]. Indeed, some tumor cells majorly rely on OXPHOS for energy production, and besides the Warburg and oxidative phenotypes, some cancer exhibits hybrid phenotypes with an acquired metabolic flexibility.

Tumor metabolic alterations recently emerged as enticing targets for the development of anticancer treatments [13–16]. To identify potential treatment strategies, the specific descriptions of biochemical pathways and metabolic alterations are commonly carried out in well-established tumor models via *in vitro* phenotyping, which provides specific tests that can define distinct metabolic profiles. *In vivo* tumor models are then generally selected based on these *in vitro* characterizations and used for preclinical studies before clinical translation. Because *in vitro* models do not reflect the complex structure and the metabolic heterogeneity of tumors, numerous factors could potentially be underestimated when translating the models from *in vitro* to *in vivo*. Vascularization, cell density, metabolic competition, cooperation, and commensalism with host cells could indeed contribute to the metabolic pattern exhibited by tumor cells.

Because some reports highlighted the potential influence of tumor environment on metabolic profile of cancer cells [17,18], the objective of the present study was to investigate if tumor models differ in their metabolic phenotypes *in vitro* and *in vivo*. To answer this question, a global metabolic study was carried out *in vitro* and *in vivo* using prototypical tumor models. The MDA-MB-231 human breast cancer model and the SiHa human cervical cancer model were selected based on a previous *in vitro* study describing the cell lines as glycolytic and oxidative, respectively [19]. Glucose metabolism was analyzed under hypoxic and oxygenated conditions. According to a paradigm extensively applied *in vitro*, we hypothesized that when passing from hypoxia to a better oxygenated state, a Warburg phenotype should conserve a glycolytic behavior, whereas an oxidative phenotype should metabolically switch from glycolysis to OXPHOS (Pasteur effect). Advanced imaging techniques including positron emission tomography (PET), electron paramagnetic resonance (EPR) imaging, and ^{13}C-hyperpolarizated magnetic resonance spectroscopy (MRS) were used to characterize the metabolic phenotype *in vivo*. Our results identified major discordances between metabolic profiles determined *in vitro* and *in vivo*, highlighting the limitations of direct extrapolation of *in vitro* findings to the *in vivo* situation.

Material and Methods

Cell Culture

MDA-MB-231 (human breast cancer) and SiHa (human cervix squamous cell carcinoma) cell lines (American Type Culture Collection) were routinely cultured in Dulbecco's modified Eagle's medium containing 4.5 g/l of glucose supplemented with 10% fetal bovine serum and 1% penicillin-streptomycin.

Metabolic Fluxes In Vitro

Glucose utilization and lactate production were measured from supernatants of cultured cells under hypoxia or after reoxygenation. Cells were seeded in six-well plates and incubated until 70% to 80% confluence under hypoxic condition (1% O_2). Before the initiation of the experiment, the incubation medium was removed. Cells were quickly washed, and medium was changed to a low-glucose medium without glutamine. The cells were returned in the incubator under hypoxic condition. After 4 hours under hypoxia, supernatant of cultured cells was sampled. Cells were then returned in the incubator to remain under constant hypoxia for 24 hours or moved to aerobic condition (21% O_2) during 20 hours. At the end of the experiment, a final sampling of supernatant was performed for each condition, constant hypoxia or reoxygenation. The protocol is summarized in Figure 1. The supernatants collected were deproteinized. Glucose and lactate concentrations in samples were measured using specific enzymatic assays on a CMA600 microdialysis analyzer (CMA Microdialysis AB, Solna, Sweden).

Animal and Tumor Models

Animal studies were undertaken in accordance with Belgian and the Université catholique de Louvain ethical committee regulations (agreements number UCL/2010/MD/001 and UCL/2014/MD/026). EPR imaging and hyperpolarized ^{13}C-MRS experiments were carried out in compliance with the Guide for the Care and Use of Laboratory Animal Resources (National Research Council, 1996) and approved by the National Cancer Institute (NCI) Animal Care and Use Committee.

To establish subcutaneous tumor models, a total of 10^7 MDA-MB-231 cells or 10^7 SiHa cells, amplified *in vitro*, were collected by trypsinization, washed three times with Hanks balanced salt solution, and resuspended in 200 µl of a 1:1 mixture of Matrigel (BD Biosciences) and Hanks balanced salt solution. For EPR spectroscopy, PET/computed tomography (CT) imaging, and microdialysis experiments, the tumor cells were inoculated subcutaneously into the right hind thigh of nude female NMRI mice (Janvier Le Genest-Saint-Isle, France). For EPR imaging and hyperpolarized ^{13}C-MRS experiments, the tumor cells were inoculated subcutaneously into the right hind thighs of athymic nude female mice supplied by Frederick Cancer Research Center (Animal Production, Frederick, MD). The mice were kept under standard housing and feeding conditions. A total of 29 MDA-MB-231 tumors and 26 SiHa tumors were scanned of this study. All the experiments were performed when tumors reached 7 mm in diameter.

Tumor Metabolic Fluxes

To evaluate the effect of different oxic conditions on tumor metabolism, tumor-bearing mice were scanned twice for the breathing challenge, air versus carbogen breathing, with 1 day between each condition. The experimental design for *in vivo* experiments is presented in Figure 2. Animals were anesthetized by inhalation of isoflurane (Forene, Abbot, England) mixed with either air (21% oxygen) or carbogen (5% CO_2/95% oxygen), depending on the breathing condition tested, in a continuous flow (2 l/min). Animals were warmed (approximately 35°C) throughout the anesthesia period, and breathing rate was maintained at 80 ± 10 breaths per minute using 1.5% to 2% isoflurane.

EPR Spectroscopy

In vivo tumor pO_2 was monitored by EPR spectroscopy using charcoal as the oxygen-sensitive probe [20,21]. EPR spectra were recorded using a 1.1-GHz EPR spectrometer (Magnettech, Berlin, Germany). According to calibration curves made by measuring the EPR line width as a function of the pO_2 [22], the EPR spectra line width was converted to pO_2. A charcoal suspension (100 mg/ml) was

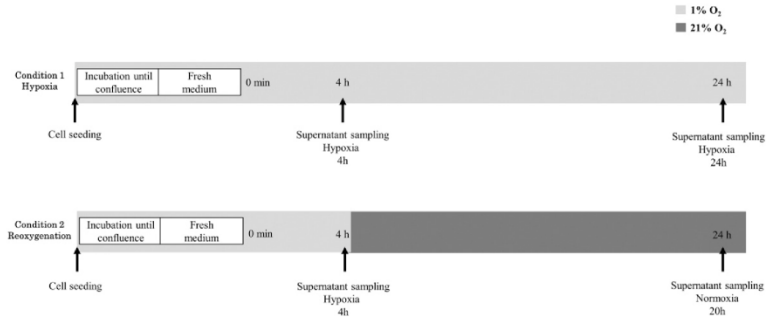

Figure 1. *In vitro* metabolic fluxes. The impact of different oxic conditions on tumor cell metabolism was investigated.

injected intratumorally (60 µl), and experiments were initiated 24 hours after EPR probe implantation [23]. For EPR readings, the tumor under study was placed in the center of the extended loop resonator whose sensitive volume extends 1 cm into the tumor mass. pO_2 measurements correspond to the average of pO_2 values in the tumor volume under study. For air condition, basal measurements were performed. For carbogen condition, pO_2 measurements were started after a 10-minute inhalation period. Crossed conditions were tested for the breathing challenge, the animal cohort was divided into two groups, and the following conditions were tested: day 1 air/day 2 carbogen or day 1 carbogen/day 2 air. The details of the protocol are presented in Figure 2*A*.

EPR Imaging

Tumor pO_2 maps were obtained under air and carbogen breathing using an EPR imaging scanner equipped with a volume leg coil resonator tuned to 300 MHz. After the animal was positioned prone with the tumor-bearing leg placed inside the resonator, the EPR oxygen probe (OXO63, GE Healthcare) was injected intravenously as a 1.125-mmol/kg bolus through a cannula placed in the tail vein. EPR signals were obtained following the RF excitation pulses (60 nanoseconds, 80 W, 70° flip angle) using an analog-to-digital converter (200 megasamples/s). The repetition time was 8 microseconds. The free induction decay curves were collected under a nested loop of the *x*, *y*, and *z* gradients, and each time point in the free induction decay curve underwent phase modulation enabling three-dimensional (3D) spatial encoding. Anatomical reference was obtained using a 3-T magnetic resonance imaging (MRI) scanner (MR Solutions, Guildford, UK). The imaging protocol is detailed in Figure 2*B*. Co-registration of EPR and MRI images and data analysis were accomplished using MATLAB software (Mathworks). From the pO_2 images of the tumor, pO_2 frequency distributions and median tumor pO_2 were calculated.

PET/CT Imaging

Tumor ^{18}F-FDG uptake was assessed during the breathing challenge using PET/CT imaging. Whole-body PET imaging was performed on a dedicated small-animal PET scanner (Mosaic, Philips Medical Systems, Cleveland, OH) with a spatial resolution of 2.5 mm (full width at half maximum). The PET scans were followed by whole-body acquisitions using a helical CT scanner (NanoSPECT/CT Small Animal Imager, Bioscan Inc., Washington DC). For each breathing condition, anesthetized mice were injected 120 µl intraperitoneally with 11.1 to 14.8 MBq of ^{18}F-FDG (Betaplus Pharma, Brussels, Belgium). A 10-minute transmission scan was first obtained in a single mode using a 370-MBq ^{137}Cs source for attenuation correction. A 10-minute static PET acquisition was then performed after a 60-minute resting period. After the correction with attenuation factors obtained from the transmission scan, images were reconstructed using a fully 3D row action maximum likelihood algorithm in a 128 × 128 × 120 matrix, with a voxel size of 1 mm^3. After PET acquisition, anesthetized animals were transferred on the same bed from the PET scanner to the CT scanner (x-ray tube voltage: 55 kVp; number of projections: 180; exposure time 1000 milliseconds). The CT projections were reconstructed with a voxel size of 0.221 × 0.221 × 0.221 mm^3. The details of the imaging protocol are presented in Figure 2*A*. Regions of Interest (ROIs) were delineated on fused PET/CT images using PMOD software (PMOD, version 3.403, PMOD Technologies Ltd., Zurich, Switzerland). Two-dimensional ROIs were established on consecutive transversal slices using a 50% isocontour tool (ROI including the pixel values larger than 50% of the maximum pixel) that semiautomatically defined a 3D volume of interest (VOI) around the tissue of interest. To avoid overestimation of the uptake within the VOI, PET/CT fused images where used to discriminate hot pixels coming from the neighboring tissues like urinary bladder. Using the mean uptake within this VOI, the global tracer uptake was assessed in tumors and expressed as percentage of injected dose per gram of tissue (%ID/g). Crossed conditions were tested for the breathing challenge, the animal cohort was divided into two groups, and the following conditions were tested: day 1 air/day 2 carbogen or day 1 carbogen/day 2 air.

Microdialysis

For the evaluation of tumor extracellular lactate content during the breathing challenge, we used microdialysis with a 6000-Da cutoff probe (Aurora Borealis) and a saline solution flux of 1 µl/min. Two probes were inserted per tumor under anesthesia 30 minutes before the collection of dialysates. Three baseline samplings were performed under air breathing. Then, the breathing gas was shifted to carbogen, and sampling was initiated after a 10-minute equilibration period

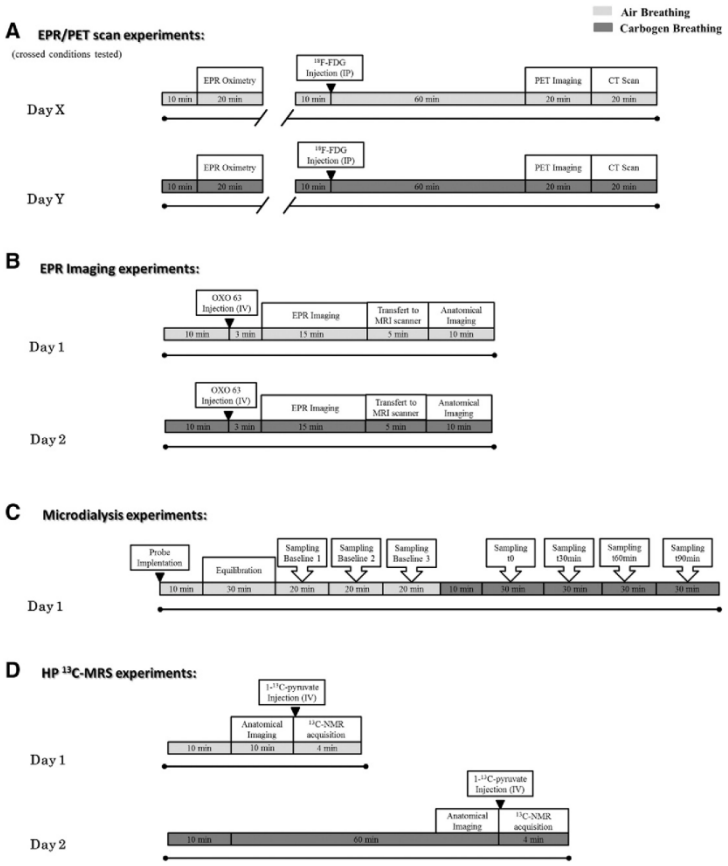

Figure 2. Experimental design built as a dynamic follow-up of the tumors during a breathing challenge. Tumor-bearing mice were scanned twice for the breathing challenge, air (light gray) versus carbogen (dark gray) breathing, with 1 day between each condition. Animals were anesthetized by inhalation of isoflurane mixed with either air (21% O_2) or carbogen (95% O_2/5% CO_2), depending on the breathing condition tested, in a continuous flow (2 l/min). Animals were warmed (approximately 35°C) throughout the anesthesia period. Anesthesia period is indicated by black lines. Breathing conditions are represented by light gray and dark gray shaded area for air and carbogen, respectively. (A) EPR spectroscopy and PET scan experiments. Crossed conditions were tested (conditions tested: day 1 air/day 2 carbogen or day 1 carbogen/day 2 air). (B) EPR imaging. (C) Microdialysis experiments. (D) Hyperpolarized ^{13}C-MRS studies.

during 90 minutes. The lactate concentration in dialysates was determined using specific enzymatic assays on a CMA600 microdialysis analyzer (CMA Microdialysis AB, Solna, Sweden). The experimental design is displayed in Figure 2*C*.

Hyperpolarized ^{13}C-MRS Studies

1-^{13}C pyruvic acid (30 µl), containing 15 mM OXO63 and 2.5 mM gadolinium chelate ProHance (Bracco Diagnostics, Milano, Italy), was hyperpolarized at 3.35 T and 1.4 K using the Hypersense DNP polarizer (Oxford Instruments, Abingdon, UK) according to the manufacturer's instructions. After 60 to 90 minutes, the hyperpolarized sample was rapidly dissolved in 4.5 ml of a superheated alkaline buffer that consisted of 50 mM Tris(hydroxymethyl) aminomethane, 75 mM NaOH, and 100 mg/l of ethylenediaminetetraacetic acid. The hyperpolarized 1-^{13}C pyruvate solution (96 mM) was intravenously injected through a catheter placed in the tail vein of the mouse (12 µl/g body weight). Hyperpolarized ^{13}C-MRS studies were performed on a 3-T scanner (MR Solutions, Guildford, UK). A home-built ^{13}C solenoid leg coil 17.5 mm in diameter and 18.5 mm in length was used to closely

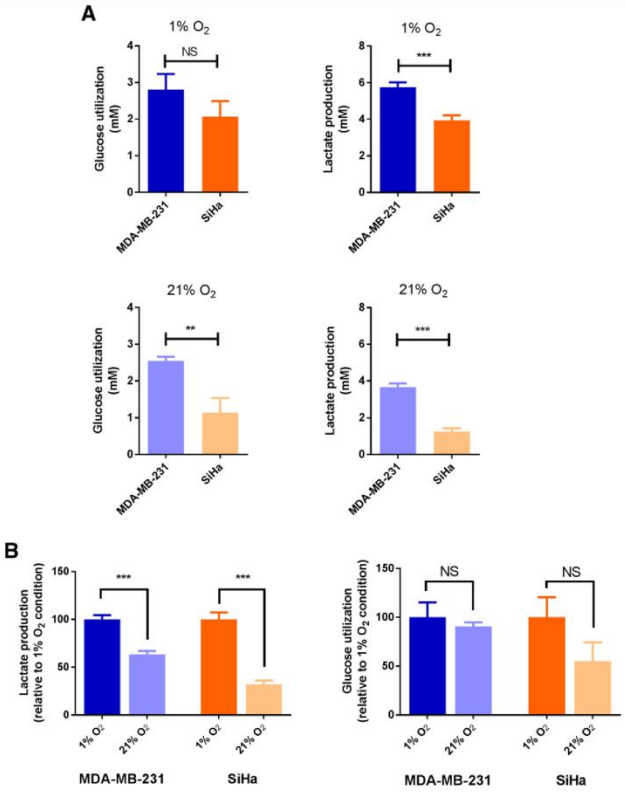

Figure 3. Metabolic behavior of MDA-MB-231 and SiHa cells under hypoxic and oxygenated conditions *in vitro*. (A) Under hypoxic condition (1% O_2), MDA-MB-231 cells produce high levels of lactate compared with SiHa cells. Under oxygenated condition (21% O_2), MDA-MB-231 cells maintained their glycolytic behavior. Data are expressed as means ± SEM. Unpaired tests were two-sided. (B) Effect of reoxygenation on lactate production and on glucose utilization in MDA-MB-231 cells and SiHa cells *in vitro*. SiHa cells are more sensitive to reoxygenation than MDA-MB-231 cells. Data are expressed as means ± SEM. Paired tests were two-sided.

conform to the size of the tumors upon measurement. After the rapid injection of hyperpolarized 1-^{13}C pyruvate, spectra were acquired every second for 240 seconds using a single pulse sequence. Data were analyzed in a model-free approach using the lactate/pyruvate ratio, calculated from the areas under the curves of the 1-^{13}C lactate peak and the 1-^{13}C pyruvate peak [24]. Additional details about the experimental design are presented in Figure 2*D*.

Statistical Analysis

Analysis was performed using the GraphPad Prism 6 software. Results are expressed as means value of parameter ± SEM. All statistical tests were two-sided. Paired *t* test was used to compare mean changes between groups (air versus carbogen) for each tumor model, and unpaired *t* test was used to compare mean changes between the two tumor models. Results with $P < .05$ (*), <.01 (**), or <.001 (***) were considered to be statistically significant.

Results

In Vitro, MDA-MB-231 Cells Exhibit a Glycolytic Behavior Even After Reoxygenation, Whereas SiHa Cells Are Oxidative Under Oxygenated Condition

To assess the impact of different oxic conditions on tumor metabolism, we first evaluated the cellular metabolic fluxes under hypoxic and oxygenated conditions. Cells were kept during 4 hours under hypoxia (1% O_2) before undergoing reoxygenation (21% O_2) or remaining under constant hypoxia. Glucose utilization and lactate production were measured during the reoxygenation period or during the same period under hypoxia ($n = 3$ per model, triplicates) (Figure 3).

Under hypoxic condition (Figure 3*A*, 1% O_2), MDA-MB-231 cells produced high levels of lactate (5.76 ± 0.26 mM) compared with SiHa cells (3.93 ± 0.29 mM) ($P < .001$), but similar glucose consumption was measured in MDA-MB-231 cells (2.80 ± 0.43 mM) and SiHa cells

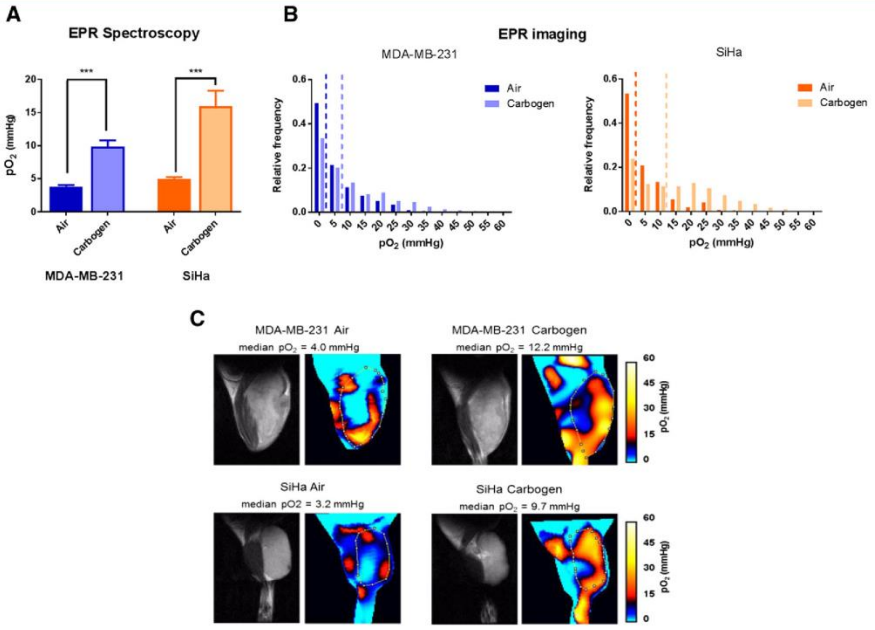

Figure 4. Effect of a breathing challenge on tumor oxygenation *in vivo*. These results show that hypoxic and oxygenated conditions are achieved under air and carbogen breathing, respectively, in MDA-MB-231 and SiHa tumors. (A) Changes of mean pO_2 under air and carbogen breathing measured by EPR spectroscopy. Data are expressed as means ± SEM. Paired tests were two-sided. (B) pO_2 frequency distributions in MDA-MB-231 and SiHa tumors as measured on EPR oxygen images. Lines indicated median pO_2 values for the collected data. (C) Representative EPR oxygen images of MDA-MB-231 and SiHa tumors obtained under air and carbogen breathing using EPR imaging. Region of interest was drawn on the tumor zone.

(2.07 ± 0.43 mM) (P = .2416). Under oxygenated condition (Figure 3*A*, 21% O_2), glucose utilization was significantly different (P = .0034) between for MDA-MB-231 cells (2.55 ± 0.11 mM) and SiHa cells (1.14 ± 0.39 mM). Also, MDA-MB-231 cells produced more lactate (3.65 ± 0.22 mM) than SiHa cells (1.25 ± 0.17 mM) (P < .001).

To highlight a metabolic shift under different oxic conditions, we compared the metabolic fluxes of each cell line under hypoxic and oxygenated conditions (Figure 3*B*). By evaluating the variation of glucose utilization or lactate production under hypoxic and oxygenated conditions in each cell line, we noted that the reoxygenation majorly impacted SiHa compared with MDA-MB-231 cell metabolism. Indeed, for lactate production, MDA-MB-231 cells exhibit a decrease of 37% (P < .001) compared with a decrease of 68% observed in SiHa cells (P < .001). Glucose utilization was slightly but not significantly decreased by 9% in MDA-MB-231 cells (P = .5710) and by 45% in SiHa cells (P = .1300).

Even after reoxygenation, MDA-MB-231 cells remained more glycolytic than SiHa cells. Our results are consistent with previous phenotyping studies reporting MDA-MB-231 and SiHa cells as Warburg [19,25] and oxidative, respectively [19,26].

MDA-MB-231 and SiHa Tumors Are Hypoxic Under Air Breathing and Are Reoxygenated Under Carbogen Breathing

To evaluate the metabolic behavior of these tumor cells *in vivo*, we designed experiments to study the global metabolism *in vivo* before and after reoxygenation induced by carbogen breathing. By changing O_2 availability in the tumor during the breathing challenge, we expected to achieve a hypoxic versus better oxygenated status in the models, thus mimicking the hypoxic versus oxygenated conditions tested *in vitro*.

In Figure 4, the effects of the breathing challenge on oxygenation were evaluated by EPR oximetry. Oxygenation increased after carbogen breathing in MDA-MB-231 (n = 16, P < .001) and in SiHa (n = 12, P < .001) tumors (Figure. 4*A*). Basal pO_2 values (air breathing) assessed by EPR spectroscopy were 3.8 ± 0.2 mm Hg for MDA-MB-231 tumors and 4.9 ± 0.3 mm Hg for SiHa tumors. Under carbogen breathing, MDA-MB-231 and SiHa tumors reached a pO_2 of 9.9 ± 0.95 mm Hg and 16.0 ± 2.3 mm Hg, respectively. These data were confirmed by EPR imaging measurements (MDA-MB-231: n = 3; SiHa: n = 5) (Figure 4, *B* and *C*). Typical pO_2 maps (Figure 4*C*) highlighted hypoxic tumors (pO_2< 10 mm Hg) under air breathing and a change of oxygenation after carbogen breathing. pO_2 frequency distributions were generated (Figure 4*B*)

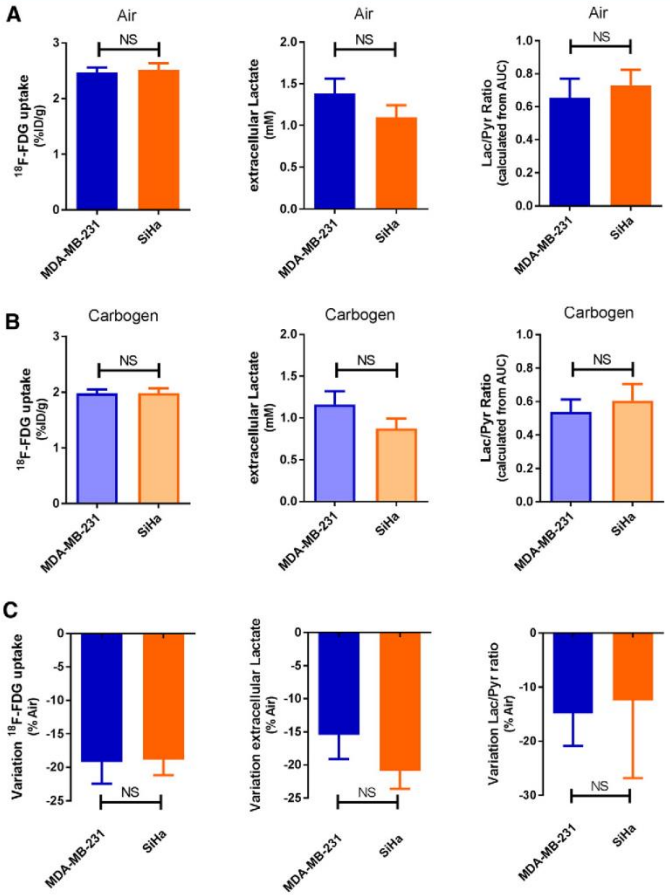

Figure 5. Metabolic behavior of MDA-MB-231 and SiHa tumors under air and carbogen breathing *in vivo*. The biomarkers tested were ^{18}F-FDG uptake, extracellular lactate content during microdialysis experiments, and the transformation of pyruvate into lactate using hyperpolarized ^{13}C-MRS. MDA-MB-231 and SiHa tumors exhibit the same phenotype under air (A) and also under carbogen (B) breathing. Data are expressed as means ± SEM. Unpaired tests were two-sided. The magnitude of response to the breathing challenge (variation) (C) is identical in both models. Data are expressed as means ± SEM. Unpaired tests were two-sided.

and highlighted the shift of median pO_2 induced by carbogen. Median pO_2 shifted from 2.6 to 6.5 mm Hg in MDA-MB-231 tumors and from 2.0 to 13.7 mm Hg in SiHa tumors.

These results demonstrate that hypoxic and oxygenated conditions are achieved under air and carbogen breathing, respectively, in both tumor models.

In Vivo, MDA-MB-231 and SiHa Tumors Exhibit the Same Phenotype Under Basal Condition and Under Carbogen Breathing

To evaluate the metabolic behavior of the models *in vivo*, glucose uptake, extracellular lactate content, and lactate flux were measured in MDA-MB-231 and SiHa tumors under air (hypoxic condition) and carbogen (oxygenated condition) breathing (Figure 5).

Under air breathing, we observed a similar glycolytic behavior in MDA-MB-231 and in SiHa tumors, assessed by a high uptake of ^{18}F-FDG, high lactate content (evaluated by microdialysis), and high lactate/pyruvate ratio (measured during hyperpolarized ^{13}C-MRS studies) (Figure 5*A*). Under carbogen breathing, there was no appreciable difference in the metabolic profile of the two models (Figure 5*B*). However, a metabolic shift was observed after reoxygenation using carbogen in MDA-MB-231 and SiHa tumors. As presented in Figure 6, ^{18}F-FDG uptake was significantly reduced in both models under carbogen (MDA: $n = 16$, $P < .001$; SiHa $n =$

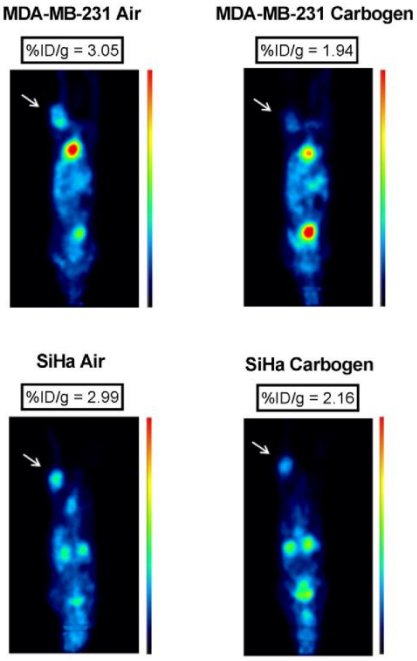

Figure 6. Representative ^{18}F-FDG PET images showing MDA-MB-231 and SiHa tumor-bearing mice imaged under air and carbogen breathing. Tumors are indicated by thin arrows. ^{18}F-FDG uptake is expressed in %ID/g. Images were normalized. ^{18}F-FDG uptake drops after carbogen breathing in MDA-MB-231 and SiHa tumors.

12, $P < .001$). The extracellular lactate content in tumors significantly decreased under carbogen (MDA: $n = 4$, $P = .0162$; SiHa $n = 4$, $P = .0021$). This metabolic shift was also noted by measuring the conversion of pyruvate to lactate in the models (Figure 7) but did not reach a statistical significance (MDA: $n = 6$, $P = .0652$; SiHa $n = 5$, $P = .3913$). We also evaluated the magnitude of response to the breathing challenge by measuring the variation of these biomarkers between air and carbogen breathing conditions (Figure 5*C*). According to all the biomarkers tested, there was no difference in behavior between MDA-MB-231 and SiHa tumors during the breathing challenge ($P > .05$).

Together, the results obtained *in vivo* indicate that the MDA-MB-231 tumors do not appear more glycolytic than SiHa tumors, both models exhibiting the same metabolic behavior under the different conditions tested.

Discussion

This study emphasizes a major limitation of describing the metabolic phenotype of tumors based on the *in vitro* studies solely. By evaluating glucose metabolism under different oxic conditions in two well-established glycolytic and oxidative tumor cell models, we challenged the Warburg and Pasteur effects, respectively. In the Warburg cellular model, in which metabolism is O_2-independent, we expected to preserve high rate of glycolysis even in the presence of oxygen, whereas in the oxidative cellular model, in which metabolism is sensitive to O_2, we expected to observe a switch from glycolysis to OXPHOS in the presence of a large amount of O_2 relative to baseline. This paradigm, extensively applied *in vitro*, has to our knowledge never been applied so far *in vivo*. By applying protocols with hypoxic and oxygenated conditions *in vitro* and *in vivo*, we identified a major difference in the metabolic behavior between both experimental conditions. *In vitro*, MDA-MB-231 cells kept their glycolytic metabolism even after reoxygenation (typical of a Warburg phenotype). On the contrary, SiHa cells shifted to an oxidative metabolism when oxygen became available, which is consistent with a Pasteur effect (Figure 3). The metabolic behavior was dramatically different *in vivo* for both tumor models: MDA-MB-231 tumors and SiHa tumors exhibited the same phenotype under hypoxia, and no difference was observed between both tumor models after reoxygenation induced by the carbogen breathing (Figure 5). These results highlight that the tumor microenvironment could be as important as the (epi)genetic profile to shape the tumor phenotype.

Our work extends recent efforts highlighting the limitation of *in vitro* studies to truly reflect the complex tumor behavior. Even if the microenvironment has already been presented as a decisive parameter determining the metabolic phenotype of tumors

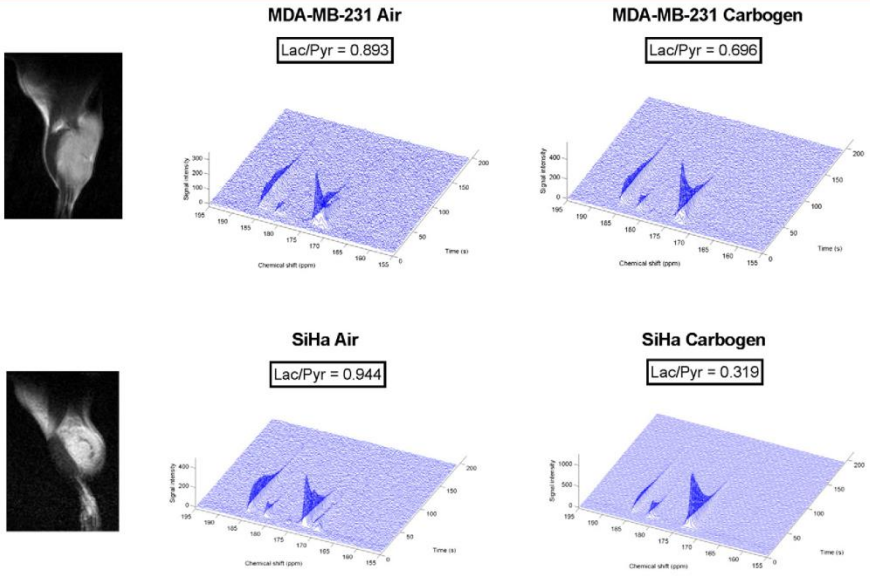

Figure 7. Typical ^{13}C-MRS spectra from representative MDA-MB-231 tumors and SiHa tumors and corresponding ^{1}H anatomical images. Lactate production, measured by the Lac/Pyr ratio, is reduced in MDA-MB-231 and SiHa tumors after carbogen breathing: pyruvate (173 ppm), lactate (185 ppm) peaks, and pyruvate hydrate (181 ppm).

[13,27,28], research has extensively focused on genetic and epigenetic alterations in cancer, and only a few studies have addressed the influence of the *in vivo* environment on the tumor metabolism. Davidson and colleagues recently investigated tissue metabolites from non–small cell lung tumors after the infusion of [U-^{13}C]glucose and [U-^{13}C]glutamine in mice [18]. Although lung cancer cells exhibited minor glucose oxidation *in vitro*, they established that glucose oxidation was required for tumor growth *in vivo*. Also, these authors identified a limited glutamine metabolism in lung tumor *in vivo* compared with lung cancer cells *in vitro* and suggested lactate as another preferred source of carbon in lung tumors. They also assessed that transplanted tumors exhibit a phenotype more similar to spontaneous lung tumors in mice compared with tumor cells in culture, highlighting the importance of model selection. In another recent study of Hensley and coworkers [17], metabolic activities related to perfusion were studied in human lung tumors based on multimodality imaging and ^{13}C-glucose infusions. Poorly perfused areas, assessed by dynamic contrast-enhanced MRI, exhibited higher glucose metabolism compared with well perfused areas that preferentially relied on alternative fuels. Both these studies performed in lung cancer were able to identify common metabolic features in preclinical models and in patients, showing minimal resemblance with *in vitro* characterization.

Our present work adds to these studies in several ways. First, we showed that tumor cell models exhibit distinct metabolic behaviors *in vitro* but present the same behavior *in vivo* as attested by a multimodality imaging study. Although we reproduced similar experimental conditions *in vitro* and *in vivo*, we assessed that the paradigm, extensively applied *in vitro*, did not recapitulate the *in vivo* behavior of these models. The results observed *in vivo* could not be attributed to the impact of anesthesia on tumor hemodynamics as it was demonstrated previously that isoflurane had negligible effect on both tumor perfusion and oxygenation [29]. Also, the measurement repeatability was demonstrated during EPR spectroscopy and PET scan experiments. Indeed, crossed conditions were tested for the breathing challenge, and no difference was observed between the two subgroups in the animal cohort. Second, we assessed the occurrence of a rapid metabolic adaptation after carbogen breathing *in vivo* in both models. Carbogen breathing had a significant impact on ^{18}F-FDG uptake and lactate content (Figure 5). This demonstrates the rapid plasticity of tumor cells to adapt their metabolism to the oxygen environment, a phenomenon known as the Pasteur effect. As already suggested by other studies [30,31], our data support that careful experimental protocol optimization is required for metabolic studies, likewise breathing conditions. However, regardless of the breathing gas used, the evaluation of tumor oxygenation in parallel to tumor metabolism studies would undoubtedly improve tumor phenotyping research. Third, the advanced imaging technologies used in the present study represent relevant tools for tumor metabolic phenotyping *in vivo*. ^{18}F-FDG PET scan is a widespread technology already used in clinical routine, and hyperpolarized ^{13}C-MRI is an emerging technology that was recently introduced in clinical research [32]. Our data suggest that molecular imaging techniques could

represent a powerful tool to identify metabolic alterations in patients and may be used as relevant biomarkers to guide treatments targeting tumor metabolism.

However, our study presents some limitations that should be addressed. First, host cells and tumor microenvironment could be involved in the divergence of metabolic metabolism between *in vitro* and *in vivo* studies. In our study, the metabolic profile was established *in vivo* considering results on the whole tumor. Using a global measurement of the tumor mass, we were not able to discriminate between host cell metabolism and cancer cell metabolism. Further investigations using co-culture models under different culture conditions should be considered to determine the role of host cell in metabolic profile measurements as well as the impact of nutrient availability, oxygenation, and acidification on tumor metabolism. Second, xenografts using immortalized cell lines represent the majority of the tumor models investigated due to their easy use. Nevertheless, this approach does not always correlate with clinical outcomes in patients, as the generation of cancer cell lines could majorly alter biologic and genetic properties and cause the loss of specific cell population. Third, the use of immunodeficient animals provides a less realistic tumor microenvironment. Therefore, it would be important to further explore primary cell cultures implanted in immunocompetent animals. Finally, comparative study involving different implantations such as subcutaneous or orthotopic should be considered.

In conclusion, our metabolic study identified distinct metabolic behaviors of two well-established tumor models *in vitro* and *in vivo*. Results suggest that there is a need to take cautiously any extrapolation of *in vitro* characterization to the *in vivo* situation. Implanted tumors and spontaneous cancer models should be preferred to identify relevant metabolic alterations within the milieu of the tumor microenvironment. When well-established tumor cell models are translated *in vivo*, additional phenotyping should be considered and could be achieved by using clinically relevant biomarkers like ^{18}F-FDG PET scan and hyperpolarized ^{13}C-MRI.

Conflict of Interest

The authors disclose no potential conflicts of interest.

Acknowledgements

This study was funded by grants from the Belgian National Fund for Scientific Research (F.S.R.-FNRS; PDR T.0107.13), the Fonds Joseph Maisin, the Action de Recherches Concertées ARC 14/19-058, Belgian Science Policy Office Interuniversity Attraction Pole IUAP #P7/03, and intramural National Institute of Health funds. M. A. N. is a Research Fellow and P. E. P. a Senior Postdoctoral Fellow of F.R.S.-FNRS. P. S. and B. F. J. are Research Associates of F.R.S.-FNRS.

References

[1] López-Lázaro M (2008). The Warburg effect: why and how do cancer cells activate glycolysis in the presence of oxygen? *Anticancer Agents Med Chem* **8**(3), 305–312. http://dx.doi.org/10.2174/187152008783961932.

[2] Upadhyay M, Samal J, Kandpal M, Singh OV, and Vivekanandan P (2013). The Warburg effect: insights from the past decade. *Pharmacol Ther* **137**(3), 318–330. http://dx.doi.org/10.1016/j.pharmthera.2012.11.003.

[3] Vander Heiden MG, Cantley LC, and Thompson CB (2009). Understanding the Warburg effect: the metabolic requirements of cell proliferation. *Science* **324**(5930), 1029–1033. http://dx.doi.org/10.1126/science.1160809.

[4] Warburg O (1925). Uber den Stoffwechsel der Carcinomzelle. *Klin Wochenschr* **4**, 534–536. http://dx.doi.org/10.1007/BF01726151.

[5] Lunt SY and Vander Heiden MG (2011). Aerobic glycolysis: meeting the metabolic requirements of cell proliferation. *Annu Rev Cell Dev Biol* **27**, 441–464. http://dx.doi.org/10.1146/annurev-cellbio-092910-154237.

[6] De Preter G, Neveu MA, Danhier P, Brisson L, Payen VL, and Porporato PE, et al (2016). Inhibition of the pentose phosphate pathway by dichloroacetate unravels a missing link between aerobic glycolysis and cancer cell proliferation. *Oncotarget* **7**(3), 2910–2920. http://dx.doi.org/10.18632/oncotarget.6272.

[7] Warburg O (1956). On respiratory impairment in cancer cells. *Science* **124**(3215), 269–270. http://dx.doi.org/10.1126/science.124.3215.267.

[8] Moreno-Sanchez R, Rodriguez-Enriquez S, Marin-Hernandez A, and Saavedra E (2007). Energy metabolism in tumor cells. *FEBS J* **274**(6), 1393–1418. http://dx.doi.org/10.1111/j.1742-4658.2007.05686.x.

[9] Moreno-Sanchez R, Marin-Hernandez A, Saavedra E, Pardo JP, Ralph SJ, and Rodriguez-Enriquez S (2014). Who controls the ATP supply in cancer cells? Biochemistry lessons to understand cancer energy metabolism. *Int J Biochem Cell Biol* **50**, 10–23. http://dx.doi.org/10.1016/j.biocel.2014.01.025.

[10] Xie J, Wu H, Dai C, Pan Q, Ding Z, and Hu D, et al (2014). Beyond Warburg effect—dual metabolic nature of cancer cells. *Sci Rep* **4**, 4927. http://dx.doi.org/10.1038/srep04927.

[11] Obre E and Rossignol R (2015). Emerging concepts in bioenergetics and cancer research: metabolic flexibility, coupling, symbiosis, switch, oxidative tumors, metabolic remodeling, signaling and bioenergetic therapy. *Int J Biochem Cell Biol* **59**, 167–181. http://dx.doi.org/10.1016/j.biocel.2014.12.008.

[12] Jose C, Bellance N, and Rossignol R (2011). Choosing between glycolysis and oxidative phosphorylation: a tumor's dilemma? *Biochim Biophys Acta* **1807**(6), 552–561. http://dx.doi.org/10.1016/j.bbabio.2010.10.012.

[13] Hanahan D and Weinberg RA (2011). Hallmarks of cancer: the next generation. *Cell* **144**(5), 646–674. http://dx.doi.org/10.1016/j.cell.2011.02.013.

[14] Porporato PE, Dhup S, Dadhich RK, Copetti T, and Sonveaux P (2011). Anticancer targets in the glycolytic metabolism of tumors: a comprehensive review. *Front Pharmacol* **2**, 49. http://dx.doi.org/10.3389/fphar.2011.00049.

[15] Tennant DA, Duran RV, and Gottlieb E (2010). Targeting metabolic transformation for cancer therapy. *Nat Rev Cancer* **10**(4), 267–277. http://dx.doi.org/10.1038/nrc2817.

[16] Bost F, Decoux-Poullot AG, Tanti JF, and Clavel S (2016). Energy disruptors: rising stars in anticancer therapy? *Oncogenesis* **5**, e188. http://dx.doi.org/10.1038/oncsis.2015.46.

[17] Hensley CT, Faubert B, Yuan Q, Lev-Cohain N, Jin E, and Kim J, et al (2016). Metabolic heterogeneity in human lung tumors. *Cell* **164**(4), 681–694. http://dx.doi.org/10.1016/j.cell.2015.12.034.

[18] Davidson SM, Papagiannakopoulos T, Olenchock BA, Heyman JE, Keibler MA, and Luengo A, et al (2016). Environment impacts the metabolic dependencies of Ras-driven non–small cell lung cancer. *Cell Metab* **23**(3), 517–528. http://dx.doi.org/10.1016/j.cmet.2016.01.007.

[19] De Preter G, Danhier P, Porporato PE, Payen VL, Jordan BF, and Sonveaux P, et al (2016). Direct evidence of the link between energetic metabolism and proliferation capacity of cancer cells in vitro. *Adv Exp Med Biol* **876**, 209–214. http://dx.doi.org/10.1007/978-1-4939-3023-4_26.

[20] Gallez B, Jordan BF, Baudelet C, and Misson PD (1999). Pharmacological modifications of the partial pressure of oxygen in murine tumors: evaluation using in vivo EPR oximetry. *Magn Reson Med* **42**(4), 627–630.

[21] Jordan BF, Baudelet C, and Gallez B (1998). Carbon-centered radicals as oxygen sensors for in vivo electron paramagnetic resonance: screening for an optimal probe among commercially available charcoals. *MAGMA* **7**(2), 121–129.

[22] Gallez B, Baudelet C, and Jordan BF (2004). Assessment of tumor oxygenation by electron paramagnetic resonance: principles and applications. *NMR Biomed* **17**(5), 240–262. http://dx.doi.org/10.1002/nbm.900.

[23] Charlier N, Beghein N, and Gallez B (2004). Development and evaluation of biocompatible inks for the local measurement of oxygen using in vivo EPR. *NMR Biomed* **17**(5), 303–310. http://dx.doi.org/10.1002/nbm.902.

[24] Hill DK, Orton MR, Mariotti E, Boult JK, Panek R, and Jafar M, et al (2013). Model free approach to kinetic analysis of real-time hyperpolarized 13C magnetic resonance spectroscopy data. *PLoS One* **8**, e71996. http://dx.doi.org/10.1371/journal.pone.0071996.

[25] Gatenby RA and Gillies RJ (2004). Why do cancers have high aerobic glycolysis? *Nat Rev Cancer* **4**(11), 891–899. http://dx.doi.org/10.1038/nrc1478.

[26] Sonveaux P, Vegran F, Schroeder T, Wergin MC, Verrax J, and Rabbani ZN, et al (2008). Targeting lactate-fueled respiration selectively kills hypoxic tumor cells in mice. *J Clin Invest* **118**(12), 3930–3942. http://dx.doi.org/10.1172/JCI36843.

[27] Cairns RA, Harris IS, and Mak TW (2011). Regulation of cancer cell metabolism. *Nat Rev Cancer* **11**(2), 85–95. http://dx.doi.org/10.1038/nrc2981.

[28] Davidson SM and Vander Heiden MG (2012). METabolic adaptations in the tumor MYCroenvironment. *Cell Metab* **15**(2), 131–133. http://dx.doi.org/10.1016/j.cmet.2012.01.005.

[29] Baudelet C and Gallez B (2004). Effect of anesthesia on the signal intensity in tumors using BOLD-MRI: comparison with flow measurements by laser Doppler flowmetry and oxygen measurements by luminescence-based probes. *Magn Reson Imaging* **22**(7), 905–912. http://dx.doi.org/10.1016/j.mri.2004.02.005.

[30] Fueger BJ, Czernin J, Hildebrandt I, Tran C, Halpern BS, and Stout D, et al (2006). Impact of animal handling on the results of 18F-FDG PET studies in mice. *J Nucl Med* **47**, 999–1006.

[31] Stout D, Berr SS, LeBlanc A, Kalen JD, Osborne D, and Price J, et al (2013). Guidance for methods descriptions used in preclinical imaging papers. *Mol Imaging* **12**, 1–15. http://dx.doi.org/10.2310/7290.2013.00055.

[32] Nelson SJ, Kurhanewicz J, Vigneron DB, Larson PE, Harzstark AL, and Ferrone M, et al (2013). Metabolic imaging of patients with prostate cancer using hyperpolarized [1-(1)(3)C]pyruvate. *Sci Transl Med* **5**(198), 198ra08. http://dx.doi.org/10.1126/scitranslmed.3006070.

DISCUSSION AND PERSPECTIVES

1. Specific aims and principal findings

The first objective of the study was to assess the metabolic effects of dichloroacetate (DCA) in tumors presenting different metabolic profiles. For this purpose, DCA effects were evaluated in terms of oxygen consumption, glucose uptake and lactate production measurements using advanced molecular imaging technologies.

Two different tumor xenografts were used. MDA-MB-231 and SiHa tumor models were selected according to their glycolytic (Gatenby, 2004) (De Preter, 2016) and oxidative (Sonveaux, 2008) (De Preter, 2016) behavior respectively.

While the effects of DCA on oxygen consumption have been extensively explored in vitro, this has never been investigated in vivo to our knowledge. Our strategy was to consider this key parameter in order to fully characterize the effects of this drug on tumor glucose metabolism. We decided to apply in tumors a direct measurement of the oxygen consumption using ^{17}O NMR. First, in order to validate the potential of ^{17}O NMR method to reveal variations of O_2 consumption rate in tumors, we evaluated the impact of mild hypothermia on oxygen consumption rate in the murine fibrosarcoma FSAII tumor model. Tumor oxygenation, assessed by EPR oximetry measurements, was progressively decreased after hypothermia induction compared to animals kept under normothermic condition. This changed in tumor pO_2 was demonstrated to result from a drop in oxygen consumption rate, as revealed by ^{17}O NMR measurements.

As ^{17}O NMR technique was able to monitor the impact of hypometabolism induction in tumors, we applied this technique with ^{18}F-FDG PET scans and

hyperpolarized ^{13}C-pyruvate NMR experiments to explore the effects of DCA in the glycolytic MDA-MB-231 tumor model and the oxidative SiHa tumor models. While a previous in vitro study revealed that metabolism of glycolytic MDA-MB-231 cells was dramatically affected by DCA treatment compared to oxidative SiHa cells (De Preter, 2016), we were surprised to see that both tumor models were unaffected by DCA treatment in vivo, as oxygen consumption, glucose uptake and lactate production remained unchanged. So contrarily to our first assumptions, glycolytic tumors did not appear more impacted than oxidative tumors and DCA treatment failed to induce a metabolic shift in the tumor models tested in vivo.

Given this major discordance in metabolic response to DCA observed in vitro and in vivo, we decided to investigate if the tumor models under study could differ in their metabolic phenotypes in vitro and in vivo. The paradigm that we used to study the metabolic behaviors of a Warburg phenotype and an oxidative phenotype was the following: the global metabolic status was studied before and after a transient tumor hyperoxia. When passing from a hypoxic state to an oxygenated state, a Warburg phenotype should not modify its consumption in oxygen and in glucose and will continue to produce lactate. On the contrary, an oxidative phenotype should metabolically switch to higher oxygen consumption, lower glucose consumption with a decrease in lactate production in favor of an increase in CO2/carbonate production. While this paradigm is obvious and has been extensively applied in vitro, it was never applied so far in vivo. In vitro, MDA-MB-231 cells were glycolytic under both hypoxic and oxygenated conditions, whereas SiHa cells underwent a metabolic shift after reoxygenation. This observation was consistent with previous

characterizations of the cell lines. In vivo, PET, EPR oximetry, microdialysis and ^{13}C-hyperpolarizated NMR were used to characterize the metabolic phenotype in the tumor models. The same animals were scanned twice during a breathing challenge. As validated by EPR oximetry, we achieved a hypoxic versus better oxygenated status in the models under air and carbogen breathing respectively. We found that both tumor models decreased their glucose uptake and lactate production under carbogen breathing but above all, we were not able to discriminate the behavior of these tumor models. Here again, we highlighted that the tumor models under study exhibited distinct metabolic behaviors under in vitro and in vivo conditions.

Consequently, our study reveals major discordances between in vitro and in vivo metabolic behaviors, highlighting limitations of direct translation of in vitro discoveries to the in vivo context. Also, our study challenges leading paradigms in the field of tumor metabolism, such as the Pasteur effect and the Warburg effect.

2. Important issues and challenges arising from this study

As we were investigating the effects of dichloroacetate in 2 well-described tumor models using molecular imaging in vivo, central questions emerged. Do tumor models and corresponding tumor cell models exhibit the same metabolic phenotype? Can imaging biomarkers reflect the in vitro phenotyping of tumor models? Further investigations of our models using oxygen as a metabolic modulator gave us some clues. Yes, molecular imaging represents a key tool to characterize tumor phenotype and metabolic modulations. Unfortunately, we undeniably confirmed dissimilarities between in vitro and in vivo behaviors of our tumor models. Further investigation using other tumor models should confirm the relevance of these findings. But above all, the factors and mechanisms involved in the metabolic deviation between in vitro and in vivo conditions in cancer should be explored and should be considered for cancer research planning. The limitations of the techniques used in this study will also be considered and the challenges remaining for translational research on oncology will be discussed.

2.1. Challenges remaining for metabolic phenotyping

2.1.1. Tumor models and metabolic heterogeneity

Metabolic discrepancy between in vitro and in vivo tumor models:

In our study, in vivo models did not recapitulate the previously observed in vitro behavior. In order to test the relevance of this finding, other tumor models should be tested. In our study, we selected the tumor models based on a metabolic profile study made within six human and murine cancer cell

lines (**Figure 21**) (De Preter, 2016). MDA-MB-231 human breast cancer cells exhibited low oxygen consumption rate, high glycolytic efficiency and low intracellular ATP content, consistent with a Warburg or glycolytic profile. On the contrary, SiHa human cervical cancer cells presented high oxygen consumption rate, low glycolytic efficiency and high intracellular ATP content, characteristic of an oxidative profile.

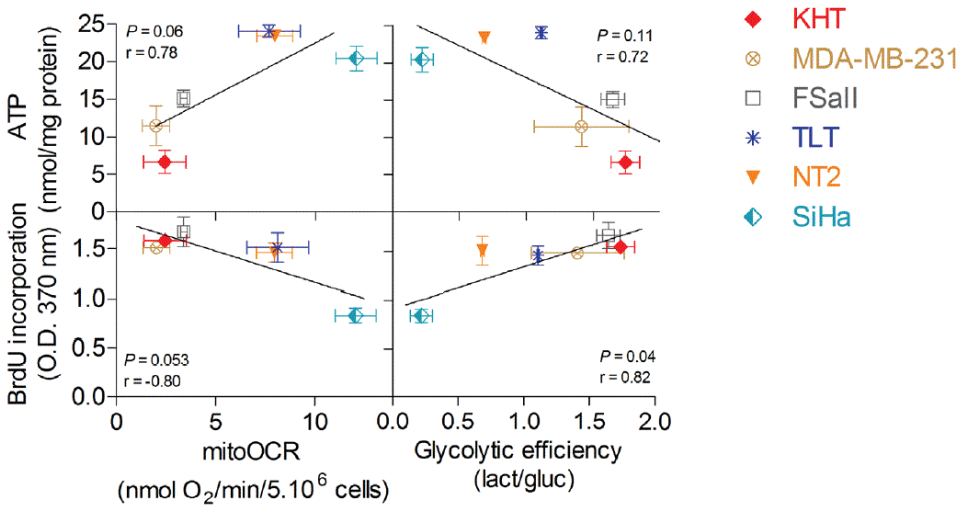

Figure 21: Glycolytic efficiency, mitochondrial oxygen consumption rate [mitoOCR], intracellular ATP content and proliferation rates of six human and murine cancer cell lines (De Preter, 2016).

A more refined strategy would be to work on cell clones only differring from one given metabolic actor or pathway. In this case, metabolism-independent influences, inherent to different genotypes, should be excluded. Also, mechanisms involved in this metabolic discrepancy should be investigated. What is the role of the local microenvironment? Is there a

metabolic shift occurring during tumor development? To study these hypotheses, engineered cell culture systems compatible with NMR systems, called bioreactors, should be considered. Their ability to control parameters such as oxygenation, flow, pH, and substrate availability to introduce perturbations in microenvironment biologically make these systems a biologically relevant approach. Associated with NMR, dynamic and steady state metabolism can be monitored in real time (Keshari, 2014). Using this approach, the same parameters and tracers could be studied with NMR in vitro and in vivo, limiting thus the impact of confounding factors occurring when in vitro and in vivo studies are performed with technologies relying on different principles.

Role of host cell in metabolic profile measurements in vivo:

Are the host cells involved in the divergence of metabolic metabolism between in vitro and in vivo studies? Solid tumors are made from an assemblage of distinct cell types, including cancer cells, cancer stem cells, immune cells, endothelial cells, pericytes and cancer-associated fibrobasts (**Figure 22**) (Hanahan, 2011).

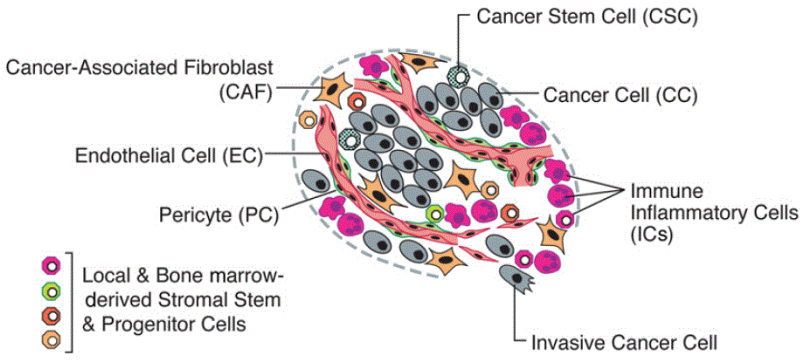

Figure 22: Individual specialized cell types in tumor masse (Hanahan, 2011).

Host cells generally undergo a metabolic reprogramming in tumors and a metabolic interplay between tumor cells and host cells can occur to support tumor expansion. For exemple, cancer cells rely on the vascular supply for metabolic homeostasis (fuel availability and waste removal) and growth, and endothelial cells rely on cancer cell release of pro-angiogenic signals (Verdegem, 2014). Similarly to cancer cells, endothelial cells increase their glycolytic rate during vessel sprouting to support cell growth and division. Also, recent studies have demonstrated that antitumoral immune cell populations rely on aerobic glycolysis and glutaminolysis, competing with cancer cells for nutrients, while pro-tumoral immune cells may act in symbiosis with cancer cells, preferring the use of metabolic waste products of tumor cells (Wang, 2014). A metabolic interplay between cancer cells and cancer associated fibroblast has also been described (Pavlides, 2009).

While a metabolic heterogeneity is already present in the cancer cell population, metabolic interplay or competition can occur between cancer cells and host cells in solid tumors. In our study, the metabolic profile was established in vivo considering results on the whole tumor. Using a global measurement of the tumor mass, we were not able to discriminate between host cell metabolism and cancer cell metabolism. Unfortunately, according to the present spatial resolution of the imaging technologies used, the application of parametric maps is not sufficient to obtain information at the cellular level. The use of co-culture models should be set-up to test the interaction of cancer cells with endothelial cells, fibroblasts and immune cells under different culture conditions (nutrient, oxygenation, acidification, etc).

2.1.2. Technical considerations

In this study, we exploited the capacity of molecular imaging to explore tumor metabolism non invasively. While ^{18}F-FDG PET is a well-known technology that has already proven its value in the management of cancer patients, we used two other innovative technologies, hyperpolarized ^{13}C-MRI and ^{17}O NMR, that still need to demonstrate their clinical relevance.

^{17}O NMR approach to study tumor oxygen consumption:

Our study demonstrated the potential of ^{17}O NMR to assess oxygen consumption in tumor. Fast and non invasive, this direct method may provide a unique way to study an important aspect of tumor metabolism. Furthermore, the technique is suitable for repeated measurements and could fit for cancer patient monitoring. Indeed, Zhu and co-workers previously demonstrated the reliability and reproducibility of the $CMRO_2$ measurement using ^{17}O MRI technology (Zhu, 2007). As cerebral $H_2{}^{17}O$ concentration quickly reaches a new steady state level after the cessation of a brief $^{17}O_2$ inhalation, it allows repeated $CMRO_2$ measurements in the same subject and experimental session. As hemodynamic and metabolism of cancer and tumor tissues are drastically different, further characterization of tumor $^{17}O_2$ metabolism is required to estimate how fast measurements could be repeated in the same subject. The use of sophisticated models for quantification including hemodynamic information, as it has already been proposed for brain studies, should be favored. In our study, we opted for a simplified quantification method to assess oxygen consumption in cancer. Complex models proposed in the brain describe that the build-up of $H_2{}^{17}O$ signal during the inhalation is tightly correlated to $CMRO_2$ (**Figure 23**).

Based on this concept, we measured the slope during the linear incorporation phase as marker of tumor oxygen consumption.

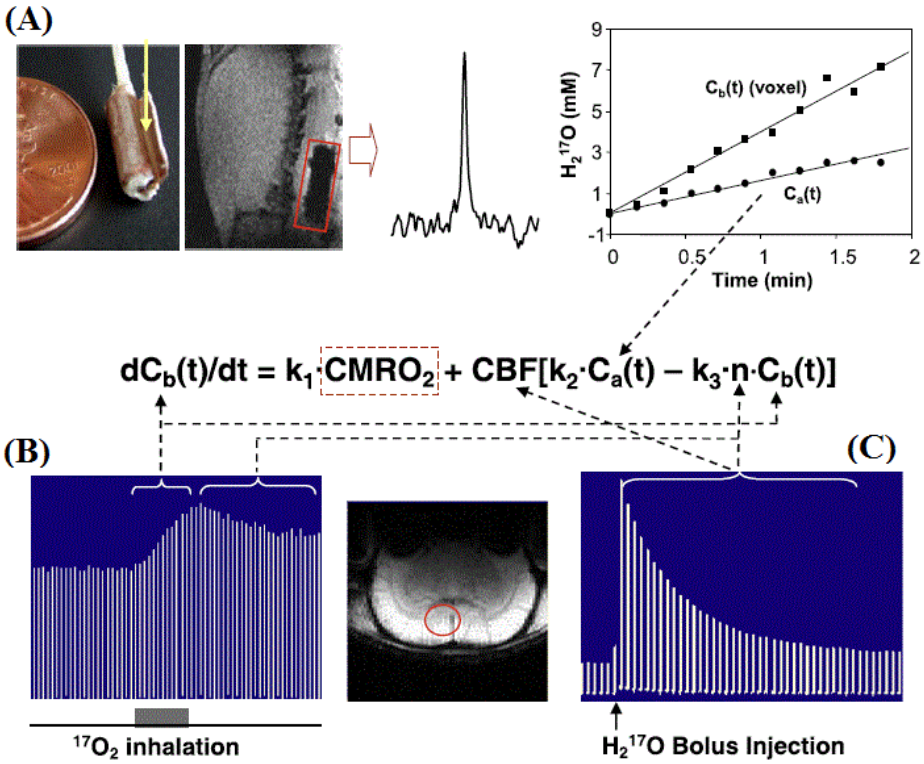

Figure 23: Schematic diagram showing the multiple in vivo ^{17}O measurements for determining $CMRO_2$ based on $C_a(t)$, $C_b(t)$ and CBF measurements.

Adapted from (Zhu, 2011)

(A) Measurement of $C_a(t)$, the $H_2{}^{17}O$ concentrations in excess of the natural abundance $H_2{}^{17}O$ concentration in the arterial blood, by using an implanted ^{17}O RF coil (the left inset). The middle insert illustrates a ^{17}O spectrum of natural abundance $H_2{}^{17}O$ obtained from the rat carotid artery blood with the implanted coil before $^{17}O_2$ inhalation. The right insert shows the time course of $C_a(t)$ (circle symbol) and $C_b(t)$ from a representative voxel (square symbol) in the same rat during the $^{17}O_2$ inhalation.

(B) Measurement of $C_b(t)$, the $H_2{}^{17}O$ concentrations in excess of the natural abundance $H_2{}^{17}O$ concentration in the brain tissue. Stacked plot of the ^{17}O spectra of the metabolic $H_2{}^{17}O$ from the same voxel acquired before (natural abundance), during (as indicated by the gray bar under the stacked plot) and after a 2-min $^{17}O_2$ inhalation.
(C) Measurement of CBF, the cerebral blood flow. Stacked plot of the ^{17}O spectra of cerebral $H_2{}^{17}O$ tracer from one representative voxel. The spectra were acquired before and after a bolus injection of $H_2{}^{17}O$.

The rate of $H_2{}^{17}O$ production depends on both oxygen tissue consumption and concentration of $^{17}O_2$ gas in the blood. Also the total amount of $H_2{}^{17}O$ measured in a tissue will depend on 3 main processes (Atkinson, 2010) (Zhu, 2011):

- oxygen utilization and local $H_2{}^{17}O$ production;
- blood perfusion and local $H_2{}^{17}O$ washout;
- blood flow recirculation of $H_2{}^{17}O$ produced in the body.

Adaptation of models proposed in brain studies to the tumor context should constitute a finer approach to assess oxygen metabolism. However, the complex vessel architecture and hemodynamic in tumors will complicate this effort. Furthermore, given the metabolic heterogeneity in tumors, spectroscopic imaging should be preferred to generate real oxygen consumption maps. Associated with the proper surface coil dedicated for superficial tumor or volume coil to assess metabolism of profound tumors, ultra-short echo imaging sequence can be designed to follow oxygen consumption in real time. The major restrain consist of finding the good

balance between ultra-fast measurements with reasonable image resolution, without signal loss (due to rapid $H_2{}^{17}O$ relaxation time decay). This can be avoided by minimizing the delay (or echo time) between the ^{17}O spin excitation pulse and NMR signal sampling (Zhu, 2011).

Hyperpolarized [1-^{13}C]pyruvate NMR to follow pyruvate metabolism:

In 2003, dissolution DNP has been successfully developed to explore ^{13}C-metabolites in biological systems (Ardenkjaer-Larsen, 2003). Rapidly, [1-^{13}C]pyruvate has become a molecule of choice to study the metabolism of tumor. By measuring the hyperpolarized ^{13}C label flux between pyruvate and lactate after hyperpolarized ^{13}C-pyruvate injection, LDH activity and lactate pool size can be rapidly assessed in various tissues (see Introduction section 3.3.1.). After numerous studies attesting the value of hyperpolarized [1-^{13}C]pyruvate to study tumor metabolism, this technology has been recently translated to the clinic in prostate cancer patients (Nelson, 2013). Although, numerous aspects are still unidentified or underestimated and should be considered if we want this technology to progress in clinical practice. Some of them will be examined hereafter.

Even if the technology seems to spread and is currently used in many imaging platforms all around the world, there is actually no standardized method for lactate labeling quantification. Different mathematical models were presented to analyze hyperpolarized kinetic data but numerous factors affect the appearance of lactate labeling including (Harrison, 2012) (Hill, 2013):

- the hyperpolarized signal relaxation rates;
- the arterial input function (AIF) and delivery of the injected tracer;

- the metabolic conversion into other metabolites;
- the pool size of metabolites;
- the transport between the intracellular and extracellular space;
- the loss of polarization due to the application of a radio-frequency pulse.

Also, it is important to mention that lactate labeling is predominantly due to isotope exchange rather than net chemical flux (Day, 2007) (Kettunen, 2010) (Brindle, 2011). Due to the high level of lactate present in tumor tissues, the LDH-catalyzed reaction will rapidly come to near-chemical equilibrium after hyperpolarized ^{13}C-pyruvate administration. This will result in a very small conversion of pyruvate into lactate but will be followed by the exchange of hyperpolarized ^{13}C label between the pyruvate and lactate pools at near chemical equilibrium. In our study, we used a simplified and fast method based on the measurement of the ratio of the total area under the curves (AUC) of the injected tracer and the generated metabolites, called the AUC ratio method. This technique has the advantage to be independent on AIF (Hill, 2013). The most commonly used kinetic models are the 2-site exchange and the 3-site exchange models (**Figure 24**) and are similar to the methods used in other areas of MRI, such as DCE-MRI. While the first one does not take cellular transport into account and assumes that hyperpolarized signals are intracellular, the second one differentiates between intracellular and extracellular spaces and thus takes metabolite efflux into account (Harrison, 2012) (Hill, 2013) (Daniels, 2016).

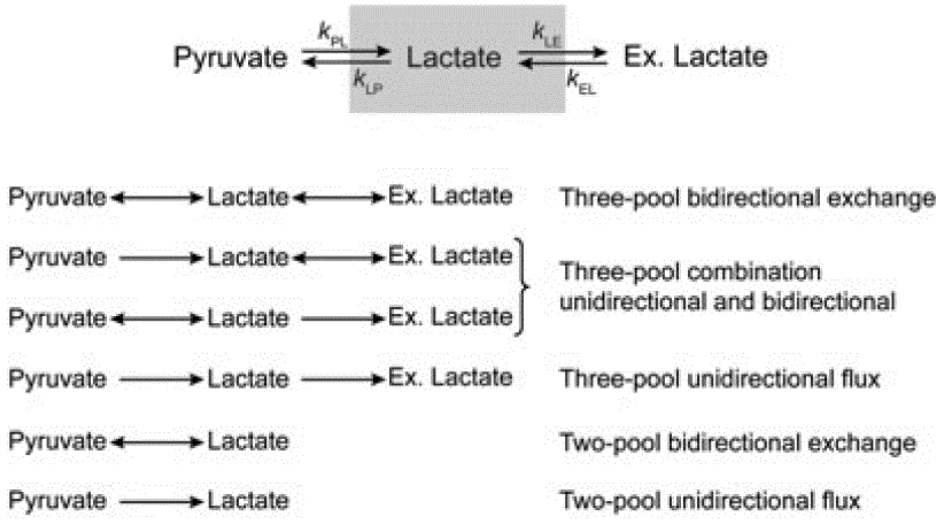

Figure 24: Two- and three-site exchange models. (Harrison, 2012)
Kij is the rate of transfer from pool i to pool j. Ex, extracellular lactate; L, lactate (total or intracellular); P, pyruvate.

Another major aspect currently missing in the field is guidelines regarding animal and patient preparation. If we compare with ^{18}F-FDG PET, strict diet is required to avoid competition between ^{18}F-FDG and glucose for uptake and phoshorylation. Also, the type of anesthesia used can mainly impact ^{18}F-FDG uptake. In hyperpolarized [1-^{13}C]pyruvate NMR experiments, transporter activity and tracer transport are recognized as key factor that can affect rate of transfer. And similar to ^{18}F-FDG, hyperpolarized [1-^{13}C]pyruvate is administered at high doses and could potentially compet for transport and metabolism. It is only recently that the group of Kevin Brindle investigated how the measurement repeatability in tumors could be affected by animal fasting (Serrao, 2016). As expected, they concluded that fasting prior to the MR examination might be preferred to ensure uniform and

constant metabolic status and lower intra-subject variability, especially for repeated experiments.

Further efforts are thus required to optimize experimental protocols for quantitative metabolic imaging with hyperpolarized [1-^{13}C]pyruvate in small animals and will benefit to current clinical studies.

To attest pyruvate metabolism, [1-^{13}C]pyruvate has been the most widely studied hyperpolarized tracer due to its high solubility in water, its ability of easily hyperpolarized, its relatively long relaxation time and its very rapid transport across the cell membrane and rapid metabolism. As already previously described, its transformation into lactate, alanine or bicarbonate can be followed in various tissues. Unfortunately, bicarbonate peak is generally undetectable in tumors due to their high rate of glycolysis but also due to the low pH affecting the balance between bicarbonate and CO_2. Also, metabolism through the Krebs cycle cannot be appraised using this tracer. As presented in **Figure 17**, [1-^{13}C]pyruvate is labeled on the carbonyl acid and transformed by the PDH into ^{13}C-CO_2 and unlabeled AcetylCoA. As the label is lost under the form of CO_2, the label cannot enter the Krebs cycle. In contrast, [2-^{13}C]pyruvate is labeled at the adjacent ketone position and is metabolized similarly to [1-^{13}C]pyruvate into lactate and alanine. However, its transformation by the PDH allows the formation of [1-^{13}C]acetylCoA which can be further metabolized though the Krebs cycle (**Figure 17**). This tracer could represent an interesting tracer to investigate tumor models that present hybrid metabolism, by attesting glycolytic process via the lactate labeling and OXPHOS via the Krebs cycle intermediates labeling, in one experiment. Nevertheless, this tracer presents a reduced relaxation time compared to the conventional [1-^{13}C]pyruvate that could impair the

detection of the metabolites in vivo. However, recent studies probing mitochondrial metabolism in normal rats (Marjanska, 2010) (Hu, 2012) (Park, 2013b) and in a rat C6 glioma model (Park, 2016) demonstrated the feasibility at different magnetic field (3T and 9.4T).

^{18}F-FDG PET to attest glucose metabolism:

^{18}F-FDG PET is a widespread technology approved in clinical practice for cancer diagnosis, staging and treatment monitoring. By highlighting enhanced glycolysis in tumors, this technology supported Warburg's hypothesis, making thus ^{18}F-FDG the tracer of choice to study tumor metabolism. This tracer is generally interpreted as a marker of glycolytic phenotypes, assuming the tumor metabolism to be aerobic (Clavo, 1995) (Waki, 1997) (Gatenby, 2004) (Miles, 2008). Unfortunately, this tracer represents a rather indirect and incomplete demonstration of a Warburg phenotype. Indeed, this tracer highlights the consequences of a glycolytic metabolism and cannot discriminate between areobic glycolysis (Warburg phenotype) and anaerobic glycolysis. Also, if the ^{18}F-FDG PET is not associated with oxygenation or oxygen consumption measurements, we cannot postulate that tumor metabolism is aerobic. Furthermore, glucose can support various metabolic pathways, other than the glycolysis itself. After its uptake, glucose is phosphorylated to glucose-6-phosphate by the hexokinase. Glucose-6-phosphate can than support three pathways, the glycolysis, the glycogen synthesis and the pentose phosphate pathway. As ^{18}F-FDG accumulation relies on GLUT and hexokinase activities, but is not further metabolized, assuming that ^{18}F-FDG represents only glycolytic process in cell would be simplistic. ^{18}F-FDG should preferably be presented as a tracer highlighting the first steps of glycolysis. It is only by combining

this tracer with oxygenation or oxygen consumption measurements and with methods describing other metabolic processes that we would be able to appraise glycolytic metabolism in tumors.

Multi-modality imaging to appraise tumor metabolism:

In general, sensitive and specific techniques are required to describe disease processes. So far, no technology can fulfill these requirements alone. And in the case of cancer, an integral evaluation of tumor metabolism and bioenergetics should be preferred to characterize the numerous metabolic alterations. Also, due to the link between metabolism and microenvironment, a multi-parametric exam could notably improve the knowledge of underlying mechanisms. As already considered in this section about the technical considerations, each technology could benefit from another. For example, ^{17}O NMR and hyperpolarized [1-^{13}C]pyruvate NMR could benefit from perfusion imaging for data analysis and quantification. ^{18}F-FDG PET evaluation could be improved by oxygenation measurements. The generation of multi-parametric map, in parallel with morphological information, should improve many aspects in oncology including diagnosis, characterization of the lesion which is crucial for treatment assignment and treatment follow-up. But of course, more is not always better. PET, MRI and other imaging techniques are complex technologies and efficient use should be examined. Appropriate protocols should be defined to answer a specific question in regard to the tissue under investigation.

2.2. The case of treatments targeting glycolysis

2.2.1. PDK inhibitors and dichloroacetate

Dichloroacetate (DCA), long used to treat lactic acidosis in various pathologies, has emerged as a promising anticancer drug (Bonnet, 2007). Through the inhibition of the pyruvate dehydrogenase kinase, DCA reverts the glycolytic metabolism and reactivates the mitochondrial function in cancer cells. Recently, our group documented that DCA was able to induce a metabolic switch preferentially in glycolytic cancer cells, leading to a more oxidative phenotype and decreasing proliferation, while oxidative cells remained less sensitive to DCA treatment (De Preter, 2016). However, using imaging biomarkers, we showed in this study that glycolytic tumors and oxidative tumors presented a similar response to DCA and we could not observe clear metabolic shift in both tumor models.

While the investigation of DCA as an efficient anticancer treatment is ongoing in patients, some recent studies indicated confusing or contradictory effects between in vitro and in vivo studies. It has been reported that the anticancer effects of DCA may rely on multiple mechanisms depending on the drug concentration, drug administration scheme (Fedorchuk, 2016) and cell type (Stockwin, 2010). Promotion of tumor growth was even observed after DCA treatment in neuroblastoma tumors (Feuerecker, 2015). It is thus not surprising that DCA did not demonstrate convincing effects in advanced non-small cell lung cancer patients during a phase II trial (Garon, 2014). Different hypotheses can be discussed to explain the lack of efficacy of DCA in vivo.

Firstly, lack of effective cellular uptake and mitochondrial targeting could impair DCA efficiency. Recently, Pathak and co-workers developed a mitochondria targeted DCA molecule, called Mito-DCA (**Figure 25.A**), by the incorporation of a lipophilic triphenylphosphonium cation through a biodegradable linker within the molecule. This new drug was able to induce a metabolic shift and apoptosis in tumor cells with dysfunctional mitochondria, while normal cells were not affected (Pathak, 2014). This approach could improve treatment efficacy by reaching appropriate intracellular drug dose. Another strategy has also been developed to selectively deliver DCA into cancer cells. Mitaplatin (**Figure 25.B**) is a compound designed from the fusion of a six-coordinate platinum (IV) complex synthesized from cisplatin, with two DCA moieties in the axial positions (Dhar, 2009). Once in the tumor cell, the drug dissociates into its respective molecules due to the negative intracellular redox potential and displays a dual-killing mode in cancer cells. This approach offers an innovative formulation and a unique mechanism by attacking both nuclear DNA with cisplatin and mitochondria with DCA in cancer cells.

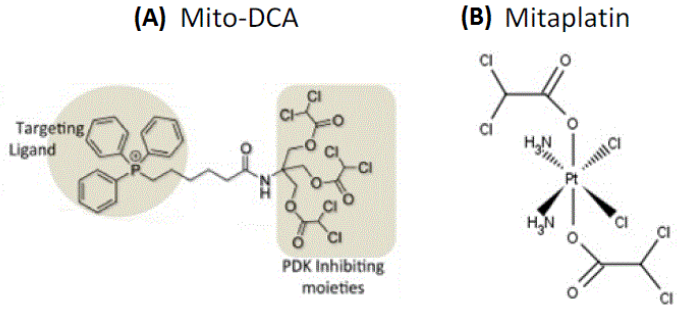

Figure 25: Structure of Mito-DCA (A) and Mitaplatin (B) (Bell, 2016)

Secondly, a change in PDK isoform expression between in vitro and in vivo model could impair DCA efficacy on tumor metabolism in vivo. Indeed, oncogene regulation but also local tumor microenvironment can affect PDK isoform, possibly leading to the expression of a PDK isoform less sensitive to DCA effects. We can thus not exclude the effect of extracellular pH on DCA efficacy in our models. The systematic comparison of PDK isoforms expression in vitro and in vivo could benefit for preclinical studies, but also the characterization in patient tumors could predict DCA efficacy and identify good candidates for DCA treament.

Thirdly, DCA could present a lack of specificity against PDK as recent finding suggested that DCA may also act by other mechanisms. A possible disruption of the balance between fatty acid β-oxidation and glucose oxidation has already been suggested (as reviewed by Sutendra, 2013). New compounds targeting of the lipoyl-binding pocket or the ATP binding pocket are under development to obtain an optimal PDK inhibition (Saunier, 2016) (Bell, 2016). Also, DCA effects on PDK and on other metabolic pathways could potentially lead to compensatory effects in the tumor cells. Indeed, external stimuli and local microenvironment are known to lead to a metabolic reorganization. For example, it has been described recently that chronic tumor acidosis induces a metabolic rewiring towards fatty acid oxidation (Corbet, 2016). As DCA is known to decrease glucose uptake and to reduce lactate within the microenvironment, other metabolic pathways such as the fatty acid oxidation, glutaminolysis or the serine pathway could potentially be affected and could lead to both anti- or procancer effects.

Finally, the metabolic alterations described in vitro that led to the development of DCA could be dramatically different in vivo. This

hypothesis has already been discussed in this manuscript but this demonstrates that the identification of relevant metabolic distortions is crucial. We have already presented numerous imaging technologies able to study glucose metabolism but some techniques are also available to study noninvasively the metabolism of various molecules such as glutamine (glu-Chemical exchange saturation transfer imaging, hyperpolarized ^{13}C-glutamine NMR, ^{18}F-fluoroglutamine PET), amino acids (^{11}C-methionine PET, ^{18}F-fluorothylthyrosine), lipid (^{31}P MRS, ^{1}H-choline MRS, ^{11}C-choline PET) or glycogen (^{18}F-NFTG PET) (Sengupta, 2016). These techniques could be used to identify new targets for anticancer treatment but also to support drug development by characterizing the mechanisms of action and drug efficacy.

In summary, challenges remain for the development of anticancer drug presenting good specificity and appropriate delivery to the target.

2.2.2. Targeting the metabolic interplay between host cell and cancer cells, a new anticancer strategy

Current anticancer strategies target specific alterations present in the tumor cells. But, as previously described, host cells collaborate with tumor cells and act as brothers in arms to support the malignant process. In order to restore a normal endothelial and immune cell function, a new strategy would be to target the metabolic interplay existing between host cells and cancer cells. For example, 3PO, a specific inhibitor of PFKBP3, has been tested for its antiangiogenic potential. 3PO reduced glycolysis in endothelial cells in vitro and impaired endothelial cell proliferation (Verdegem, 2014). The reactivation of exhausted T cells by adjusting their metabolism has also

been presented as a potential strategy (Mockler, 2014). The possibilities of modulating the metabolic interplay existing in the tumor mass may represent a promising way to treat cancer and necessitates further investigation.

2.2.3. Multi-modality imaging to assess treatment response

Many agents targeting tumor metabolism are cytostatic (Tennant, 2010). Therefore tumor shrinkage may not be seen and the use of conventional anatomical imaging techniques would not be optimal for treatment response assessment. Functional and molecular imaging techniques may play a unique role as it offers the possibility of an early assessment of the tumor response by reflecting the biologic activity in tumors (Figueiras, 2011) (Serkova, 2011). Nevertheless, the imaging technologies previously proposed for tumor phenotyping are not able to fully explain the effects of targeted drug. Indeed, changes in metabolic biomarkers observed after treatment could also result from impaired perfusion or cell loss. Multi-modality imaging attesting morphology, perfusion, cellularity and metabolism are thus essential to describe tumor response to treatment targeting metabolism.

2.3. Chances and challenges of translation to the clinic

2.3.1. Tumor models for translational cancer research

Understanding the mechanisms involved in the metabolic discrepancy between in vitro and in vivo conditions will considerably affect cancer research. Nevertheless, efforts to find relevant tumor models that reflect

tumor patient heterogeneity and patient outcomes are essential. Some approaches currently used will be discussed in this section.

In syngeneic tumor models, animal tumor cell lines are grafted in syngeneic immunocompetent animals. Using this approach, intact immune system can interact with the developing tumor. Unfortunately, these tumor models do not generally reflect the biological properties and the cellular heterogeneity of patient tumors (Huszthy, 2012). Human tumor xenografts are thus generally preferred.

Xenografts using conventional human cell lines represent the majority of the tumor models investigated due to its easy use. Nevertheless, this approach do not always correlate with clinical outcomes in patients, as the generation of cancer cell lines could majorly alter biologic and genetic properties and cause the loss of specific cell population (Hidalgo, 2014). Human tumor samples engrafted directly into immune-compromised mice may offer several advantages over standard cell-line xenograft models (Huszthy, 2012). By maintaining the 3D structure of the tissue, the sample will contain the different tumor cell clones, host cells and also component from the extracellular matrix. This approach has the advantage to be biologically stable even after a few passages in mice and global gene-expression patterns, mutational status, metastatic potential, drug responsiveness and tumor architecture are preserved (Tentler, 2014). However, the use of immunodeficient animals provides a less realistic tumor microenvironment. Human tumor xenografts in humanized mouse models should be preferred to better mimic the human local microenvironment. This is also a preferable approach for immunotherapy studies.

Genetically engineered mouse (GEM) models are useful to study the effect of specific mutations during tumor progression but cannot fully reproduce the genetic complexity of human tumors. As only a few mutations can be studied and that tumor development is slow and variable, this approach is time consuming, expensive and difficult to validate (Richmond, 2008).

Human tumor samples approach could thus provide a more-relevant preclinical system to examine clinically directed hypothesis, to identify new targets for anticancer treatment and to test drug activity or new drug combinations. However, challenges remain to validate this approach, as no common methodology is currently applied. Standard procedures for biopsy sampling, biopsy preparation/preservation and tissue implantation should be defined. Once validated, another pertinent strategy would be to use animal tumor models to improve patient management in a concept called co-clinical trial (**Figure 26**) (Hidalgo, 2014). Parallel studies in patients and in animal models generated from these patients could be useful:

- to identify potential biomarkers for patient enrolment;
- to assess drug response simultaneously in the patient and the animal model;
- to identify mechanisms of resistance;
- to interrogate other novel drug combinations.

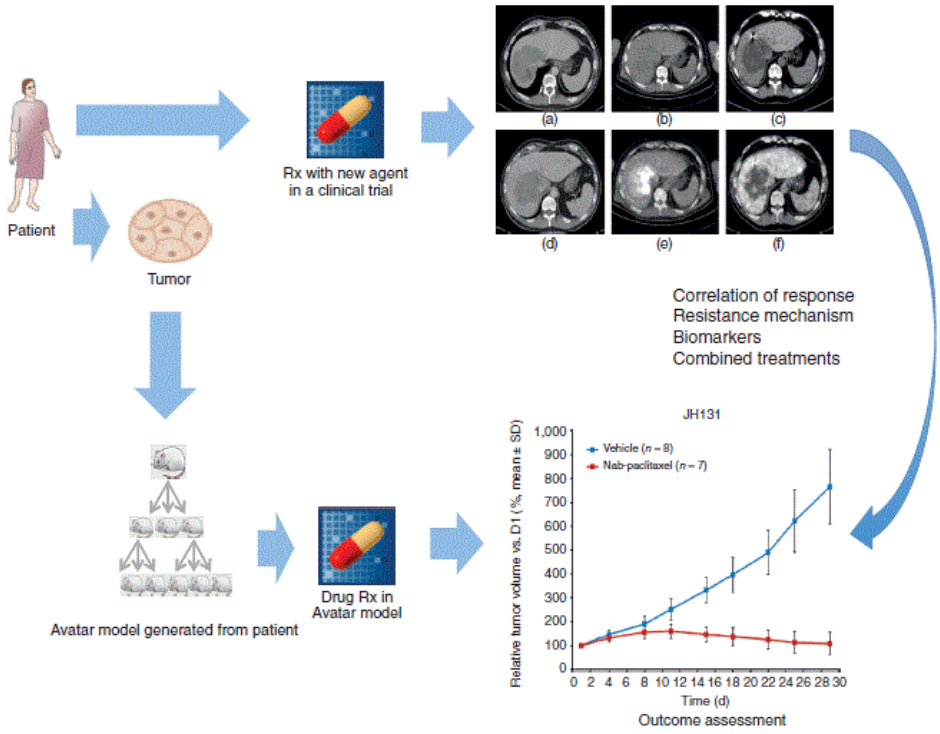

Figure 26: Co-clinical trial approach with human xenograft tumor model developed from a patient enrolled and treated in a clinical trial with a novel agent (Hidalgo, 2014).

2.3.2. Imaging technology refinement for clinical use

^{18}F-FDG PET has already been used for decades in human and strong guidelines has emerged from this long clinical practice to ensure relevant use for this technique in cancer patients. Unfortunately, this is not yet the case for emerging technologies like hyperpolarized ^{13}C-MRI or ^{17}O MRS.

For ^{17}O MRS experiments, the high cost of ^{17}O-labeled gas remains a major limitation. Isotope recovery systems, already developed for pig studies, should be considered (Tailor, 2004) (Baumgardner, 2008). Also the low sensitivity at low magnetic field could impair the impact of the technology in center not enjoying high field MRI scanner. Finally, RF coil, gas delivery and models for oxygen consumption quantification need to be adapted for clinical use, as the human body size, lung capacity and respiration rate as well as blood circulation speed are drastically different from those in small animals (Zhu, 2002) (Zhu, 2005) (Zhu, 2011). Protocols proposed by studies performed in pigs, which are animals with lung capacity similar to humans, could help for protocol design in humans (Tailor, 2004) (Baumgardner, 2008). However, the steadily growing number of study performed in humans will certainly help for the translation of ^{17}O MRS into clinical practice (Hoffmann 2011) (Hoffmann 2014) (Borowiak, 2014).

For hyperpolarized ^{13}C-MRI studies, patient handling, tracer safety need to be defined during the ongoing clinical trials. Furthermore, the polarizers need to be adapted to provide an automated process with minimal operator intervention but still ensuring quality control and sterility (Ardenkjaer-Larsen, 2016). Anyway, the limited number of technicians familiar with the MRI and MRS and complex data processing are factors that will limit the impact of the technology in the clinical setting (Lin, 2014).

Beside the limitations of each individual technique, another challenge consists in the development of protocols for multi-modality imaging in patients in which patient care needs to be optimized. The protocol has to provide a fast and relevant approach that will benefit to the patient. The development of PET/MR systems will certainly improve these aspects.

Using this kind of device, PET and MR sequences can be started at the same time during one examination, providing multiparametric data with a good image fusion. A recent study has investigated the feasibility of this approach using a combined clinical PET/MRI scanner in canine cancer patients (Gutte, 2015). Performed within 2 hours, they successfully visualized ^{18}F-FDG uptake and [1-^{13}C]pyruvate transformation. However, the impact of multi-injection of tracers should be investigated, especially to avoid competing uptake or metabolism that may distort the results.

3. General conclusions

In this study, we designed a multi-modality imaging project to identify metabolic signature inside solid tumors based on metabolic modulations. ^{18}F-FDG PET, hyperpolarized [1-^{13}C]pyruvate MRI, EPR oximetry and ^{17}O MRS were used to study the impact of DCA treatment and carbogen breathing in glycolytic and oxidative tumor models. The current study established a metabolic discrepancy between in vitro and in vivo conditions. While tumor cell lines presented distinct behaviors according to their metabolic profiles, the tumors models presented similar metabolic patterns in vivo. The absence of true correlation between in vitro and in vivo tumor models suggested the key role of local microenvironment and host cells to shape tumor features. In the future, multimodal non invasive imaging should be considered to identify relevant metabolic alterations in patients, which would help for anticancer treatment development. Animal tumor models derived from patients could be used to test treatment efficacy, mechanisms of resistance and drug combinations. However today, emerging techniques, like hyperpolarized ^{13}C-MRI or ^{17}O MRS, still require improvements for optimal use of these methods in patients and appropriate protocols for animal models generation has still to be determined.

BIBLIOGRAPHY

(Abildgaard, 2014)

Abildgaard C, Dahl C, Basse AL, Ma T, Guldberg P. Bioenergetic modulation with dichloroacetate reduces the growth of melanoma cells and potentiates their response to BRAFV600E inhibition. Journal of Translational Medicine 2014;12:247

(Adams, 2010)

Adams MC, Turkington TG, Wilson JM, Wong TZ. A systematic review of the factors affecting accuracy of SUV measurements. AJR American journal of roentgenology 2010;195(2):310-320

(Andronesi, 2013)

Andronesi OC, Rapalino O, Gerstner E, Chi A, Batchelor TT, Cahill DP, Sorensen AG, Rosen BR. Detection of oncogenic IDH1 mutations using magnetic resonance spectroscopy of 2-hydroxyglutarate. The Journal of clinical investigation 2013;123(9):3659-3663

(Arai, 1990)

Arai T, Nakao S, Mori K, Ishimori K, Morishima I, Miyazawa T, Fritz-Zieroth B. Cerebral oxygen utilization analyzed by the use of oxygen-17 and its nuclear magnetic resonance. Biochemical and Biophysical Research Communications. 1990;169(1):153-158

(Arai, 1991)

Arai T, Mori K, Nakao S, Watanabe K, Kito K, Aoki M, Mori H, Morikawa S, Inubushi T. In vivo oxygen-17 nuclear magnetic resonance for the estimation of cerebral blood flow and oxygen consumption. Biophysical Research Communications. 1991;179(2):954-61

(Ardenkjaer-Larsen, 2003)

Ardenkjaer-Larsen JH, Fridlund B, Gram A, Hansson G, Hansson L, Lerche MH, Servin R, Thaning M, Golman K. Increase in signal-to-noise ratio of > 10,000 times in liquid-state NMR. Proceedings of the National Academy of Sciences of the United States of America 2003;100(18):10158-10163

(Ardenkjaer-Larsen, 2016)

Ardenkjaer-Larsen JH. On the present and future of dissolution-DNP. Journal of magnetic resonance 2016;264:3-12

(Atkinson, 2010)

Atkinson IC, Thulborn KR. Feasibility of mapping the tissue mass corrected bioscale of cerebral metabolic rate of oxygen consumption using 17-oxygen and 23-sodium MR imaging in a human brain at 9.4 T. NeuroImage 2010;51(2):723-733

(Avril, 2007)

Avril N, Propper D. Functional PET imaging in cancer drug development. Future Oncology. 2007;3(2):215-228

(Bhat, 2015)

Bhat TA, Kumar S, Chaudhary AK, Yadav N, Chandra D. Restoration of mitochondria function as a target for cancer therapy. Drug discovery today 2015;20(5):635-643

(Baumgardner, 2008)

Baumgardner JE, Mellon EA, Tailor DR, Mallikarjunarao K, Borthakur A, Reddy R. Mechanical ventilator for delivery of $^{17}O_2$ in brief pulses. Open Biomed Eng J. 2008;2:57-63

(Bell, 2016)

Bell H, Parkin E. Pyruvate dehydrogenase kinase inhibition: Reversing the Warburg effect in cancer therapy. International Journal of Cancer Therapy and Oncology 2016;4(2):4215

(Biaglow, 1998)

Biaglow JE, Manevich Y, Leeper D, Chance B, Dewhirst MW, Jenkins WT, Tuttle SW, Wroblewski K, Glickson JD, Stevens C, Evans SM. MIBG inhibits respiration: potential for radio- and hyperthermic sensitization. International Journal of radiation oncology, biology, physics 1998;42(4):871-876

(Bonnet, 2007)

Bonnet S, Archer SL, Allalunis-Turner J, Haromy A, Beaulieu C, Thompson R, Lee CT, Lopaschuk GD, Puttagunta L, Bonnet S, Harry G, Hashimoto K, Porter CJ, Andrade MA, Thebaud B, Michelakis ED. A mitochondria-K+ channel axis is suppressed in cancer and its normalization promotes apoptosis and inhibits cancer growth. Cancer cell 2007;11(1):37-51

(Borowiak, 2014)

Borowiak R, Groebner J, Haas M, Hennig J, Bock M. Direct cerebral and cardiac 17O-MRI at 3 Tesla: initial results at natural abundance. Magma 2014;27(1):95-99

(Brindle, 2008)

Brindle K. New approaches for imaging tumour responses to treatment. Nature reviews Cancer 2008;8(2):94-107

(Brindle, 2011)

Brindle KM, Bohndiek SE, Gallagher FA, Kettunen MI. Tumor imaging using hyperpolarized 13C magnetic resonance spectroscopy. Magnetic resonance in medicine 2011;66(2):505-519

(Brindle, 2012)

Brindle K. Watching tumours gasp and die with MRI: the promise of hyperpolarised 13C MR spectroscopic imaging. The British journal of radiology 2012;85(1014):697-708

(Brindle, 2015)

Brindle KM. Imaging metabolism with hyperpolarized (13)C-labeled cell substrates. Journal of the American Chemical Society 2015;137(20):6418-6427

(Butler, 2013)

Butler EB, Zhao Y, Munoz-Pinedo C, Lu J, Tan M. Stalling the engine of resistance: targeting cancer metabolism to overcome therapeutic resistance. Cancer research 2013;73(9):2709-2717

(Cairns, 2011)

Cairns RA, Harris IS, Mak TW. Regulation of cancer cell metabolism. Nature reviews Cancer 2011;11(2):85-95

(Castillo, 1996)

Castillo M, Kwock L, Mukherji SK. Clinical applications of proton MR spectroscopy. AJNR American Journal of Neuroradiology. 1996;17(1):1-15

(Chaumeil, 2013)

Chaumeil MM, Larson PE, Yoshihara HA, Danforth OM, Vigneron DB, Nelson SJ, Pieper RO, Phillips JJ, Ronen SM. Non-invasive in vivo assessment of IDH1 mutational status in glioma. Nature communications 2013;4:2429

(Chen, 2008)

Chen AP, Kurhanewicz J, Bok R, Xu D, Joun D, Zhang V, Nelson SJ, Hurd RE, Vigneron DB. Feasibility of using hyperpolarized [1-13C]lactate as a substrate for in vivo metabolic 13C MRSI studies. Magnetic resonance imaging 2008;26(6):721-726

(Choi, 2013)

Choi YK, Park KG. Metabolic roles of AMPK and metformin in cancer cells. Molecules and cells 2013;36(4):279-287

(Chu, 2015)

Chu QS, Sangha R, Spratlin J, Vos LJ, Mackey JR, McEwan AJ, Venner P, Michelakis ED. A phase I open-labeled, single-arm, dose-escalation, study of dichloroacetate (DCA) in patients with advanced solid tumors. Investigational new drugs 2015;33(3):603-610

(Clavo, 1995)

Clavo AC, Brown RS, Wahl RL. Fluorodeoxyglucose uptake in human cancer cell lines is increased by hypoxia. Journal of Nuclear Medicine 1995;36(9):1625-1632

(Corbet, 2016)

Corbet C, Pinto A, Martherus R, Santiago de Jesus JP, Polet F, Feron O. Acidosis Drives the Reprogramming of Fatty Acid Metabolism in Cancer Cells through Changes in Mitochondrial and Histone Acetylation. Cell metabolism 2016;24(2):311-323

(Costa, 2014)

Costa A, Scholer-Dahirel A, Mechta-Grigoriou F. The role of reactive oxygen species and metabolism on cancer cells and their microenvironment. Seminars in cancer biology 2014;25:23-32

(Dang, 2011)

Dang CV, Hamaker M, Sun P, Le A, Gao P. Therapeutic targeting of cancer cell metabolism. Journal of molecular medicine 2011;89(3):205-212

(Dang, 2012)

Dang CV. Links between metabolism and cancer. Genes & development 2012;26(9):877-890

(Daniels, 2016)

Daniels CJ, McLean MA, Schulte RF, Robb FJ, Gill AB, McGlashan N, Graves MJ, Schwaiger M, Lomas DJ, Brindle KM, Gallagher FA. A comparison of quantitative methods for clinical imaging with hyperpolarized (13)C-pyruvate. NMR in biomedicine 2016;29(4):387-399

(Day, 2007)

Day SE, Kettunen MI, Gallagher FA, Hu DE, Lerche M, Wolber J, Golman K, Ardenkjaer-Larsen JH, Brindle KM. Detecting tumor response to treatment using hyperpolarized 13C magnetic resonance imaging and spectroscopy. Nature medicine 2007;13(11):1382-1387

(de Graaf, 2003)

de Graaf RA, Mason GF, Patel AB, Behar KL, Rothman DL. In vivo 1H-[13C]-NMR spectroscopy of cerebral metabolism. NMR in biomedicine 2003;16(6-7):339-357

(de Graaf, 2007)

de Graaf RA. Basic Principles. In Vivo NMR Spectroscopy: John Wiley & Sons, Ltd; 2007. p 1-42

(de Graaf, 2011)

de Graaf RA, Rothman DL, Behar KL. State of the art direct 13C and indirect 1H-[13C] NMR spectroscopy in vivo. A practical guide. NMR in biomedicine 2011;24(8):958-972

(De Preter, 2016)

De Preter G, Neveu MA, Danhier P, Brisson L, Payen VL, Porporato PE, Jordan BF, Sonveaux P, Gallez B. Inhibition of the pentose phosphate pathway by dichloroacetate unravels a missing link between aerobic glycolysis and cancer cell proliferation. Oncotarget 2016;7(3):2910-2920

(Delaney, 2015)

Delaney LM, Ho N, Morrison J, Farias NR, Mosser DD, Coomber BL. Dichloroacetate affects proliferation but not survival of human colorectal cancer cells. Apoptosis : an international journal on programmed cell death 2015;20(1):63-74

(Dhar, 2009)

Dhar S, Lippard SJ. Mitaplatin, a potent fusion of cisplatin and the orphan drug dichloroacetate. Proceedings of the National Academy of Sciences of the United States of America 2009;106(52):22199-22204

(Doherty, 2013)

Doherty JR, Cleveland JL. Targeting lactate metabolism for cancer therapeutics. The Journal of clinical investigation 2013;123(9):3685-3692

(Draoui, 2011)

Draoui N, Feron O. Lactate shuttles at a glance: from physiological paradigms to anti-cancer treatments. Disease models & mechanisms 2011;4(6):727-732

(Draoui, 2014)

Draoui N, Schicke O, Seront E, Bouzin C, Sonveaux P, Riant O, Feron O. Antitumor activity of 7-aminocarboxycoumarin derivatives, a new class of potent inhibitors of lactate influx but not efflux. Molecular cancer therapeutics 2014;13(6):1410-1418

(D'Souza, 2011)

D'Souza GG, Wagle MA, Saxena V, Shah A. Approaches for targeting mitochondria in cancer therapy. Biochimica et biophysica acta 2011;1807(6):689-696

(Dunbar, 2014)

Dunbar EM, Coats BS, Shroads AL, Langaee T, Lew A, Forder JR, Shuster JJ, Wagner DA, Stacpoole PW. Phase 1 trial of dichloroacetate (DCA) in adults with recurrent malignant brain tumors. Investigational new drugs 2014;32(3):452-464

(Dutta, 2013)

Dutta P, Martinez GV, Gillies RJ. A New Horizon of DNP technology: Application to In-vivo 13C Magnetic Resonance Spectroscopy and Imaging. Biophysical reviews 2013;5(3):271-281

(El Sayed, 2013)

El Sayed SM, Mahmoud AA, El Sawy SA, Abdelaal EA, Fouad AM, Yousif RS, Hashim MS, Hemdan SB, Kadry ZM, Abdelmoaty MA, Gabr AG, Omran FM, Nabo MM, Ahmed NS. Warburg effect increases steady-state ROS condition in cancer cells through decreasing their antioxidant capacities (anticancer effects of 3-bromopyruvate through antagonizing Warburg effect). Medical hypotheses 2013;81(5):866-870

(Fais, 2014)

Fais S, Venturi G, Gatenby B. Microenvironmental acidosis in carcinogenesis and metastases: new strategies in prevention and therapy. Cancer metastasis reviews 2014;33(4):1095-1108

(Fang, 2010)

Fang M, Shen Z, Huang S, Zhao L, Chen S, Mak TW, Wang X. The ER UDPase ENTPD5 promotes protein N-glycosylation, the Warburg effect, and proliferation in the PTEN pathway. Cell 2010;143:711–724

(Farwell, 2014)

Farwell MD, Pryma DA, Mankoff DA. PET/CT imaging in cancer: current applications and future directions. Cancer 2014;120(22):3433-3445

(Fedorchuk, 2016)

Fedorchuk AG, Pyaskovskaya ON, Gorbik GV, Prokhorova IV, Kolesnik DL and Solyanik GI. Effectiveness of sodium dichloroacetate against glioma C6 depends on administration schedule and dosage. Experimental oncology 2016; 38(2):80-83

(Feron, 2009)

Feron O. Pyruvate into lactate and back: from the Warburg effect to symbiotic energy fuel exchange in cancer cells. Radiotherapy and oncology 2009;92(3):329-333

(Feuerecker, 2015)

Feuerecker B, Seidl C, Pirsig S, Bruchelt G and Senekowitsch-Schmidtke R. DCA promotes progression of neuroblastoma tumors in nude mice. American Journal of Cancer Research 2015; 5(2):812-820

(Figueiras, 2011)

Figueiras RG, Padhani AR, Goh VJ, Vilanova JC, González SB, Martín CV, Caamaño AG, Naveira AB, Choyke PL. Novel oncologic drugs: what they do and how they affect images. Radiographics 2011;31(7):2059-2091

(Gallagher, 2008)

Gallagher FA, Kettunen MI, Day SE, Hu DE, Ardenkjaer-Larsen JH, Zandt R, Jensen PR, Karlsson M, Golman K, Lerche MH, Brindle KM. Magnetic resonance imaging of pH in vivo using hyperpolarized 13C-labelled bicarbonate. Nature 2008;453(7197):940-943

(Gallez, 2004)

Gallez B, Baudelet C, Jordan BF. Assessment of tumor oxygenation by electron paramagnetic resonance: principles and applications. NMR in biomedicine 2004;17(5):240-262

(Ganapathy-Kanniappan, 2013)

Ganapathy-Kanniappan S, Geschwind JF. Tumor glycolysis as a target for cancer therapy: progress and prospects. Molecular Cancer 2013;12:152

(Garcia-Figueiras, 2016)

Garcia-Figueiras R, Baleato-Gonzalez S, Padhani AR, Oleaga L, Vilanova JC, Luna A, Cobas Gomez JC. Proton magnetic resonance spectroscopy in oncology: the fingerprints of cancer? Diagnostic and interventional radiology 2016;22(1):75-89

(Garon, 2014)

Garon EB, Christofk HR, Hosmer W, Britten CD, Bahng A, Crabtree MJ, Hong CS, Kamranpour N, Pitts S, Kabbinavar F, Patel C, von Euw E, Black A, Michelakis ED, Dubinett SM, Slamon DJ. Dichloroacetate should be considered with platinum-based chemotherapy in hypoxic tumors rather than as a single agent in advanced non-small cell lung cancer. Journal of cancer research and clinical oncology 2014;140(3):443-452

(Gatenby, 2014)

Gatenby RA, Gillies RJ. Why do cancers have high aerobic glycolysis? Nature reviews Cancer 2004;4(11):891-899

(Gillies, 1994)

Gillies RJ, Liu Z, Bhujwalla Z. 31P-MRS measurements of extracellular pH of tumors using 3-aminopropylphosphonate. American Journal of Physiology. 1994;267(1 Pt 1):C195-203

(Gillies, 2008)

Gillies RJ, Robey I, Gatenby RA. Causes and consequences of increased glucose metabolism of cancers. Journal of nuclear medicine 2008;49 Suppl 2:24S-42S

(Golman, 2003)

Golman K, Olsson LE, Axelsson O, Mansson S, Karlsson M, Petersson JS. Molecular imaging using hyperpolarized 13C. The British journal of radiology 2003;76 Spec No 2:S118-127

(Golman, 2006a)

Golman K, Petersson JS. Metabolic imaging and other applications of hyperpolarized 13C1. Academic radiology 2006;13(8):932-942

(Golman, 2006b)

Golman K, in 't Zandt R, Thaning M. Real-time metabolic imaging. Proceedings of the National Academy of Sciences of the United States of America 2006;103(30):11270-11275

(Golman, 2006c)

Golman K, Zandt RI, Lerche M, Pehrson R, Ardenkjaer-Larsen JH. Metabolic imaging by hyperpolarized 13C magnetic resonance imaging for in vivo tumor diagnosis. Cancer research 2006;66(22):10855-10860

(Gonzalez, 2014)

Gonzalez CD, Alvarez S, Ropolo A, Rosenzvit C, Bagnes MF, Vaccaro MI. Autophagy, Warburg, and Warburg reverse effects in human cancer. BioMed research international 2014;2014:926729

(Granchi, 2012)

Granchi C, Minutolo F. Anticancer agents that counteract tumor glycolysis. ChemMedChem 2012;7(8):1318-1350

(Granchi, 2014)

Granchi C, Fancelli D, Minutolo F. An update on therapeutic opportunities offered by cancer glycolytic metabolism. Bioorganic & medicinal chemistry letters 2014;24(21):4915-4925

(Grégoire, 2007)

Grégoire V, Haustermans K, Geets X, Roels S, Lonneux M. PET-based treatment planning in radiotherapy: a new standard? Journal of Nuclear Medicine 2007;48 Suppl 1:68S-77S

(Guimarães, 2015)

Guimarães IS, Nayara G. Tessarollo, Paulo C.M. Lyra-Júnior, Diandra Z. dos Santos, Roger C. Zampier, Laura F.R.L. de Oliveira, Krislayne V. Siqueira, Ian V. Silva, Leticia B.A. Rangel (2015). Targeting the PI3K/AKT/mTOR Pathway in Cancer Cells, Updates on Cancer Treatment, Prof. Letícia Rangel (Ed.), InTech, DOI: 10.5772/61676. Available from: http://www.intechopen.com/books/updates-on-cancer-treatment/targeting-the-pi3k-akt-mtor-pathway-in-cancer-cells

(Gupta, 2012)

Gupta SC, Hevia D, Patchva S, Park B, Koh W, Aggarwal BB. Upsides and downsides of reactive oxygen species for cancer: the roles of reactive oxygen species in tumorigenesis, prevention, and therapy. Antioxidants & redox signaling 2012;16(11):1295-1322

(Gutte, 2015)

Gutte H, Hansen AE, Larsen MM, Rahbek S, Henriksen ST, Johannesen HH, Ardenkjaer-Larsen J, Kristensen AT, Hojgaard L, Kjaer A. Simultaneous Hyperpolarized 13C-Pyruvate MRI and 18F-FDG PET (HyperPET) in 10 Dogs with Cancer. Journal of nuclear medicine 2015;56(11):1786-1792

(Hanahan, 2011)

Hanahan D, Weinberg RA. Hallmarks of cancer: the next generation. Cell 2011;144(5):646-674

(Hardie, 2013)

Hardie DG. AMPK: a target for drugs and natural products with effects on both diabetes and cancer. Diabetes 2013;62(7):2164-2172

(Harrison, 2012)

Harrison C, Yang C, Jindal A, DeBerardinis RJ, Hooshyar MA, Merritt M, Dean Sherry A, Malloy CR. Comparison of kinetic models for analysis of pyruvate-to-lactate exchange by hyperpolarized 13 C NMR. NMR in biomedicine 2012;25(11):1286-1294

(Hashemi, 2012)

Hashemi RH, Bradley WG, Lisanti CG. MRI: The Basics. Lippincott Williams & Wilkins; 2012

(Hidalgo, 2014)

Hidalgo M, Amant F, Biankin AV, Budinska E, Byrne AT, Caldas C, Clarke RB, de Jong S, Jonkers J, Maelandsmo GM, Roman-Roman S, Seoane J, Trusolino L, Villanueva A. Patient-derived xenograft models: an emerging platform for translational cancer research. Cancer Discov 2014;4(9):998-1013

(Hill, 2013)

Hill DK, Orton MR, Mariotti E, Boult JK, Panek R, Jafar M, Parkes HG, Jamin Y, Miniotis MF, Al-Saffar NM, Beloueche-Babari M, Robinson SP, Leach MO, Chung YL and Eykyn TR. Model Free Approach to Kinetic Analysis of Real-Time Hyperpolarized 13C Magnetic Resonance Spectroscopy Data. PLoS ONE. 2013; 8(9):e71996

(Hockenbery, 2013)

Hockenbery DM, Tom M, Abikoff C, Margineantu D. The Warburg Effect and Beyond: Metabolic Dependencies for Cancer Cells. 2013:35-51

(Hoffmann, 2011)

Hoffmann SH, Begovatz P, Nagel AM, Umathum R, Schommer K, Bachert P, Bock M. A measurement setup for direct 17O MRI at 7 T. Magnetic resonance in medicine 2011;66(4):1109-1115

(Hoffmann, 2014)

Hoffmann SH, Radbruch A, Bock M, Semmler W, Nagel AM. Direct (17)O MRI with partial volume correction: first experiences in a glioblastoma patient. Magma 2014;27(6):579-587

(Hou, 2013)

Hou H, Mupparaju SP, Lariviere JP, Hodge S, Gui J, Swartz HM, Khan N. Assessment of the changes in 9L and C6 glioma pO2 by EPR oximetry as a prognostic indicator of differential response to radiotherapy. Radiation research 2013;179(3):343-351

(Hu, 2012)

Hu S, Yoshihara HA, Bok R, Zhou J, Zhu M, Kurhanewicz J, Vigneron DB. Use of hyperpolarized [1-13C]pyruvate and [2-13C]pyruvate to probe the effects of the anticancer agent dichloroacetate on mitochondrial metabolism in vivo in the normal rat. Magnetic resonance imaging 2012;30(10):1367-1372

(Huszthy, 2012)

Huszthy PC, Daphu I, Niclou SP, Stieber D, Nigro JM, Sakariassen PO, Miletic H, Thorsen F, Bjerkvig R. In vivo models of primary brain tumors: pitfalls and perspectives. Neuro-oncology 2012;14(8):979-993

(Hutchins, 2008)

Hutchins GD, Miller MA, Soon VC, Receveur T. Small animal PET imaging. ILAR Journal 2008;49(1):54-65

(Hwang, 2015)

Hwang JH, Choi CS. Use of in vivo magnetic resonance spectroscopy for studying metabolic diseases. Experimental & molecular medicine 2015;47:e139

(Icard, 2012)

Icard P, Lincet H. A global view of the biochemical pathways involved in the regulation of the metabolism of cancer cells. Biochimica et biophysica acta 2012;1826(2):423-433

(Jadvar, 2005)

Jadvar, H, Parker, JA. PET radiotracers. Clinical PET and PET/CT. Springer-Verlag London; 2005:45–67

(Jordan, 2010a)

Jordan BF, Gallez B. Non-Invasive Imaging of the Tumor Microenvironment. Tumor Microenvironment: John Wiley & Sons, Ltd; 2010. p 229-270

(Jordan, 2010b)

Jordan BF, Gallez B. Surrogate MR markers of response to chemo- or radiotherapy in association with co-treatments: a retrospective analysis of multi-modal studies. Contrast Media & Molecular Imaging 2010;5(6):323-332

(Jordan, 2012)

Jordan BF, Sonveaux P. Targeting tumor perfusion and oxygenation to improve the outcome of anticancer therapy. Frontiers in pharmacology 2012;3:94.

(Jose, 2011)

Jose C, Bellance N, Rossignol R. Choosing between glycolysis and oxidative phosphorylation: a tumor's dilemma? Biochimica et biophysica acta 2011;1807(6):552-561.

(Kankotia, 2014)

Kankotia S, Stacpoole PW. Dichloroacetate and cancer: new home for an orphan drug? Biochimica et biophysica acta 2014;1846(2):617-629

(Karroum, 2012)

Karroum O, Kengen J, Danhier P, Magat J, Mignion L, Bouzin C, Verrax J, Charette N, Starkel P, Calderon PB, Sonveaux P, Feron O, Grégoire V, Gallez B, Jordan BF. Tumor reoxygenation following administration of Mitogen-Activated Protein Kinase inhibitors: a rationale for combination with radiation therapy. Radiotherapy and Oncology. 2012;105(1):64-71.

(Keshari, 2009)

Keshari KR, Wilson DM, Chen AP, Bok R, Larson PE, Hu S, Van Criekinge M, Macdonald JM, Vigneron DB, Kurhanewicz J. Hyperpolarized [2-13C]-fructose: a hemiketal DNP substrate for in vivo metabolic imaging. Journal of the American Chemical Society 2009;131(48):17591-17596

(Keshari, 2014)

Keshari KR, Wilson DM. Chemistry and biochemistry of 13C hyperpolarized magnetic resonance using dynamic nuclear polarization. Chemical Society reviews 2014;43(5):1627-1659

(Kettunen, 2010)

Kettunen MI, Hu DE, Witney TH, McLaughlin R, Gallagher FA, Bohndiek SE, Day SE, Brindle KM. Magnetization transfer measurements of exchange between hyperpolarized [1-13C]pyruvate and [1-13C]lactate in a murine lymphoma. Magnetic resonance in medicine : official journal of the Society of Magnetic Resonance in Medicine / Society of Magnetic Resonance in Medicine 2010;63(4):872-880

(Kircher, 2012)

Kircher MF, Hricak H, Larson SM. Molecular imaging for personalized cancer care. Molecular oncology 2012;6(2):182-195

(Koritzinsky, 2015)

Koritzinsky M. Metformin: A Novel Biological Modifier of Tumor Response to Radiation Therapy. International journal of radiation oncology, biology, physics 2015;93(2):454-464

(Krishna, 2012)

Krishna MC, Matsumoto S, Yasui H, Saito K, Devasahayam N, Subramanian S, Mitchell JB. Electron paramagnetic resonance imaging of tumor pO(2). Radiation research 2012;177(4):376-386

(Kurhanewicz, 2008)

Kurhanewicz J, Bok R, Nelson SJ, Vigneron DB. Current and potential applications of clinical 13C MR spectroscopy. Journal of nuclear medicine 2008;49(3):341-344

(Lagadinou, 2013)

Lagadinou ED, Sach A, Callahan K, Rossi RM, Neering SJ, Minhajuddin M, Ashton JM, Pei S, Grose V, O'Dwyer KM, Liesveld JL, Brookes PS, Becker MW, Jordan CT. BCL-2 inhibition targets oxidative phosphorylation and selectively eradicates quiescent human leukemia stem cells. Cell stem cell 2013;12(3):329-341

(LeBleu, 2014)

LeBleu VS, O'Connell JT, Gonzalez Herrera KN, Wikman H, Pantel K, Haigis MC, de Carvalho FM, Damascena A, Domingos Chinen LT, Rocha RM, Asara JM, Kalluri R. PGC-1alpha mediates mitochondrial biogenesis and oxidative phosphorylation in cancer cells to promote metastasis. Nature cell biology 2014;16(10):992-1003, 1001-1015

(Leone, 2014)

Leone A, Di Gennaro E, Bruzzese F, Avallone A, Budillon A. New perspective for an old antidiabetic drug: metformin as anticancer agent. Cancer treatment and research 2014;159:355-376

(Li, 2015)

Li Y, Park I, Nelson SJ. Imaging tumor metabolism using in vivo magnetic resonance spectroscopy. Cancer journal 2015;21(2):123-128

(Liberti, 2016)

Liberti MV, Locasale JW. The Warburg Effect: How Does it Benefit Cancer Cells? Trends in biochemical sciences 2016;41(3):211-218

(Lin, 2014)

Lin G, Chung YL. Current opportunities and challenges of magnetic resonance spectroscopy, positron emission tomography, and mass spectrometry imaging for mapping cancer metabolism in vivo. BioMed research international 2014;2014:625095

(López-Lázaro, 2008)

López-Lázaro M. The Warburg Effect : why and how do cancer cells activate glycolysis in the presence of oxygen? Anti-Cancer Agents in Medicinal Chemistry 2008;8:305-312

(Lu, 2012)

Lu M, Atthe B, Mateescu GD, Flask CA, Yu X. Assessing mitochondrial respiration in isolated hearts using (17)O MRS. NMR in biomedicine 2012;25(6):883-889

(Lunt, 2011)

Lunt SY, Vander Heiden MG. Aerobic glycolysis: meeting the metabolic requirements of cell proliferation. Annual review of cell and developmental biology 2011;27:441-464

(Lynch, 2014)

Lynch K, O'Brien R. (1)H magnetic resonance spectroscopy: a review of the current literature and its potential utility in veterinary oncology. Veterinary journal 2014;200(2):240-247

(Marjanska, 2010)

Marjanska M, Iltis I, Shestov AA, Deelchand DK, Nelson C, Ugurbil K, Henry PG. In vivo 13C spectroscopy in the rat brain using hyperpolarized [1-(13)C]pyruvate and [2-(13)C]pyruvate. Journal of magnetic resonance 2010;206(2):210-218

(Michelakis, 2008)

Michelakis ED, Webster L, Mackey JR. Dichloroacetate (DCA) as a potential metabolic-targeting therapy for cancer. British journal of cancer 2008;99(7):989-994

(Miles, 2008)

Miles KA, Williams RE. Warburg revisited: imaging tumour blood flow and metabolism. Cancer imaging 2008;8:81-86

(Mockler, 2014)

Mockler MB, Conroy MJ, Lysaght J. Targeting T cell immunometabolism for cancer immunotherapy; understanding the impact of the tumor microenvironment. Frontiers in oncology 2014;4:107

(Moreno-Sanchez, 2007)

Moreno-Sanchez R, Rodriguez-Enriquez S, Marin-Hernandez A, Saavedra E. Energy metabolism in tumor cells. The FEBS journal 2007;274(6):1393-1418

(Moreno-Sanchez, 2014)

Moreno-Sanchez R, Marin-Hernandez A, Saavedra E, Pardo JP, Ralph SJ, Rodriguez-Enriquez S. Who controls the ATP supply in cancer cells? Biochemistry lessons to understand cancer energy metabolism. The international journal of biochemistry & cell biology 2014;50:10-23

(Narazaki, 2013)

Narazaki M, Kanazawa Y, Koike S, Ando K, Ikehira H. Quantitative 17O imaging towards oxygen consumption study in tumor bearing mice at 7 T. Magnetic resonance imaging 2013;31(5):643-650

(Nelson, 2013)

Nelson SJ, Kurhanewicz J, Vigneron DB, Larson PE, Harzstark AL, Ferrone M, van Criekinge M, Chang JW, Bok R, Park I, Reed G, Carvajal L, Small EJ, Munster P, Weinberg VK, Ardenkjaer-Larsen JH, Chen AP, Hurd RE, Odegardstuen LI, Robb FJ, Tropp J, Murray JA. Metabolic imaging of patients with prostate cancer using hyperpolarized [1-(1)(3)C]pyruvate. Science translational medicine 2013;5(198):198ra108

(Ngo, 2015)

Ngo DC, Ververis K, Tortorella SM, Karagiannis TC. Introduction to the molecular basis of cancer metabolism and the Warburg effect. Molecular biology reports 2015;42(4):819-823

(Nielsen, 2001)

Nielsen FU, Daugaard P, Bentzen L, Stødkilde-Jørgensen H, Overgaard J, Horsman MR, Maxwell RJ. Effect of changing tumor oxygenation on glycolytic metabolism in a murine C3H mammary carcinoma assessed by in vivo nuclear magnetic resonance spectroscopy. Cancer Res. 2001;61(13):5318-5325

(Obre, 2015)

Obre E, Rossignol R. Emerging concepts in bioenergetics and cancer research: metabolic flexibility, coupling, symbiosis, switch, oxidative tumors, metabolic remodeling, signaling and bioenergetic therapy. The international journal of biochemistry & cell biology 2015;59:167-181

(Overhauser, 1953)

Overhauser AW. Polarization of Nuclei in Metals. Physical Review 1953;92(2):411-415

(Papandreoui, 2011)

Papandreou I, Goliasova T, Denko NC. Anticancer drugs that target metabolism: Is dichloroacetate the new paradigm? International journal of cancer Journal international du cancer 2011;128(5):1001-1008

(Park, 2013a)

Park JM, Recht LD, Josan S, Merchant M, Jang T, Yen YF, Hurd RE, Spielman DM, Mayer D. Metabolic response of glioma to dichloroacetate measured in vivo by hyperpolarized (13)C magnetic resonance spectroscopic imaging. Neuro-oncology 2013;15(4):433-441

(Park, 2013b)

Park JM, Josan S, Grafendorfer T, Yen YF, Hurd RE, Spielman DM, Mayer D. Measuring mitochondrial metabolism in rat brain in vivo using MR Spectroscopy of hyperpolarized [2-(1)(3)C]pyruvate. NMR in biomedicine 2013;26(10):1197-1203

(Park, 2016)

Park JM, Josan S, Jang T, Merchant M, Watkins R, Hurd RE, Recht LD, Mayer D, Spielman DM. Volumetric spiral chemical shift imaging of hyperpolarized [2-(13) c]pyruvate in a rat c6 glioma model. Magnetic resonance in medicine 2016;75(3):973-984

(Pathak, 2014)

Pathak RK, Marrache S, Harn DA, Dhar S. Mito-DCA: a mitochondria targeted molecular scaffold for efficacious delivery of metabolic modulator dichloroacetate. ACS Chem Biol 2014;9(5):1178-1187

(Pathania, 2009)

Pathania D, Millard M, Neamati N. Opportunities in discovery and delivery of anticancer drugs targeting mitochondria and cancer cell metabolism. Advanced drug delivery reviews 2009;61(14):1250-1275

(Pauwels, 2000)

Pauwels EK, Sturm EJ, Bombardieri E, Cleton FJ, Stokkel MP. Positron-emission tomography with [18F]fluorodeoxyglucose. Part I. Biochemical uptake mechanism and its implication for clinical studies. Journal of Cancer Research and Clinical Oncology. 2000;126(10):549-559

(Pavlides, 2009)

Pavlides S, Whitaker-Menezes D, Castello-Cros R, Flomenberg N, Witkiewicz AK, Frank PG, Casimiro MC, Wang C, Fortina P, Addya S, Pestell RG, Martinez-Outschoorn UE, Sotgia F, Lisanti MP. The reverse Warburg effect: aerobic glycolysis in cancer associated fibroblasts and the tumor stroma. Cell cycle 2009;8(23):3984-4001

(Payen, 2016)

Payen VL, Porporato PE, Baselet B, Sonveaux P. Metabolic changes associated with tumor metastasis, part 1: tumor pH, glycolysis and the pentose phosphate pathway. Cellular and Molecular Life Sciences 2016 73(7):1333-1348

(Peiris-Pages, 2016)

Peiris-Pages M, Martinez-Outschoorn UE, Pestell RG, Sotgia F, Lisanti MP. Cancer stem cell metabolism. Breast cancer research 2016;18(1):55

(Pfeiffer, 2001)

Pfeiffer T, Schuster S, Bonhoeffer S. Cooperation and competition in the evolution of ATP-producing pathways. Science 2001;292(5516):504-507

(Phelps, 2000)

Phelps ME. Positron emission tomography provides molecular imaging of biological processes. Proceedings of the National Academy of Sciences of the United States of America 2000;97(16):9226-9233

(Porporato, 2011)

Porporato PE, Dhup S, Dadhich RK, Copetti T, Sonveaux P. Anticancer targets in the glycolytic metabolism of tumors: a comprehensive review. Frontiers in pharmacology 2011;2:49

(Qian, 2014)

Qian Y. Inhibitors of glucose transport and glycolysis as novel anticancer therapeutics. World Journal of Translational Medicine 2014;3(2):37

(Reiser, 2008)

Reiser MF, Semmler W, Hricak H. Basics of Magnetic Resonance Imaging and Magnetic Resonance Spectroscopy, in Magnetic Resonance Tomography, Springer-Verlag Berlin Heidelberg, 2008. p 3-168

(Richmond, 2008)

Richmond A, Su Y. Mouse xenograft models vs GEM models for human cancer therapeutics. Disease models & mechanisms 2008;1(2-3):78-82

(Rodrigues, 2005)

Rodrigues TB, Cerdán S. 13C MRS: An outstanding tool for metabolic studies. Concepts in Magnetic Resonance Part A 2005;27A(1):1-16

(Rodrigues, 2014)

Rodrigues TB, Serrao EM, Kennedy BW, Hu DE, Kettunen MI, Brindle KM. Magnetic resonance imaging of tumor glycolysis using hyperpolarized 13C-labeled glucose. Nature medicine 2014;20(1):93-97

(Rohren, 2004)

Rohren EM, Turkington TG, Coleman RE. Clinical applications of PET in oncology. Radiology. 2004;231(2):305-332

(Ros, 2013)

Ros S, Schulze A. Balancing glycolytic flux: the role of 6-phosphofructo-2-kinase/fructose 2,6-bisphosphatases in cancer metabolism. Cancer&Metabolism. 2013;1(1):8

(Salibi, 1998)

Salibi N, Brown MA. Clinical MR Spectroscopy: First Principles: John Wiley & Sons, Inc; 1998. p 5-17

(Saunier, 2016)

Saunier E, Benelli C, Bortoli S. The pyruvate dehydrogenase complex in cancer: An old metabolic gatekeeper regulated by new pathways and pharmacological agents. International journal of cancer Journal international du cancer 2016;138(4):809-817

(Schroeder, 2009)

Schroeder MA, Atherton HJ, Ball DR, Cole MA, Heather LC, Griffin JL, Clarke K, Radda GK, Tyler DJ. Real-time assessment of Krebs cycle metabolism using hyperpolarized 13C magnetic resonance spectroscopy. FASEB journal 2009;23(8):2529-2538

(Sengupta, 2016)

Sengupta D, Pratx G. Imaging metabolic heterogeneity in cancer. Molecular cancer 2016;15:4

(Serkova, 2011)

Serkova NJ. Translational imaging endpoints to predict treatment response to novel targeted anticancer agents. Drug resistance updates : reviews and commentaries in antimicrobial and anticancer chemotherapy 2011;14(4-5):224-235

(Serrao, 2016)

Serrao EM, Rodrigues TB, Gallagher FA, Kettunen MI, Kennedy BW, Vowler SL, Burling KA, Brindle KM. Effects of fasting on serial measurements of hyperpolarized [1-(13) C]pyruvate metabolism in tumors. NMR in biomedicine 2016;29(8):1048-1055

(Seth, 2011)

Seth P, Grant A, Tang J, Vinogradov E, Wang X, Lenkinski R, Sukhatme VP. On-target Inhibition of Tumor Fermentative Glycolysis as Visualized by Hyperpolarized Pyruvate. Neoplasia 2011;13(1):60-71

(Smith, 2003)

Smith JJ, Sorensen AG, Thrall JH. Biomarkers in imaging: realizing radiology's future. Radiology. 2003;227(3):633-638

(Sonveaux, 2008)

Sonveaux P, Vegran F, Schroeder T, Wergin MC, Verrax J, Rabbani ZN, De Saedeleer CJ, Kennedy KM, Diepart C, Jordan BF, Kelley MJ, Gallez B, Wahl ML, Feron O, Dewhirst MW. Targeting lactate-fueled respiration selectively kills hypoxic tumor cells in mice. The Journal of clinical investigation 2008;118(12):3930-3942

(Stacpoole, 1989)

Stacpoole PW. The pharmacology of dichloroacetate. Metabolism 1989;38(11):1124-1144

(Stacpoole, 2003)

Stacpoole PW, Nagaraja NV, Hutson AD. Efficacy of Dichloroacetate as a Lactate-Lowering Drug. The Journal of Clinical Pharmacology 2003;43(7):683-691

(Stockwin, 2010)

Stockwin LH, Yu SX, Borgel S, Hancock C, Wolfe TL, Phillips LR, Hollingshead MG, Newton DL. Sodium dichloroacetate selectively targets cells with defects in the mitochondrial ETC. International Journal of Cancer 2010;127(11):2510-2519

(Surti, 2015)

Surti S. Update on time-of-flight PET imaging. Journal of nuclear medicine 2015;56(1):98-105

(Sutendra, 2013)

Sutendra G, Michelakis ED. Pyruvate dehydrogenase kinase as a novel therapeutic target in oncology. Frontiers in oncology 2013;3:38

(Swartz, 2004)

Swartz HM. Using EPR to measure a critical but often unmeasured component of oxidative damage: oxygen. Antioxidants & Redox Signaling. 2004;6(3):677-686

(Swartz, 2014)

Swartz HM, Williams BB, Zaki BI, Hartford AC, Jarvis LA, Chen EY, Comi RJ, Ernstoff MS, Hou H, Khan N, Swarts SG, Flood AB, Kuppusamy P. Clinical EPR: unique opportunities and some challenges. Academic radiology 2014;21(2):197-206

(Szablewski, 2013)

Szablewski L. Expression of glucose transporters in cancers. Biochimica et biophysica acta 2013;1835(2):164-169

(Tailor, 2004)

Tailor DR, Baumgardner JE, Regatte RR, Leigh JS, Reddy R. Proton MRI of metabolically produced H2 17O using an efficient 17O2 delivery system. NeuroImage 2004;22(2):611-618

(Tee, 2015)

Tee SS, Keshari KR. Novel Approaches to Imaging Tumor Metabolism. Cancer journal 2015;21(3):165-173

(Tennant, 2010)

Tennant DA, Duran RV, Gottlieb E. Targeting metabolic transformation for cancer therapy. Nature reviews Cancer 2010;10(4):267-277

(Tentler, 2012)

Tentler JJ, Tan AC, Weekes CD, Jimeno A, Leong S, Pitts TM, Arcaroli JJ, Messersmith WA, Eckhardt SG. Patient-derived tumour xenografts as models for oncology drug development. Nat Rev Clin Oncol 2012;9(6):338-350

(Tomasi, 2012)

Tomasi G, Rosso L. PET imaging: implications for the future of therapy monitoring with PET/CT in oncology. Current opinion in pharmacology 2012;12(5):569-575

(Upadhyay, 2013)

Upadhyay M, Samal J, Kandpal M, Singh OV, Vivekanandan P. The Warburg effect: insights from the past decade. Pharmacology & therapeutics 2013;137(3):318-330

(van der Mijn, 2016)

van der Mijn JC, Panka DJ, Geissler AK, Verheul HM, Mier JW. Novel drugs that target the metabolic reprogramming in renal cell cancer. Cancer & metabolism 2016;4:14

(Vander Heiden, 2011)

Vander Heiden MG. Targeting cancer metabolism: a therapeutic window opens. Nature reviews Drug discovery 2011;10(9):671-684

(Vaupel, 2012)

Vaupel P, Mayer A. Availability, not respiratory capacity governs oxygen consumption of solid tumors. The international journal of biochemistry & cell biology 2012;44(9):1477-1481

(Vegran, 2011)

Vegran F, Boidot R, Michiels C, Sonveaux P, Feron O. Lactate influx through the endothelial cell monocarboxylate transporter MCT1 supports an NF-kappaB/IL-8 pathway that drives tumor angiogenesis. Cancer research 2011;71(7):2550-2560

(Verdegem, 2014)

Verdegem D, Moens S, Stapor P, Carmeliet P. Endothelial cell metabolism: parallels and divergences with cancer cell metabolism. Cancer & metabolism 2014;2(1):1-19

(Viale, 2015)

Viale A, Corti D, Draetta GF. Tumors and mitochondrial respiration: a neglected connection. Cancer research 2015;75(18):3685-3686

(Waki, 1997)

Waki A, Fujibayashi Y, Yonekura Y, Sadato N, Ishii Y, Yokoyama A. Reassessment of FDG uptake in tumor cells: high FDG uptake as a reflection of oxygen-independent glycolysis dominant energy production. Nuclear Medicine and Biology 1997;24(7):665-670

(Walenta, 2002)

Walenta S, Schroeder T, Mueller-Klieser W. Metabolic mapping with bioluminescence: basic and clinical relevance. Biomolecular Engineering 2002;18(6):249-262

(Wang, 2010)

Wang F, Ogasawara MA, Huang P. Small mitochondria-targeting molecules as anti-cancer agents. Molecular aspects of medicine 2010;31(1):75-92

(Wang, 2014)

Wang T, Liu G, Wang R. The Intercellular Metabolic Interplay between Tumor and Immune Cells. Frontiers in immunology 2014;5:358

(Warburg, 1925)

Warburg O. Uber den Stoffwechsel der Carcinomzelle. Klinische Wochenschrift 1925;4:534-536

(Warburg, 1956)

Warburg O. On respiratory impairment in cancer cells. Science 1956;124(3215):269-270

(Ward, 2012)

Ward PS, Thompson CB. Metabolic reprogramming: a cancer hallmark even warburg did not anticipate. Cancer cell 2012;21(3):297-308

(Warmoes, 2014)

Warmoes MO, Locasale JW. Heterogeneity of glycolysis in cancers and therapeutic opportunities. Biochemical pharmacology 2014;92(1):12-21

(Weinberg, 2015)

Weinberg SE, Chandel NS. Targeting mitochondria metabolism for cancer therapy. Nature chemical biology 2015;11(1):9-15

(Wojtkowiak, 2011)

Wojtkowiak JW, Verduzco D, Schramm KJ, Gillies RJ. Drug resistance and cellular adaptation to tumor acidic pH microenvironment. Molecular pharmaceutics 2011;8(6):2032-2038

(Yeung, 2008)

Yeung SJ, Pan J, Lee MH. Roles of p53, MYC and HIF-1 in regulating glycolysis - the seventh hallmark of cancer. Cellular and molecular life sciences : CMLS 2008;65(24):3981-3999

(Yoshida, 2015)

Yoshida GJ. Metabolic reprogramming: the emerging concept and associated therapeutic strategies. Journal of experimental & clinical cancer research : CR 2015;34:111

(Zannella, 2013)

Zannella VE, Dal Pra A, Muaddi H, McKee TD, Stapleton S, Sykes J, Glicksman R, Chaib S, Zamiara P, Milosevic M, Wouters BG, Bristow RG, Koritzinsky M. Reprogramming metabolism with metformin improves tumor oxygenation and radiotherapy response. Clinical cancer research 2013;19(24):6741-6750

(Zheng, 2012)

Zheng J. Energy metabolism of cancer: Glycolysis versus oxidative phosphorylation (Review). Oncology letters 2012;4(6):1151-1157

(Zhu, 2001)

Zhu XH, Merkle H, Kwag JH, Ugurbil K, Chen W. 17O relaxation time and NMR sensitivity of cerebral water and their field dependence. Magnetic resonance in medicine 2001;45(4):543-549

(Zhu, 2002)

Zhu XH, Zhang Y, Tian RX, Lei H, Zhang N, Zhang X, Merkle H, Ugurbil K, Chen W. Development of (17)O NMR approach for fast imaging of cerebral metabolic rate of oxygen in rat brain at high field. Proceedings of the National Academy of Sciences of the United States of America 2002;99(20):13194-13199

(Zhu, 2005)

Zhu XH, Zhang N, Zhang Y, Zhang X, Ugurbil K, Chen W. In vivo 17O NMR approaches for brain study at high field. NMR in biomedicine 2005;18(2):83-103

(Zhu, 2007)

Zhu XH, Zhang Y, Zhang N, Ugurbil K, Chen W. Noninvasive and three-dimensional imaging of CMRO(2) in rats at 9.4 T: reproducibility test and normothermia/hypothermia comparison study. Journal of cerebral blood flow and metabolism : official journal of the International Society of Cerebral Blood Flow and Metabolism 2007;27(6):1225-1234

(Zhu, 2010)

Zhu XH, Zhang Y, Chen W. In vivo 17O MRS imaging for assessing myocardial oxygen metabolism in rat heart at 9.4 T. Proceedings of the 18th Annual Meeting of ISMRM; Stockholm, Sweden. 2010. p. 172

(Zhu, 2011)

Zhu XH, Chen W. In vivo oxygen-17 NMR for imaging brain oxygen metabolism at high field. Progress in nuclear magnetic resonance spectroscopy 2011;59(4):319-335

(Zong, 2016)

Zong WX, Rabinowitz JD, White E. Mitochondria and Cancer. Molecular cell 2016;61(5):667-676